Alzheimer's and inflammation: exploring the interplay between immune cells in the peripheral immune system and the central nervous system through single-cell RNA-seq

Dissertation

zur

Erlangung des Doktorgrades (Dr. rer. nat.)

der

Mathematisch-Naturwissenschaftlichen Fakultät

der

Rheinischen Friedrich-Wilhelms-Universität Bonn

vorgelegt von

Emily Hinkley

aus

London, dem Vereinigten Königreich

Bonn, 2024

Angefertigt mit Genehmigung der Mathematisch-Naturwissenschaftlichen Fakultät

der Rheinischen Friedrich-Wilhelms-Universität Bonn

Erstgutachter: Prof. Dr. Joachim L. Schultze

Zweitgutachter: Priv.-Doz. Dr. Marc Beyer

Tag der Promotion: 2nd February 2024

Erscheinungsjahr: 2024

Declaration of originality

Hiermit erkläre ich an Eides statt, dass ich die vorliegende Arbeit selbstständig und nur unter Verwendung der angegebenen Quellen und Hilfsmittel verfasst habe,

die vorgelegte Arbeit nicht bereits anderweitig als Dissertation eingereicht worden ist,

ich keine früheren Promotionsversuche unternommen habe,

für die Erstellung der vorgelegten Arbeit keine fremde Hilfe, insbesondere keine entgeltliche Hilfe von Vermittlungs- oder Beratungsdiensten in Anspruch genommen wurde.

Index

Abstract

Alzheimer's disease (AD) is a progressive neurodegenerative disease that is the most common cause of dementia and the sixth leading cause of death globally (Haque & Levey, 2019; World Health Organization, 2017). Increases in ageing populations are exacerbating the problem and by 2050 the number of people with a dementia diagnosis is predicted to reach 132 million (World Health Organization, 2017). This will have a significant social and economic cost, however despite the active and growing field of research that has arisen to tackle this problem AD remains a disease with no curative treatment and relatively limited options for management (Revi, 2020). Diagnosis is also challenging, as pre-mortem diagnosis struggles to definitively distinguish AD from other types of dementia with similar presentation and the long prodromal phase in AD can mean that detection is only possible after neuronal damage has already begun (Jack Jr et al., 2018).

The impact of inflammation both in the central nervous system (CNS) and peripheral immune system (PIS) has recently become a highly discussed area of research in the field and advances in our understanding of immune privilege have led to new opportunities to interrogate AD pathogenesis. We now know that systemic inflammation can play a role in the progression of CNS pathologies. Studies have demonstrated that peripheral immune stimuli can trigger long-term immune training in the CNS and worsen the Amyloid-β (Aβ) burden in AD (Wendeln et al., 2018). When we consider this alongside evidence that these peripheral inflammatory events have an impact in the CNS far earlier than previously thought (Jack Jr et al., 2018) then it is clear that elucidating this early stage relationship could be critical to the development of effective interventions.

Our study aims to investigate the interplay between AD and peripheral inflammation through analysis of single-cell RNA sequencing (scRNA-seq) data of circulating immune cells in both the CNS and PIS. We sought to identify changes at transcriptional and cellular level between the two systems in parallel by profiling peripheral blood mononuclear cells (PBMCs) from the PIS and immune cells isolated from cerebrospinal fluid (CSF). The study cohort recruited donors via the existing DELCODE, DESCRIBE and DANCER studies at DZNE and used

clinical biomarkers to classify these donors using the AT(N) diagnostic framework (Jack Jr et al., 2018).

In my thesis, I identified changes in the CSF myeloid cell compartment of AD donors which suggested inflammation-triggered recruitment from the PIS into the CSF. This was in line with previous observations reporting transitioning of blood-borne myeloid progenitors into a microglia-like myeloid subtype in other neuroinflammatory pathologies (Esaulova et al., 2020). I also identified a separate subset of apparently dysfunctional CSF-specific microglia that were strongly linked to iron metabolism which is known to be dysfunctional in AD (Kenkhuis et al., 2021). No statistically verifiable transcriptional or cellular level changes were identified in the PBMC compartment of AD donors compared to healthy donors. However, this does not rule out that further studies of the PBMC compartment in the early and prodromal phases of AD could generate valuable insights.

Taken together, this work suggests that using scRNA-seq to decipher the transcriptional profiles of peripheral blood and CSF immune cells in AD offers a unique perspective on the progression and pathogenesis of this disease. Characterising the immune landscape in both systems throughout the course of disease may hold the key to identify new biomarkers and develop potential future therapies targeting the peripheral immune system.

Index of figures

Index of supplementary figures

Index of tables

Abbreviations

Remark: The list of abbreviations does not include gene names, chemicals, and acronyms of computational tools or wet-lab technologies.

ACh	Acetylcholine
AChEIs	Acetylcholinesterase inhibitors
AD	Alzheimer's disease
APR	Acute-phase reactant
ASO	Antisense oligonucleotides
AT(N)	Amyloid Tau (Neurodegeneration)
BAM	Border-associated macrophage
BBB	Blood-brain barrier
B-CSF-B	Blood-cerebrospinal fluid barrier
cDC	Conventional dendritic cell
CEL-seq	Cell expression by linear amplification and sequencing
ChP	Choroid plexus
CMT	Carrier-mediated transport
CNS	Central Nervous system
CSF	Cerebrospinal fluid
CyTOF	Time-of-flight mass cytometry
EOAD	Early-onset AD
FACS	Fluorescence-activated cell sorting
FDA	US Food and Drug Administration

FDG	Fluoro- deoxyglucose
FDR	False discovery rate
GEM	Gel beads in Emulsion
HLA	Human leukocyte antigen
ISF	Interstitial fluid
JC	John Cunningham virus
MCI	Mild cognitive impairment
MMST/MMSE	Mini-Mental-Status-Test/Exam
MRI	Magnetic resonance imaging
MTG	Middle temporal gyrus
NFTs	Neurofibrillary tangles
NGS	Next-generation sequencing
LOAD	Late-onset AD
pB	Peripheral blood
PBMC	Peripheral blood mononuclear cells
PCA	Principal component analysis
PCs	Principal components
PCR	Polymerase chain reaction
PET	Positron emission tomography
PML	Progressive multifocal leukoencephalopathy
RMT	Receptor-mediated transcytosis
scRNA-seq	Single-cell RNA sequencing

TCM	Central memory T
TCR	T cell receptor signalling
TEM	Effector memory T
TEMRA	T effector memory CD45RA+
UMAP	Uniform Manifold Approximation and Projection algorithm
UMI	Unique molecular indices

1. Introduction

1.1. Inflammation and the immune system

The human immune system is comprised of two major effector arms: the innate and the adaptive immune systems. As their names suggest the innate immune system originates at birth whilst the adaptive immune system is acquired as we grow and retains a memory of the pathogens it is exposed to. Both systems have their own cell types. In the innate immune system, these are grouped under the term myeloid cells and include monocytes, macrophages, dendritic cells, mast cells and granulocytes. In the adaptive immune system, they are termed lymphocytes which encompasses: T cells, B cells and natural killer (NK) cells. The two systems work together, with the lymphocytes receiving information on their target pathogens through the presentation of antigens (small fragments of pathogens) by myeloid cells known as antigen-presenting cells (APC) (specifically dendritic cells, macrophages and monocytes).

Inflammation is a key component of the innate immune system's response to external threats such as microbes, viruses or any other kind of physical damage. It functions as an early defensive response, setting about a complex chain reaction tailored to the perceived threat. First, threat-specific signals are sent, for example, the lysis of cells can release proteins which trigger cytokine production in the extracellular space (Nathan, 2002). This is just one starting point, amongst many others which begin the recruitment and activation of the multiple immune cell types that constitute an immune response. Normally this immune response is contained by anti-inflammatory responses which limit inflammatory signals and eventually restore homeostatic conditions within the affected area. However, inflammation has long been considered by immunologists as a double-edged sword, where healing potential is balanced against the risk of an out-of-control immune response which in the worst scenarios can lead to sepsis and death (Tracey, 2002).

Excessive inflammatory responses have been linked to many disease pathologies including rheumatoid arthritis, Crohn's disease, atherosclerosis, diabetes, multiple sclerosis, cerebral myocardial ischaemia and Alzheimer's disease (Tracey, 2002; Ardura-Fabregat et al., 2017; Boyko et al., 2017; Lai et al., 2017; Paouri and Georgopoulos, 2019). In Alzheimer's disease, proteins associated with detrimental β-amyloid plaques trigger inflammatory signalling pathways in immune cells specific to the central nervous system and begin an immune response that has both positive and negative consequences (Ardura-Fabregat et al., 2017; Boyko et al., 2017; Paouri & Georgopoulos, 2019; Weiner & Selkoe, 2002). This is an example of a pathology-related inflammatory response in the CNS which is physically separate from the peripheral immune system with its own cell types. In this study, we explore the increasing evidence of crossover between these two systems and the impact this has on CNS diseases like Alzheimer's. We would like to investigate the extent of detectable change in the PIS during a pathological event in the CNS such as AD. A better understanding of these different immune landscapes may contribute to new insights into the pathogenesis of AD.

1.2. The relationship between the central and peripheral immune system

Traditionally the CNS has been considered an immune-privileged site that is closed to access from the PIS. This is a neuroprotective mechanism which protects the brain from unnecessary inflammation which could cause damage. Both pathogens and cells of the PIS are prevented from accessing this area by physical structures that control access to the CNS architecture.

Recent interest in the relationship between the central (neuroimmune) system and the peripheral immune system has centred on the structures forming the boundary that keeps them separate. The first of these structures is the blood-brain barrier (BBB), which specifically refers to the endothelial membrane of the vascular network that supplies the brain and covers its surface (Sweeney et al., 2018). The capillaries of this network are walled by tightly packed endothelial cells enmeshed in a basement membrane which they share with pericytes and structurally supportive astrocyte end-feet (Figure 1). As well as providing a structural divide, the BBB is a regulator of solute transport into the brain. In optimal conditions, it is impermeable

to PIS cells and has low uptake and transport rates for macromolecules. When macromolecules do cross this is facilitated by carrier-mediated transport (CMT) for carbohydrates, amino acids, fatty acids, nucleotides, hormones and vitamins or receptor-mediated transcytosis (RMT) for proteins and peptides (Sweeney et al., 2018). Lipid-soluble molecules with a molecular weight under 400–600 Da can pass via transmembrane diffusion (Bellettato & Scarpa, 2018). Smaller molecules such as oxygen and carbon dioxide have no problem diffusing across the barrier rapidly. This ensures a highly-regulated CNS environment with favourable conditions for neurons to function.

The second structure that separates the PIS and CNS is the blood-cerebrospinal fluid barrier (B-CSF-B) which is found in the choroid plexus (ChP) and the arachnoid membrane, also known as the arachnoid mater. The arachnoid mater is the middle of the three layers that protect the brain which collectively are known as the meninges. Within the arachnoid mater is the subarachnoid space which is filled with CSF and contains small arterial vessels (Ransohoff & Engelhardt, 2012) (Figure 1). The ChPs are found in the four ventricles of the brain and act as a B-CSF-B as well as the main production centre for CSF. Their structure consists of capillaries surrounded by endothelial cells and connective tissue surrounded by vilified epithelial cells facing outwards into the CSF-filled ventricles (Figure 1). Once in the ventricles, CSF flows from the lateral to the third ventricle to the fourth ventricle to enter the central canal of the spinal cord or the subarachnoid space. From the subarachnoid space CSF can be reabsorbed into the systemic circulation or lymph nodes (Lun et al., 2015; Proulx, 2021).

Like the BBB, the B-CSF-B in healthy individuals is considered impenetrable to cells of the peripheral immune system. However recent work has shown that during injury and disease it can become similarly compromised. For example, the ChP is described as a route of recruitment of lymphocytes into the CSF in spinal cord injury (Kunis et al., 2013; Lun et al., 2015; Schwartz & Baruch, 2014). Monocytes are also suggested to use this route to transit into the CSF to reach lesion sites in spinal cord injuries (Shechter et al., 2013). Furthermore, the epithelial cell layer of the B-CSF-B is known to mediate monocyte migration in the presence of IFN-γ release from TH1 effector memory T cells (Kunis et al., 2013).

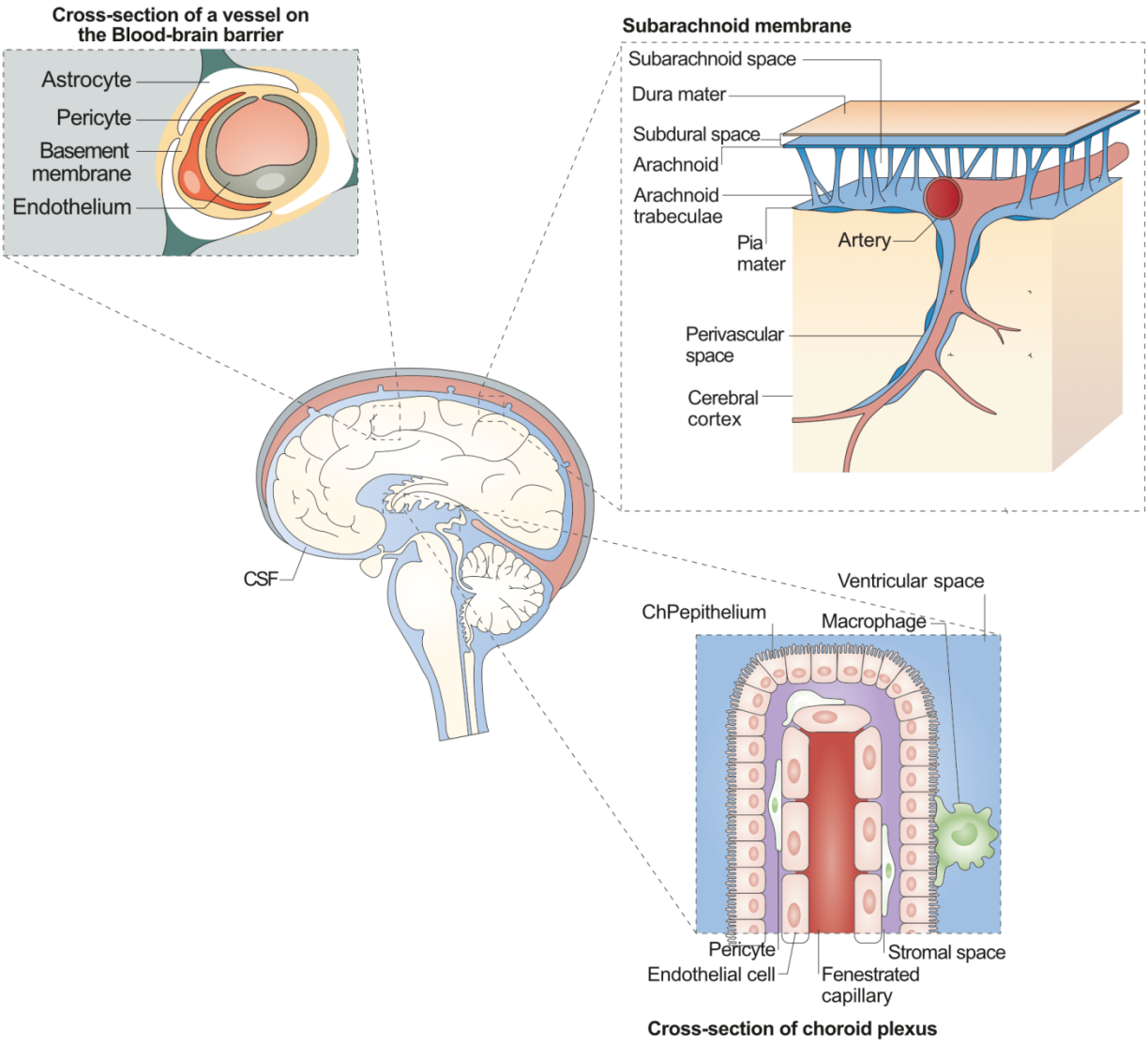

Figure 1. Structural barriers between the CNS and PIS. Overview of the blood-brain barrier and choroid plexus and blood-CSF barrier in the brain. Figure adapted from (Lun et al., 2015; Ransohoff & Engelhardt, 2012; Sweeney et al., 2018).

1.3. The CSF compartment and its cell types

The CSF provides a protective cushion for the brain and spinal cord as well as maintaining homeostatic conditions in the CNS. Studies estimate healthy adults produce CSF constantly at a rate of 400-500 ml/day (Brown et al., 2004; Sakka et al., 2011). This turnover in humans equates to the replacement of the total volume an average of four times every twenty hours. The ChP of the lateral ventricles and the tela choroidea of the third and fourth ventricles produce sixty to seventy-five percent of this volume (Sakka et al., 2011). The production of CSF comes mostly from the diffusion of arterial blood through the ChP, though as already described the B-CSF-B filters out larger and cellular components of the blood. Interstitial fluid (ISF) also contributes to CSF volume but accounts for only a small fraction (Ransohoff & Engelhardt, 2012). Reabsorption of CSF occurs at two points. Some of it will drain via the arachnoid villi in the arachnoid mater, through the dura mater and into venous blood vessels (Ransohoff & Engelhardt, 2012). Alternatively, some of it will pass from the subarachnoid space through the cribriform plate to the nasal mucosa and deep cervical lymph nodes. It has been demonstrated that APCs from the PIS can access these lymph nodes and an antigen introduced to the CSF can be detected in these lymph nodes as soon as two hours later, which is an example of communication between these two systems (Laman & Weller, 2013).

Cell populations of the CSF come predominantly from immune cells trafficked from the PIS. The percentages found are 90% T cells, 5% B cells, 5% monocytes, and <1% dendritic cells (Ransohoff & Engelhardt, 2012). Granulocytes have not been observed and presence of Neutrophils is still under debate with one study reporting a small population (<2%) (Farhadian et al., 2019).

1.3.1. Microglia-like phenotypes in the CSF

Local myeloid cells of the CNS are primarily found within the tissues or traversing across them rather than free-living in the CSF. CNS macrophages are found on the tissue borders and can be divided into location-based categories such as perivascular (pvMΦ), meningeal (mMΦ) and choroid plexus macrophages (cpMΦ) (also called CNS-associated macrophages) (Goldmann et al., 2016). Microglia are generally parenchymal and phenotypic variability has been observed dependent on what region of the brain they are sampled from (Jiang-Shieh et al., 2003). Unlike the bone-marrow-derived monocytes and macrophages of the PIS, microglia originate from a fetal yolk sac progenitor and are thought to enter the CNS through the ChP and then progress through the CSF to the brain tissue where they are typically found (Ginhoux et al., 2010; Lun et al., 2015).

Single-cell techniques have previously been utilised to characterise microglial transcriptional states in both homeostasis and disease. A recent comprehensive study combined scRNA-seq with time-of-flight mass cytometry (CyTOF) to describe eight heterogenous microglial clusters (which they name *C1–C3, C5–C9)* from human brain tissue (Sankowski et al., 2019). They used the mCEL-Seq2 protocol (Herman et al., 2018) to generate data from 4,396 microglia from 15 donors undergoing surgery for tumours or epilepsy. Whilst around 30% of cells were enriched for a bulk-RNAseq microglia signature the remaining cells displayed age and region-dependent transcriptional signatures. Two of these signatures (*C6* & *C7*) have high expression of the Gene Ontology pathway for “antigen processing and presentation of peptide antigen” (0048002) and were later identified in a CSF dataset from two HIV patients in a study that aimed to investigate neuroinflammation (Esaulova et al., 2020). Esaulova *et al*. suggested that this CSF-specific population of microglia could be coming from blood-derived progenitors that act as a microglial replacement when the BBB is disrupted. These blood-derived replacement microglia can take on a gene signature which is extremely similar to their fetal-derived counterparts (Shemer et al., 2018). The entry route that these blood-derived progenitors take to then transition into replacement microglia is still not fully understood, however, the presence of chemokine receptors CCR1, CCR5, CXCR4, and CX3CR1 suggests that they are being recruited. Whether they remain in the CSF or if this study is

providing a snapshot of these cells in transit to the parenchyma is not yet known (Esaulova et al., 2020).

The CSF microglia highlighted in Esaulova *et al*. also exhibited high levels of C1q genes which encode the C1q subcomponent of the classical complement activation pathway (Gani, 2021; Schäfer et al., 2000). The classical complement activation pathway is one of three pathways that make up the complement system, an important feature of the innate immune system that is present in both the PIS and the CNS (Figure 2). The three main pathways are activated in response to different stimuli: the classical pathway is activated by the formation of the C1-complex when antibody-antigen complexes bind together with C1q, the alternative pathway is activated by C3 hydrolysis and the lectin pathway is activated by either C3 hydrolysis or antigens without the presence of antibodies (Gani, 2021).

Whilst this system is important for its defensive role during immune activation it also functions on a maintenance level, for example, it is involved in synaptic pruning by microglia during early brain development and for the clearance of cellular debris (Bachiller et al., 2018; Carroll & Isenman, 2012). Previous studies have linked the classical complement activation pathway with microglial dysfunction, especially in relation to neurodegenerative diseases like AD (Hong et al., 2016; Terai et al., 1997).

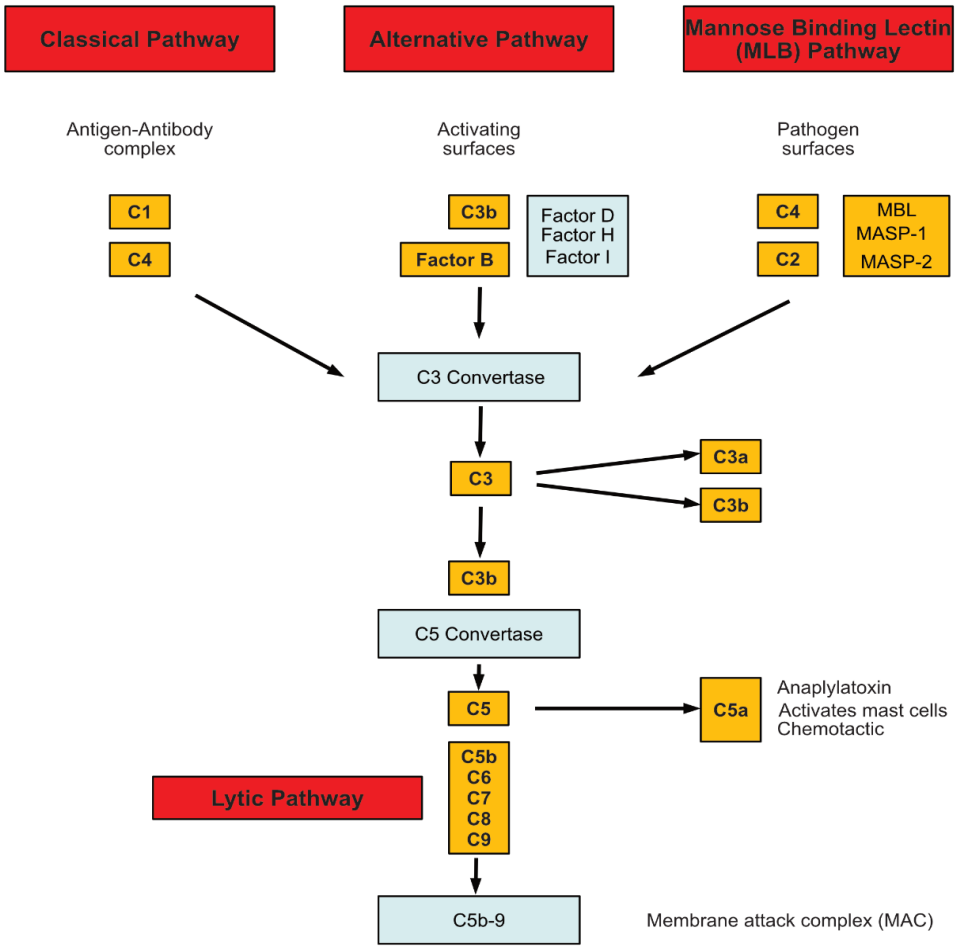

Figure 2. Complement pathways. Figure edited from (Gani, 2021).

1.4. Exploring cellular heterogeneity through single-cell Omics

The advent of scRNA-seq has allowed the generation of massive datasets faster than ever before. A single run on some of the leading platforms can now profile the transcripts of thousands of cells. Alongside this, we are seeing increases in sensitivity and the types of data parameters that can be measured, meaning not only is there a greater quantity of data available but we also have more options to improve on quality and specificity.

1.4.1. The rise of single-cell Omics

Over the last two decades, next-generation sequencing (NGS) and scRNA-seq have become the cutting-edge technology for deciphering gene transcription differences at single-cell resolution (Figure 3). These pioneering techniques have allowed us to profile highly variable gene expression across diverse cell types and complex organisms at the single-cell level (Cao et al., 2017). With projects such as the Human Cell Atlas now able to profile over a million individual cells in parallel, it is clear that the reach and potential of this technology are still rapidly expanding (Rozenblatt-Rosen et al., 2017).

This expansion has had an impact on the quality as well as the quantity of data produced. Researchers can now evaluate gene transcription dynamics in an unbiased manner, uncovering cell type specific expression profiles in heterogeneous cell populations (Shahan, 2019). Furthermore, advanced scRNA-seq techniques have recently made it possible to assess a large number of multi-tissue samples simultaneously, stratifying complex comparisons such as diseases versus controls in a single experiment (Gate et al., 2020; Mathys et al., 2019).

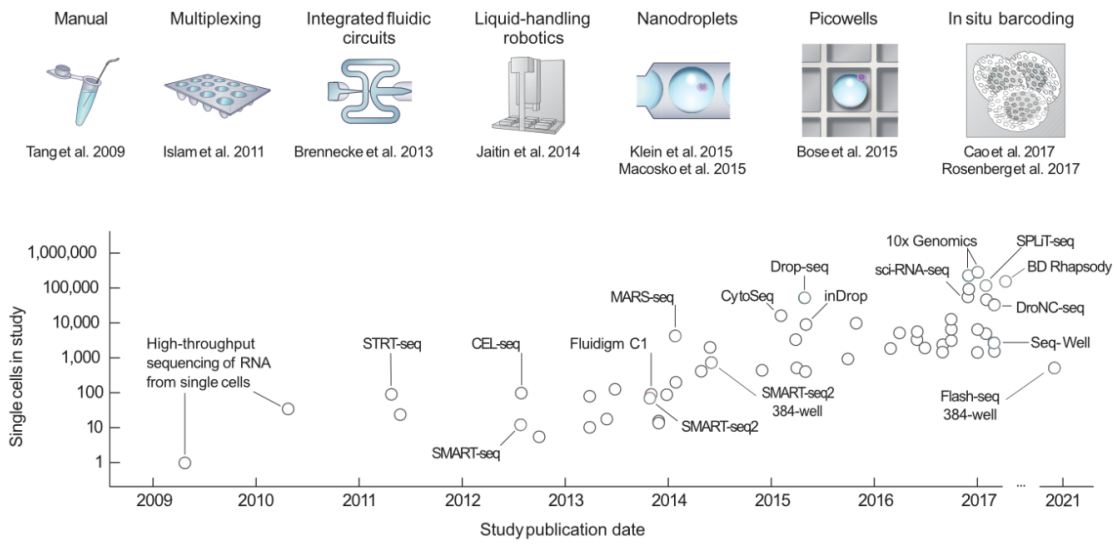

Figure 3. Timeline and scaling of scRNA-seq experiments. Cell numbers reported in representative publications up to 2018. Figure edited from (Svensson et al., 2018).

One of the first challenges in the development of new single-cell techniques is the isolation of mRNA from single-cells in the smallest possible reaction volume but on the largest possible scale. Early scRNA-seq protocols were developed as low-throughput methods involving the containment of a cell in a single tube, well or plate. In 2009 the first study to describe single-cell mRNA sequencing modified a cDNA amplification method from microarray analyses (Kurimoto et al., 2006) to assess gene expression profiles at single-cell resolution (F. Tang et al., 2009). Following on from this the single-cell tagged reverse-transcription sequencing (STRT-seq) method (Islam et al., 2011) utilised a template-switching PCR to amplify full-length cDNA. Whilst this method sequenced only the 5′-end fragment of the cDNA generated, a new method called SMART-seq was published next, which captured and sequenced fragments from the full-length cDNA (Picelli et al., 2013). Around the same time, a protocol called CEL-seq (cell expression by linear amplification and sequencing) was released which worked on a similar basis but barcoded and pooled the cells before using *in vitro* transcription for linear amplification of the mRNA (Hashimshony et al., 2012). Later MARS-seq (massively parallel scRNA-seq) scaled up the use of *in vitro* transcription, reporting the transcriptional states for thousands of cells (Jaitin et al., 2014).

Increases in the scale of single-cell experiments continued with the development of microfluidics to capture cells in droplets rather than wells. The first commercial system to move away from well-based methodologies was Fluidgm's C1 microfluidic chip-based system which captured up to 96 single-cells in individual reaction chambers where it used SMART-seq methodology to reverse transcribe mRNA (DeLaughter, 2018). The next development were droplet-based microfluidics which are characterised by the oil-based partitioning of a cell and a bead barcoded with unique molecular indices (UMIs) and oligonucleotide primers in the same droplet. Reverse transcription within these isolated droplets results in barcoded cDNA that is amplified during library preparation to generate a NGS-ready cDNA library. Early examples of this are the inDrop (Klein et al., 2015) and Drop-seq (Macosko et al., 2015) protocols. More recently the commercial release of the 10x Chromium platform from 10x Genomics (Zheng et al., 2017) has been a hugely popular tool and is used in numerous scRNA-seq studies (Gate et al., 2020; Jordão et al., 2019; Mathys et al., 2019; Ochocka et

al., 2021; Olah et al., 2020; Schafflick et al., 2020). The principle of the system is similar to previous droplet-based methods and creates Gel beads in EMulsion (GEM) on an 8-channel microfluidic chip through the capture of around 100,000 barcoded gel beads in droplets. Single cells are then loaded into these individual GEMs which act as reaction chambers for reverse transcription.

The method of using UMI barcoded beads is not unique to microfluidic techniques and is often used for techniques that do not include fluorescence-activated cell sorting (FACS) in their workflow. Seq-Well uses random deposition of cells through gravity into tiny picolitre wells on a silicon chip which also contain UMI barcoded beads (Gierahn et al., 2017). The number of cells loaded is calculated to the highest possible number that will still be sufficiently diluted to avoid the introduction of “doublets”, where more than one cell joins with a single bead. These can also be identified in the quality control (QC) of data in downstream bioinformatics analyses. The BD Rhapsody is another commercial platform which uses random distribution into picoliter wells, this time on a prefabricated cartridge (Chang et al., 2019). Like Seq-Well, the process does not offer full-length transcripts. While Seq-Well captures only the 3’-end, the BD Rhapsody protocol gets fragment cDNA by priming at random points along the length of synthesised first-strand cDNA.

Random cellular deposition into tiny picolitre wells is also used in new ultra-high throughput techniques like sci-RNA-seq3 (Cao et al., 2017). It uses probability and three-level single-cell combinatorial indexing and was recently used to profile gene expression in four million single cells from one hundred and twenty-one samples (Cao et al., 2020). These ultra-high throughput techniques have opened up new levels of data collection and new challenges in terms of data storage and analysis for the researchers using them.

The BD Rhapsody is one of several current technologies that have the capacity to take a multi-omic approach to data collection. This increasingly popular integrative approach combines scRNA-seq data with other omics technologies, like proteomics. The Rhapsody does this by simultaneously collecting single-cell protein expression data in an additional library prep protocol (BD AbSeq). Other examples of multi-omics include CITE-seq which also

combines scRNA-seq with protein expression data (Stoeckius et al., 2017), G&T-seq which captures DNA alongside scRNA-seq (Macaulay et al., 2015) and single-cell nucleosome, methylome and transcriptome sequencing (scNMT-seq) which combines chromatin accessibility, DNA methylation and scRNA-seq (Clark et al., 2018).

The last few years have marked a new era of scRNA-seq with the rise of spatial transcriptomics where single-molecule fluorescent *in situ* hybridization allows the spatial context of cells within a tissue to be captured. New methods such as cyclic smFISH (Codeluppi et al., 2018) and STARmap (spatially-resolved transcript amplicon readout mapping) (X. Wang et al., 2018), as well as commercial platforms like the Visium from 10X and the GeoMx Digital Spatial Profiler from Nanostring, have revealed information on cell and tissue structure heterogeneity that was previously lost during tissue dissociation for single cell isolation (Ståhl et al., 2016).

1.4.2. Computational analysis of scRNA-seq data

Over the last decade, the scale of datasets generated by scRNA-seq experiments has grown at an astonishing rate. In early publications, researchers described just one cell (F. Tang et al., 2009) and now studies are profiling thousands to millions of single cells at a time (Baßler et al., 2020; Cao et al., 2017; Hamed et al., 2022; Schulte-Schrepping et al., 2020; Wendisch et al., 2021). Data of this size presents significant challenges in downstream processing, it requires considerable computational power to conduct meaningful analyses and often it can be sparse containing missing or noisy entries. Data quality can be affected at all stages of the protocol, from poor cell lysis rates during isolation to low numbers of cells captured, issues with indices in library preparation and errors in sequencing.

Downstream analysis of scRNA-seq data manages these potential pitfalls through rigorous QC. One part of QC is the identification and removal of data artefacts, for example, cells with high levels of mitochondrial genes should be removed as this can indicate that the cell was under stress during the early isolation stages of the protocol (Zhao et al., 2002). Specifically,

the cytoplasmic RNA of damaged or dying cells is the first to leach out of the cell membrane leaving behind the mitochondrial RNA to be overrepresented in the dataset (Ilicic et al., 2016). Setting a maximum threshold at around 20% for mitochondrial gene expression and filtering during QC can prevent false clusters from appearing in the data later on. Another early QC step is to set a minimum threshold for UMIs per cell and genes per cell as this will remove any cells where barcoding or amplification was unsuccessful. As with the mitochondrial RNA, these low gene/UMI per cells can make the identification of clusters and subsequently cell populations more difficult.

Another source of false clusters in scRNA-seq data that uses barcoded beads is doublets. These are data points that are the combination of two cells with the same UMI, usually due to the two cells settling within the same reaction compartment. These can be identified by analysis packages such as DoubletFinder (McGinnis et al., 2019) or Scrublet (Wolock et al., 2019). These packages come with both advantages and disadvantages which have been previously evaluated and compared (Xi & Li, 2021). Extracellular RNA known as ambient RNA can also cause transcriptional changes in the data and should be removed. To achieve this, packages such as SoupX (Young & Behjati, 2020) provide tools that allow us to distinguish between native and ambient RNA.

1.4.3. Single-cell transcriptomic approaches to Alzheimer's disease

Whilst scRNA-seq is not new to AD research, the majority of work done to date has focused on elucidating differences and pathological mechanisms in brain tissue (R. Chen et al., 2017; Olah et al., 2020; Zeisel et al., 2015). Different neuronal and glial cell types and brain regions have been extensively profiled across stages of pathological change identifying disease-associated cell type-specific gene regulatory changes (Mathys et al., 2019). The role of microglia in AD has also attracted a great deal of attention with investigations finding new levels of heterogeneity (Sankowski et al., 2019) and subpopulations with disease signatures (Keren-Shaul et al., 2017; Olah et al., 2020). Areas that have been covered less extensively

in AD scRNA-seq are the non-parenchymal tissues and CSF in the CNS and the wider circulating PIS.

The CSF has been addressed in broader neuroinflammatory work (Esaulova et al., 2020; Roostaei et al., 2021; Schafflick et al., 2020) and more specifically in regards to AD where transcriptionally distinct immune cell subpopulations have been identified and linked to both inflammation and disease stage (Gate et al., 2020). The study from Gate *et al.* also included PBMC data which identified increased CD8+ T effector memory CD45RA+ (T_{EMRA}) cells in PBMC through CyTOF. This finding was further substantiated through scRNA-seq of TEMRA cells and revealed enhanced T cell receptor (TCR) signalling in this T cell population in AD. More recently, a study focused solely on scRNA-seq PBMC analysis in AD profiling immune cell types from three AD patients and two age-matched healthy controls (H. Xu & Jia, 2021). They speculated that the peripheral adaptive immune response, especially mediated by T cells, may have a role in the pathogenesis of AD and their results identified thirty-one cell type-specific genes some of which were human leukocyte antigen genes.

With the exception of the studies mentioned above, datasets comparing PBMCs of AD patients against those of healthy controls are still relatively uncommon, perhaps because this sort of data collection presents challengingly high background variation which requires analysis of a high number of individuals to overcome this variability and identify meaningful patterns. The sparsity of prior work in this area opens up the potential for the discovery of novel blood biomarkers and early detection markers, but finding a viable signal amongst so much noise may only become achievable as we begin to harness deep learning techniques.

1.5. Alzheimer's Disease

Alzheimer’s disease is a progressive neurodegenerative disease that is the most common cause of dementia, accounting for 60-70% of cases (MOE, 2017). Fifty-five million people worldwide have a diagnosis of dementia and with increasing rates of the population ageing,

this is expected to reach 132 million people by 2050 (MOE, 2017). Owing to the substantial burden of AD and economic cost, there is an active and growing field of research attempting to better understand the pathophysiology and develop effective treatments and preventative measures.

1.5.1. Definition of the disease

Alzheimer's disease manifests with progressing cognitive deficits affecting memory, language, motor skills, behavioural function and recognition ability (Burns et al., 2002; Dai & Shen, 2021). When the disease was first documented by Alois Alzheimer in 1901, he first observed in his patient (Auguste D) changes in behaviour and memory impairment (Burns et al., 2002). Years later following a subsequent post-mortem histological investigation he made the following description:

"in the centre of an otherwise almost normal cell, there stands out one or several fibrils due to their characteristic thickness and peculiar impregnability. Numerous small miliary foci are found in the superior layers. They are determined by the storage of a peculiar substance in the cerebral cortex. All in all, we have to face a particular disease process." (Stelzmann et al., 1995)

This description, published in his 1907 paper, refers to the intracellular neurofibrillary tangles of hyperphosphorylated tau and deposits of amyloid plaques. In modern science amyloid-beta plaques and neurofibrillary tangles are considered two hallmark characteristics of Alzheimer's disease and are innately associated with neuronal loss and synaptic damage (Goedert, 2009; Golde, 2022).

Stages of pathological changes within the CNS in AD were described in 1991 and are known as Braak stages (Braak & Braak, 1991). There are six Braak stages which start with increasingly severe alterations in the transentorhinal region of the brain (stages I and II) and then damage progresses to limbic regions in the middle stages (III and IV), before finally

reaching the isocortex (stages V and VI) (Braak & Braak, 1991). These stages can also be applied to Parkinson's disease. Another term that is also related to AD is mild cognitive impairment (MCI), this was coined in the 1980s and refers to the transitional phase between healthy cognitive function and the onset of dementia (Petersen et al., 2014).

Finally, AD can be separated into hereditary early-onset AD (EOAD) and sporadic late-onset AD (LOAD) pathologies. Diagnosis before 65 years of age is generally considered to be EOAD and accounts for 5–10% of cases (Reitz et al., 2020). Unlike the sporadic LOAD, EOAD is more often inherited and likely to follow an autosomal dominant inheritance pattern caused by mutations in *APP*, *PSEN1*, and *PSEN2*, however, in some instances, EOAD can still be sporadic (Reitz et al., 2020).

1.5.2. Pathogenesis, development and progression of AD

The pathogenesis of AD centres around the two hallmark characteristics introduced in the previous section: extracellular amyloid-beta plaques and intraneuronal neurofibrillary tangles (NFTs). Aβ peptides form the constituents of these amyloid-beta plaques. They are formed when amyloid precursor protein (APP) in the neuronal membrane comes into contact with beta-secretase and gamma-secretase, which cleave the protein into Aβ peptides (Ciudad et al., 2020; Pospich & Raunser, 2017) (Figure 4). These Aβ peptides known as Aβ(1–40) and Aβ(1–42) are polymorphs of different lengths with heterogeneous structures which have added to the complexity of their study and have been suggested to result in different pathogenicities (Fändrich et al., 2009). The shorter Aβ(1–40) is the most abundant isoform in AD, however, Aβ(1–42) is generally considered to have higher toxicity and plaque-forming capacities (Mori et al., 1992; Näslund et al., 1994; Schmidt et al., 2009). In the healthy brain Aβ peptides are cleared away by microglia, however, lack of clearance allows them to build up into densely-packed toxic aggregates which ultimately destroy surrounding neurons (Serrano-Pozo et al., 2011).

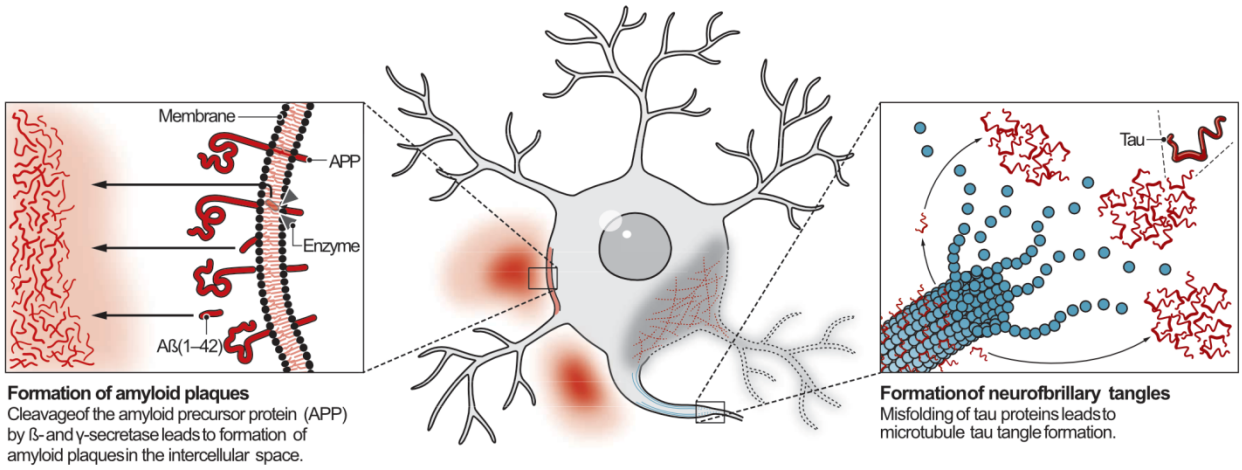

Figure 4. **Overview of amyloid plaques and neurofibrillary tangles that accumulate in the AD brain**. Adapted from (Pospich & Raunser, 2017)

NFTs are structures made up of tau. Normally tau proteins are found associated with the microtubule of neuronal axons but can also be found at lower levels in glial cells. Tau is encoded by a gene called microtubule-associated protein tau (*MAPT*) which is located on sixteen exons of the long arm on chromosome seventeen (17q21) (Andreadis, 2006). Exons 2, 3, and 10 can generate six isoforms of tau through alternative splicing (Rinaldi & Wood, 2018).

In healthy physiology, tau is a soluble, unfolded protein that when phosphorylated has a critical function in maintaining the stability of the axonal structure (Figure 4) (Weingarten et al., 1975). Phosphorylation of specific amino acid residues in tau is a normal post-translational protein modification occurring at eighty-five potential serine, threonine, and tyrosine phosphorylation sites (Noble et al., 2013). A higher rate of tau phosphorylation occurs in AD and is known as hyperphosphorylation, this happens when tau kinase and tau phosphatase activity becomes disrupted (Medeiros et al., 2011; Meng et al., 2022). The effects of this disruption are two-fold: firstly tau becomes less suited for microtubules and secondly, it is more resistant to degradation by the calcium-activated neutral proteases of the ubiquitin-proteosome pathway (Alonso et al., 2001). The redundant dysfunctional hyperphosphorylated tau instead aggregates into insoluble NFTs (Medeiros et al., 2011). The build-up of NFTs is

damaging to the neuron in itself but is especially fatal when accompanying the loss of axonal function due to insufficient maintenance of structural stability (Bloom, 2014). This process of tau hyperphosphorylation is not unique to AD but also occurs in other tauopathies such as Pick's disease, progressive supranuclear palsy, corticobasal degeneration, and argyrophilic grain disease (Rinaldi & Wood, 2018).

Identification of AD-related inflammatory pathways that are present in both the PIS and CNS is an important step toward building a more comprehensive understanding of the disease. An example of this is the identification of two inflammatory pathways activated during the early MCI stages of AD (Pillai et al., 2019). Levels of inflammatory proteins in the CSF and blood plasma were assessed to establish a better picture of the pathophysiology of inflammatory changes in AD. The authors found that phosphorylated tau levels were associated most highly with the tumour necrosis signalling pathway and $A\beta_{42}$ levels associated with the complement and coagulation cascade. Gene expression transcripts in post-mortem brain tissue were confirmatory and showed enrichment of genes from the same inflammatory pathways.

Inflammasomes are intracellular protein complexes found in innate immune cells that respond to pathogens and damage-associated molecular patterns (DAMPs) (Hu et al., 2019). In age-related diseases, microglial cells show strong inflammasome activation, which can exacerbate disease pathology. Inflammasome formation leads to extracellular secretion of cleaved IL1β and IL18, which induce nearby cells to produce proinflammatory factors such as IFNγ, TNFα, and ROS (Hu et al., 2019). Inflammasome activation has been observed in PBMCs from MCI and AD patients, where release of proinflammatory cytokine IL-1β was strongly associated with disease progression (Rui et al., 2021).

1.5.3. The challenge of diagnosis

Diagnosis of AD in pre-mortem patients is widely acknowledged to be difficult for several reasons. Firstly, the definite diagnosis of AD requires confirmation of Aβ and NFTs in the parenchymal brain tissues. The most effective and conclusive way to achieve this is post-

mortem histological staining of the plaques and bundles on a microscopy slide (Jack Jr et al., 2018). This means that often AD diagnosis is only considered definite on autopsy, and in living patients is referred to as probable AD (McKhann et al., 1984). Biopsy of pre-mortem brain tissue is a costly, dangerous and invasive procedure that is not part of the normal diagnostic practice for AD. When a patient is already undergoing a biopsy for other reasons such as surgical removal of tumours it can be possible to observe these AD hallmarks in the staining process but this is a secondary finding in the fine-mapping of the tumour and is not performed for the sole purpose of AD diagnosis. The outcome of this is that pre-mortem diagnosis of AD through histology is largely not an option. A purely symptom-based diagnosis of AD often fails to distinguish it from other forms of dementia due to variation in early symptoms which do not always start with defects in episodic memory (Deture & Dickson, 2019). Increasingly, studies acknowledge that there is a long prodromal phase in AD which occurs before the onset of clear symptoms (Buchhave et al., 2012; Holtzman et al., 2011; Jack et al., 2013). In a disease where irreparable neuronal damage is a prerequisite of symptoms, potential treatments could arguably only be effective in combination with early diagnosis.

1.5.3.1. Current methods for diagnosis of pre-mortem patients

Currently, a range of techniques are employed for the detection of AD, all come with advantages and disadvantages and for this reason, it is common for clinical diagnosis to rely on multiple diagnostic approaches. Distinguishing AD through cognitive symptoms is difficult. Cognitive testing is not standardised and the test used will vary between clinics and countries. One popular version is the Mini-Mental-Status-Test (MMST), also known as the Mini-Mental-Status-Exam (MMSE). This was developed in 1975 and scores the patient out of thirty based on their responses to thirty-three general questions (Folstein et al., 1975). The MMST is not designed specifically for AD and instead is used to detect a range of aphasic and amnestic syndromes (Folstein et al., 1975). As well as this lack of specificity for AD, there is the issue that patients will have natural variations in baseline levels of cognition. This means that these tests work best as a supportive tool for highlighting symptomatic aspects of the disease rather than a comprehensive diagnostic tool.

Neuroimaging is an area which has brought big advances to the field of AD research as well as the wider study of neurodegenerative disease. It is non-invasive and two types are commonly used to diagnose forms of dementia: positron emission tomography (PET) and magnetic resonance imaging (MRI). PET shows emissions from radioactively labelled metabolically active chemicals injected into the patient's bloodstream, common examples of PET tracers used in AD are fluoro-deoxyglucose (FDG) and Pittsburgh compound B for Aβ and flortaucipir for tau (Figure 5). Images produced with PET can highlight deposits of Aβ and tau in the brain parenchyma and surrounding tissues (Chien et al., 2013; Jack Jr et al., 2018; Villemagne et al., 2014, 2015). This is also true for MRI, which does not use radioactive tracers but generates images through radio waves and can show regional atrophy in the brain (Golde, 2022). The extent to which these images can be used to diagnose AD is debated, with some studies suggesting that both forms of neuroimaging are not sufficiently specific to AD but function better as more general indicators of neurological damage (Jack Jr et al., 2018; Wirth et al., 2013). Other studies have described PET as a powerful differential diagnostic tool in identifying and localising Aβ and tau burdens in the brain (Mattsson & Hansson, 2019).

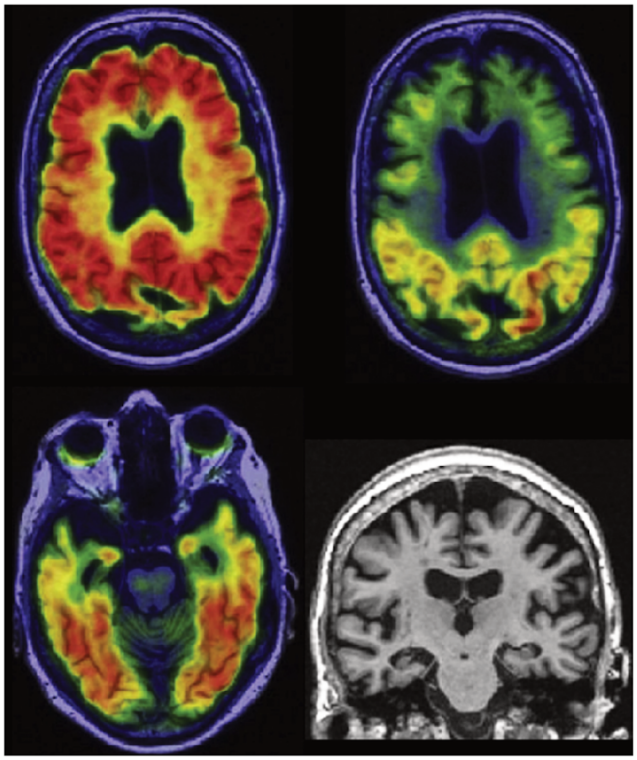

Figure 5. **Example of neuroimaging in a 75-year-old woman with amnestic multidomain dementia.** Abnormal Aβ PET with Pittsburgh compound B (top left), tau PET with flortaucipir (top right and bottom left), and atrophy on MRI (bottom right). Taken from (Jack Jr et al., 2018).

Fluid biomarkers are the other key tool in current AD diagnosis and when used in the right combinations have the potential to predict MCI and AD as early as the prodromal phase and before the development of obvious symptoms (Mattsson & Hansson, 2019). Initially, fluid biomarker studies focused on proteins expressed in the CSF that are measurable signs of Aβ and tau deposition in the brain parenchyma (Jack et al., 2013, 2016), however recent studies have moved towards validating blood-borne biomarkers (Fandos et al., 2017; Janelidze et al., 2021; Mielke et al., 2018). Typical CSF biomarkers measured are Aß42/40 ratio, p-tau-181 (phosphorylated tau-181) and total tau (t-tau), however agreement over cut-off levels used for these biomarkers varies and standardisation across clinics and countries is currently still ongoing.

1.5.3.2. Development of a biomarker-based classification system

The development of a unified classification system for the diagnosis of dementia is important in moving away from classical symptomatic diagnosis to a symptom-agnostic classification system based on measurable biological parameters in living patients. This has the double advantage of shifting the focus onto early detection, instead of diagnosing based on symptoms which are a consequence of damage, and greater clarity through the power of combined tools. In 2018 the National Institute on Aging-Alzheimer's Association (NIA-AA) published a research framework called AT(N) designed to achieve these goals (Hampel et al., 2021). This framework was aimed at improving diagnostic standards in research rather than clinical diagnosis, however, improvement in one area is likely to have future effects in the other. The framework is structured around three groups of biomarkers that can be measured through both imaging and fluid biopsy techniques: Aβ deposition, tau-mediated pathophysiology, and neurodegeneration [AT(N)] (Table1). The system was designed in a way that allows diagnosis through imaging or CSF biomarkers alone, however, a mixture of the two methods is also allowed, providing flexibility where available techniques are limited (Jack Jr et al., 2018).

Table 1. **Groups of the AT(N) framework and their biomarkers**. Biomarkers of Aβ deposition ("A") include cortical amyloid PET ligand binding or low CSF Aβ 42. Biomarkers of NFT ("T") are cortical tau PET ligand binding or raised CSF p-tau. Biomarkers of neurodegeneration or neuronal injury ["(N)"] are FDG PET hypometabolism, brain atrophy on MRI or CSF t-tau. Adapted from (Jack Jr et al., 2018).

AT(N)	Group description	Neuroimaging	CSF biomarkers
A	Aggregated Aß or associated pathology	Amyloid PET	Aß42 Aß42/ Aß40 ratio
T	Aggregated tau (NFT) or associated pathology	Tau PET	p-tau
(N)	Neurodegeneration or neuronal injury	Anatomic MRI FDG PET	t-tau

Patients can be scored as either positive or negative for each biomarker [A, T and (N)] which offers a further level of categorization as this profile then indicates one of four biomarker categories: Normal AD biomarkers, Alzheimer's disease, Alzheimer's pathological change, Alzheimer's and concomitant suspected non-Alzheimer's pathologic change or Non-AD pathologic change (Table 2). In 2021 a proposal was published to update the AT(N) system to the ATX(N) system which would include novel candidate biomarkers like neuroimmune dysregulation, synaptic dysfunction and alterations to the blood-brain barrier (Hampel et al., 2021).

Table 2. **AT(N) profiles and categories**. Adapted from (Jack Jr et al., 2018).

AT(N) Profile	Biomarker category
A-T-(N)-	Normal AD biomarkers
A+T-(N)-	Alzheimer's pathological change
A+T+(N)-	Alzheimer's disease
A+T+(N)+	Alzheimer's disease
A+T-(N)+	Alzheimer's and concomitant suspected non-Alzheimer's pathological change
A-T+(N)-	Non-AD pathological change
A-T-(N)+	Non-AD pathological change
A-T+(N)+	Non-AD pathological change

1.5.4. Management and therapeutic developments

Despite a strong research community and numerous clinical trials, AD remains a disease without curative treatment (Revi, 2020). There are therapeutic options that can interfere with disease progression allowing clinicians some degree of management depending on how early the disease is detected. Here, we explore current management strategies and recent clinical trials.

1.5.4.1. Management

Therapies for AD have so far targeted Aβ, and tau or have been for symptomatic management. Management strategies can be summarised by three main therapeutic approaches (i) Acetylcholinesterase inhibitors (AChEIs), (ii) Memantine hydrochloride (NMDA) and (iii) Antipsychotics (Olanzapine).

The deficiency of neurotransmitter acetylcholine (ACh) is a theorised pathology of Alzheimer's. Acetylcholinesterase (AChE) is an enzyme that hydrolyzes ACh to acetate and choline (Figure 6) (Akıncıoğlu & Gülçin, 2020). The role of AChEIs in the treatment of AD has been to restore levels of ACh by inhibiting its clearance.

AChEIs have been reported to have a role in the protection of cells from Aβ injury and damage from free radical toxicity (Tabet, 2006). There is evidence to suggest that AChEIs play an anti-inflammatory role, inhibiting the release of cytokines from microglia and monocytes in the CNS (Tabet, 2006). AChEIs have also shown a reduction of the Aβ burden by impeding Aβ assembly (Korabecny et al., 2019; Mezeiova et al., 2019).

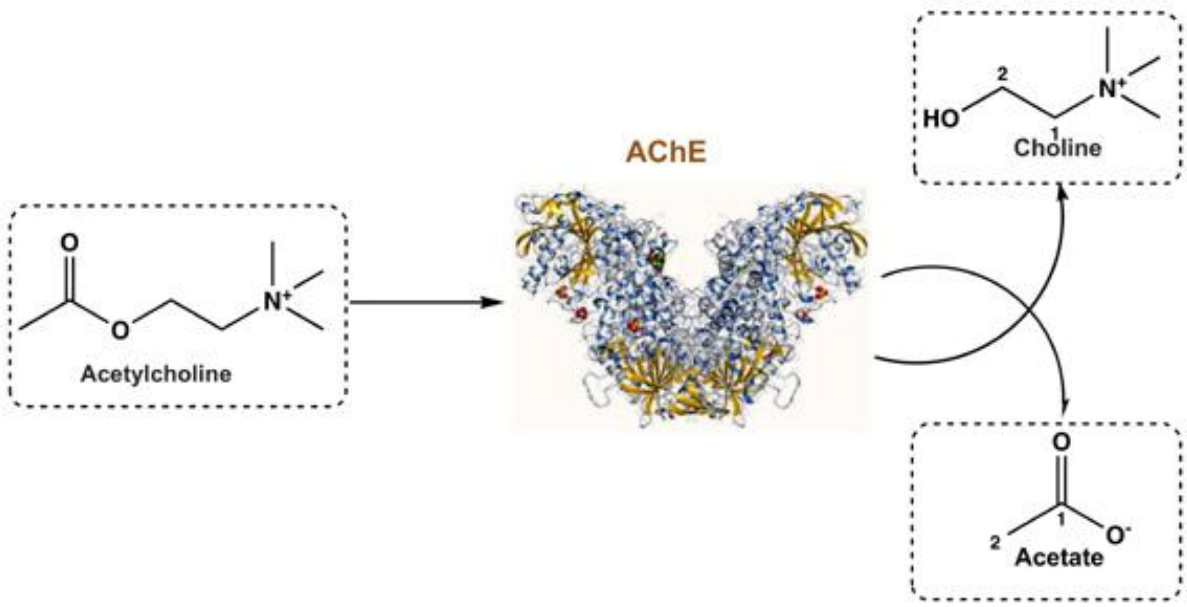

Figure 6. **Hydrolysis of ACh to acetate and choline by AChE**. Taken from (Akıncıoğlu & Gülçin, 2020).

In AD the overstimulation of N-methyl-D-Aspartate (NMDA) receptors results in calcium and glutamate-mediated excitotoxicity (J. Liu et al., 2019), ultimately leading to free radical generation and associated tau phosphorylation (Zhang et al., 2016). The use of non-competitive NMDA receptor antagonists is thought to ameliorate the component of neurodegeneration caused by this neurotoxicity.

Behavioural dysfunction, such as thought disturbance, aggression and hallucinations, are possible symptoms of AD and there are various pharmaceutical (e.g. Olanzapine) and non-pharmaceutical methods to try to improve this. The use of typical and atypical antipsychotic medication is licensed for use in AD with the aim of symptom control (Calsolaro et al., 2019). Increasing awareness around safety concerns relating to the use of antipsychotics has reduced the prevalence of use in AD patients (Ballard et al., 2011).

1.5.4.2. Developments in antisense oligonucleotide (ASO) therapies

A promising therapeutic approach currently being developed for AD are antisense oligonucleotides (ASOs). These are synthetic RNA-altering single-stranded oligodeoxynucleotides which cause the subsequent reduction or changes in protein expression depending on their design mechanism (Rinaldi & Wood, 2018). The BBB prevents oligonucleotide access into the CNS from the peripheral blood stream. To circumnavigate this, ASOs are delivered via intrathecal injection. At present only a handful of ASO-mediated therapies are already approved and successfully used in the US for the treatment of neuroinflammatory demyelinating diseases of the CNS, for example, Duchenne muscular dystrophy (Eteplirsen (Lim et al., 2017)) and spinal muscular atrophy (Nusinersen (Neil & Bisaccia, 2019)).

ASO approaches in AD have so far focused on targeting the tau production gene MAPT. This 16-exon gene has 6 known isoforms, all of which are capable of the hyperphosphorylation associated with AD pathologies. Murine studies have demonstrated that morpholino-induced skipping on exons 1, 5 or 7 results in a frameshift that can cause tau reduction (Sud et al., 2014). Treatment with ASOs has also been shown to reverse some effects of AD pathologies in aged mice and non-human primates as well as prolonging survival (DeVos et al., 2017). Recently, Biogen completed phase 2 testing for the anti-tau ASO Ionis-MAPTRX, which targets tauopathies via the MAPT gene. Their cohort consists of forty-four mild AD patients and whilst the study is complete no results have been reported yet (Lane et al., 2017).

In summary, ASO therapies are a fast-progressing therapeutic area, however their application is currently more advanced in other neuroinflammatory pathologies. The dual mechanism of amyloid plaques and tau in AD pathology also presents a problem. At present, AD ASO therapies are largely based around targeting tauopathies. To fully address the disease, ASO development will also need to slow the formation of amyloid plaques.

1.5.4.3. Immunotherapy in Alzheimer's Disease

Immunotherapies in AD are a promising idea, and currently include vaccinations, antibodies (targeting Aβ and tau), and biologicals targeting microglia molecules and inflammasome modulation. Many of the vaccines being trialled aim to train immune system recognition of Aβ plaques and subsequently trigger Aβ antibody production. GV1001 is currently the most advanced AD vaccine, having started phase III trials in 2023. It uses a different mechanism, inhibiting production of Aβ induced ROS in neurons by mimicking human telomerase reverse transcriptase (Koh et al., 2021).

One of the best-known therapies trialled in humans in recent years is the human monoclonal antibody aducanumab. The FDA approved this drug in 2021, making it the first new AD drug in over eighteen years to be approved in the US (Mullard, 2021). In transgenic murine models aducanumab allowed dose-dependent reductions in soluble and insoluble Aβ aggregations (Sevigny et al., 2016). In Europe, the treatment reached phase III trials before being discontinued in 2019 due to a lack of significant effect on cognitive decline in humans. Other Aβ monoclonal antibodies to be trialled in the last decade include solanezumab and crenezumab (Selkoe & Hardy, 2016), however, these have not been approved in Europe or the US.

Recently, promising data has been released on a IgG1 monoclonal antibody called Lecanemab. It binds with high specificity to Aβ peptides and, for the first time in a phase III study, has demonstrably slowed cognitive decline. Patients' decline in overall mental skills was reduced by 27% over 18 months (van Dyck et al., 2023). In late 2022, lecanamab was approved by the FDA despite safety concerns because of bleeding events in preconditioned individuals.

In summary, the last decade has seen the development of numerous new therapies for AD, but it is the advent of antibody therapies which brings the most tangible progress in the field. This immune aspect of neurodegenerative medicine makes it even more critical that research fully elucidates the relationship between the CNS and PIS. Understanding communication

between these systems may allow the development of more effective targets and improve management for exacerbatory neuroinflammation. As well as this there is potential for better diagnostics and disease monitoring in both the CSF and pB. Techniques like scRNA-seq could be used to monitor cell population changes in both these areas and inform treatment efficacy during drug development.

2. Aim of the thesis

The last decade of research has seen a shift in our understanding of the relationship between the CNS and PIS. The concept of immune privilege in the CNS has been challenged as new techniques uncover further evidence that the two systems are not as separate as previously thought. The CNS is vulnerable to peripheral inflammatory events and systemic inflammation is now known to play a role in the progression of neurodegenerative pathologies like AD. Alongside this, there is now evidence suggesting that these peripheral inflammatory events are having effects in the CNS far earlier than previously thought (Flores-Cordero et al., 2022; Jack Jr et al., 2018; Wyss-Coray & Rogers, 2012). This emphasises the importance of understanding the early and prodromal phases of pathologies like AD to fully uncover the pathogenesis and develop effective interventions.

Research in AD has traditionally focused on changes occurring in the neurons and their surrounding parenchymal tissues in the brain. There are several commonly used biomarkers and many more in development, however, these are generally designed to measure levels of AD-associated proteins such as phosphotau-181 and Aβ in the CSF. In the last years, the analysis of biomarkers has been extended to the peripheral blood, but only a handful of studies have approached this at a single-cell level and even fewer have attempted to elucidate transcriptional changes in immune cells between the two systems in parallel.

Therefore, this thesis aims to provide more insight into the interplay between AD and peripheral inflammation through analysis of scRNA-seq data of circulating immune cells in the CSF and peripheral blood. More specifically, we would like to know whether, during a pathological event in the CNS such as AD, we can also observe changes in the PIS detectable through scRNA-seq. We hypothesise that the high-resolution data made available through scRNA-seq technology will allow a better characterization of the immune landscape in both systems and contribute to our understanding of the cellular and molecular pathways in AD pathogenesis.

3. Materials

3.1. General laboratory consumables, equipment and reagents

3.1.1. Equipment

Table 3: Overview of equipment

Reagent or resource	Source	Identifier
Instruments		
Thermo Scientific Megafuge 40R with TX-1000 rotor	Thermo Fisher Scientific	PN 75004518
BD Rhapsody Express instrument	Becton Dickinson	Cat# 633702
BD Rhapsody Scanner	Becton Dickinson	Cat# 633701
BD Rhapsody P1200M and P5000M pipettes	Becton Dickinson	Cat. No. 633704, Cat.No. 633705
Eppendorf ThermoMixer C	Eppendorf	Cat# 5382000015
Magnetic separation stand (0.2 ml; 5ml)	V&P Scientific, Inc	Cat# VP 772F4-1, VP 772FB-1A, VP772FB-1
DynaMag-2 Magnet	ThermoFisher Scientific	Cat# 12321D
Mr. Frosty Freezing Container	ThermoFisher Scientific	Cat# 5100-0001
Countess 3 Automated Cell Counter	ThermoFisher Scientific	Cat# AMQAX2000
Agilent 4200 TapeStation system	Agilent	Cat# G2991BA
BD FACSymphony	BD bioscience	Cat# FACSymphony A5 SE

3.1.2. Reagents and kits

Table 4: Overview of reagents, kits and oligonucleotides

Reagent or resource	Source	Identifier
Critical commercial assays and kits		
RPMI 1640 Medium	GIBCO	Cat# 11875093
Fetal Bovine Serum	Pan Biotec	Cat# 3302
BD Pharmingen Stain buffer	Becton Dickinson	Cat# 563794
Pancoll human, Density: 1.077 g/ml	Pan Biotech	Cat# P04-601000
Dulbecco'S Phosphate Buffered Saline, MO	Sigma-Aldrich	Cat# D8537
Nuclease-Free Water	Invitrogen	Cat# AM9937
TE Buffer, pH8.0, 1mM disodium EDTA	Thermo Fisher	Cat# 12090015
SPRIselect	Beckmann Coulter	Cat# B23318
10% Tween 20	BIO-RAD	Cat# 1662404
Buffer EB	QIAGEN	Cat# 19086
Ethanol, Absolute	Fisher Bioreagents	Cat# BP2818-500
BD Rhapsody WTA Amplification Kit	Becton Dickinson	Cat# 633801
BD Rhapsody Cartridge Kit	Becton Dickinson	Cat# 633733
BD Cartridge Reagent Kit	Becton Dickinson	Cat# 633731
BD Rhapsody cDNA Kit	Becton Dickinson	Cat# 633773
High Sensitivity D5000 ScreenTape	Agilent	Cat# 5067-5592
TapeStation HS D5000 Reagents (Buffer & Ladder)	Agilent	Cat#5067-5593
Qubit dsDNA HS Assay Kit	ThermoFisher	Cat# Q32854
NextSeq 500/550 High Output Kit v2.5 (150 Cycles)	Illumina	Cat# 20024907
Trypan Blue	Invitrogen	Cat# T10282
FACS Clean	BD Bioscience	Cat# BD 340345
FACS Rinse	BD Bioscience	Cat# 340346

OneComp/UltraComp compensation beads	Invitrogen	Cat# 01-2222-42
DAPI	SigmaAldrich	Cat# 28718-90-3
2 mM Calcein AM	Thermo Fisher Scientific	Cat# C1430
DRAQ7	BD Bioscience	Cat. No. 564904
DMSO	SigmaAldrich	Cat# 200-664-3
INCYTO disposable hemocytometer	INCYTO	Cat. No. DHC-N01-5
High Sensitivity D5000 ScreenTape	Agilent	Cat#5067-5592
NEBNext High-Fidelity 2x PCR Master Mix	NEB	Cat#M0541L
Nextera XT DNA Library Preparation Kit (96 samples)	Illumina	Cat#FC-131-1096
2x Kapa Hifi HotStart Readymix	Kapa Biosystems	Cat#KK-2602
NextSeq 500/550 High Output Kit v2.1 (75 cycles)	Illumina	Cat#20030410
NextSeq PhiX Control Kit	Illumina	Cat#FC-110-3002
NxGen™ RNase Inhibitor	Lucigen	Cat#F83923-1
Exonuclease I	NEB	Cat#M0293S
Maxima H Minus Reverse Transcriptase	Thermo Fisher	Cat#EPO0753
dNTP	NEB	Cat#N04465
Oligonucleotides		
Tn5ME-B Oligo: 5`-GTCTCGTGGGCTCGGAGATGTGTATAAGAGACAG-3`	IDT	custom
Tn5MErev Oligo: 5`-[phos]CTGTCTCTTATACACATCT-3`	IDT	custom
TSO primer	IDT	custom
P5-SMART-PCR primer	IDT	custom
barcoded primer	IDT	custom
N70X Oligo	Illumina	custom
SMART PCR primer	Eurofins Scientific	Cat#74998995

3.1.3. Consumables

Table 5: Overview of consumables

Reagent or resource	Source	Identifier
Consumables		
AMPure XP beads	Beckman Coulter	Cat#A63881
mRNA Capture beads	Chemgenes	Cat#MACOSKO-2011-10
1.5/2 ml reaction tubes	Eppendorf	Cat# 0030121023.
PCR reaction tubes	Sarstedt	Cat#72.737.002
Falcon Tube (15 ml)	Corning®	Cat# CLS430053-500EA
Falcon Tube (50 ml)	Corning®	Cat# CLS430290-500EA
Flow cytometry tubes	Sarstedt	Cat# 55.1579.002
Cell strainers (70µM, 100µM)	BD, Falcon	Cat# 352350
Serological pipettes	Sarstedt	Cat# 86.1253.001
LifterSlip	Electron Microscopy Science	Cat#72186-60
Transwell polycarbonate membrane cell culture inserts	Corning	Cat#3422
184 Silicone Encapsulant Clear 0.5kg kit	Dow SYLGARD™	Dow 184 SIL ELAST KIT 0.5KG
Polycarbonate (PCTE) membrane filters, 0.01 MICRON, 62MM X 22MM	Sterlitech	Cat#PCT00162X221 00
Countess Cell Counting Chamber Slides	ThermoFisher Scientific	Cat# C10228

3.2. Software

Table 6: Overview of software

Reagent or resource	Source	Identifier
Software and algorithms		
AUCell	(Aibar et al., 2017)	v1.6.1 (CRAN)
Seurat (R package)	(Butler et al., 2018; Hafemeister & Satija, 2019; Stuart et al., 2019)	v2.3.4 (CRAN)
umap	(McInnes, Healy, & Melville, 2018)	https://cran.r-project.org/web/packages/umap/index.html
pheatmap	(Raivo Kolde, 2019)	v1.0.12
ComplexHeatmap (R package)	(Gu et al., 2016)	v1.20.0 (Bioconductor)
ggplot2	(Wickham, 2016)	v3.3.6 (CRAN)
ClusterProfiler (R package)	(Yu et al., 2012)	v3.10.1 (CRAN)
R statistical programming	R Core Team	v3.1.5, v4.0.3 (CRAN)
RStudio	RStudio, Inc.	v2022.02.01
Harmony (R package)	(Korsunsky et al., 2019)	v1.0
DoubletFinder	(McGinnis et al., 2019)	https://github.com/chris-mcginnis-ucsf/DoubletFinder
SingleR	(Aran et al., 2019)	https://github.com/dviraran/SingleR
scRAD	(Li et al., 2011)	v0.99.0
scCODA	(Büttner et al., 2021)	v0.1.8
STAR: RNA-seq aligner	(Dobin et al., 2013)	v2.6.1b
Azimuth	(Hao et al., 2021)	v 0.4.5

3.3. Donors

3.3.1. Donor cohort for Seq-Well

Table 7: Demographic and clinical characteristics of Seq-Well donor cohort

Donor	Age	Gender	Condition	MMST	PBMC	CSF
AD001	51	Female	Control	29	Y	-
AD002	56	Male	AD	-	Y	-
AD003	60	Female	Control	30	Y	-
AD004	61	Male	AD	-	Y	-
AD006	68	Male	Control	30	Y	-
AD007	63	Female	AD	-	Y	-
AD008	77	Female	AD	-	Y	-
AD009	70	Female	Control	-	Y	-
AD010	79	Male	Control	-	Y	-
AD011	90	Male	Control	-	Y	-
AD012	81	Female	AD	-	Y	-
AD013	72	Male	Control	-	Y	-
AD014	57	Female	AD	-	Y	-
AD015	58	Male	Control	-	Y	-
AD016	58	Male	Control	-	Y	-
AD017	56	Female	AD	27	Y	-
AD018	71	Male	Control	-	Y	-
AD019	75	Female	Control	30	Y	-
AD020	-	Male	AD	28	Y	-

Table 8: Medications from donors of the Seq-Well cohort

Donor	NSAID	steroid	anti-hypertension	anti-coagulant	thyroid hormone	anti-diabetic	anti-depressant	antibiotics	proton pump inhibitor	Vitamin	anti-cholesterol	diuretics	Dementia medication		
													Donepezil	Rivastigmine	Memantine
AD001					+	+									
AD002															
AD003															
AD004															
AD006								+							
AD007													+		
AD008			+		+										
AD009			+							+					
AD010	+		+						+						
AD011				+											
AD012		+					+						+		
AD013			+									+			
AD014			+				+							+	
AD015					+					+					
AD016															
AD017														+	
AD018															
AD019			+							+					
AD020							+							+	

3.3.2. Donor cohort for BD Rhapsody

Table 9: Demographic and clinical characteristics of the Rhapsody donor cohort

Donor	Age	Gender	Condition	MMST	PBMC	CSF
AD005	76	Female	AD	-	Y	-
AD008	77	Female	AD	-	Y	-
AD009	70	Female	Non-Biomarker Control	-	Y	-
AD011	90	Male	Non-Biomarker Control	-	Y	-
AD012	81	Female	AD	-	Y	-
AD013	72	Male	Non-Biomarker Control	-	Y	-
AD014	57	Female	AD	-	Y	-
AD015	58	Male	Non-Biomarker Control	-	Y	-
AD016	58	Male	Non-Biomarker Control	-	Y	-
AD017	56	Female	AD	27	Y	-
AD018	71	Male	Non-Biomarker Control	-	Y	-
AD019	75	Female	Non-Biomarker Control	30	Y	-
AD020	-	Male	AD	28	Y	-
AD022	80	Female	Control	28	-	Y
AD023	66	Female	Non-Biomarker Control	30	Y	-
AD024	72	Female	Control	-	Y	Y
AD025	57	Male	Control	-	Y	Y
AD026	49	Female	Non-Biomarker Control	-	Y	-
AD027	58	Male	Non-Biomarker Control	-	Y	Y
AD028	87	Female	Non-Biomarker Control	-	-	Y
AD031	61	Male	Non-Biomarker Control	29	Y	-
AD033	68	Male	Non-Biomarker Control	30	Y	-
AD034	76	Male	Non-Biomarker Control	29	Y	-
AD036	62	Female	Non-Biomarker Control	30	Y	-
AD037	68	Female	Non-Biomarker Control	25	Y	-
AD038	76	Male	AD	27	Y	-
AD039	54	Female	Non-Biomarker Control	30	Y	-
AD041	71	Male	AD	27	Y	-
AD042	62	Female	Non-Biomarker Control	30	Y	-
AD043	64	Male	Non-Biomarker Control	30	Y	-
AD044	76	Female	Non-Biomarker Control	30	Y	-
AD045	-	Female	Control	25	Y	Y
AD046	-	Male	AD	25	-	Y
AD047	56	Female	AD	28	Y	Y
AD048	70	Female	Non-AD Pathological change	8	Y	Y
AD049	69	Male	Non-Biomarker Control	30	Y	-
AD050	76	Male	AD	26	Y	Y

AD051	71	Male	Control	20	Y	Y
AD052	77	Female	Non-Biomarker Control	28	Y	-
AD055	66	Male	Control	19	Y	Y
AD056	55	Male	Control	27	Y	Y
AD057	83	Female	AD Pathological change	25	Y	Y
AD060	57	Female	Non-Biomarker Control	-	Y	Y
AD061	55	Female	Control	29	Y	Y
AD062	73	Male	AD	24	Y	Y
AD063	69	Female	Control	26	Y	Y
AD064	69	Female	AD	29	Y	Y
AD065	78	Female	Non-Biomarker Control	30	Y	-
AD066	79	Male	Non-Biomarker Control	29	Y	-
AD067	45	Female	Non-AD Pathological change	18	Y	-
AD068	70	Male	AD Pathological change	24	Y	Y
AD069	62	Male	Control	30	Y	Y
AD070	69	Female	AD	27	Y	Y
AD071	71	Female	Non-AD Pathological change	-	-	Y
AD072	78	Female	AD	-	Y	Y
AD073	77	Male	Non-AD Pathological change	27	Y	Y

Table 10: Medications from donors of the Rhapsody donor cohort

Donor	NSAID	steroid	anti-hypertension	anti-coagulant	thyroid hormone	anti-diabetic	anti-depressant	antibiotics	proton pump inhibitor	Vitamin	anti-cholesterol	diuretics	Dementia medication		
													Donepezil	Rivastigmine	Memantine
AD005															
AD008			+		+										
AD009			+							+					
AD011				+											
AD012		+					+						+		
AD013			+									+			
AD014			+				+							+	
AD015					+					+					
AD016															
AD017														+	
AD018															
AD019			+							+					

AD020							+							+	
AD022			+									+			
AD023					+										
AD024															
AD025															
AD026															
AD027											+				
AD028			+		+				+			+			
AD031															
AD033					+										
AD034					+										
AD036															
AD037															
AD038					+										
AD039					+										
AD041	+		+												
AD042					+										
AD043															
AD044						+					+				
AD045			+		+		+				+	+			
AD046			+						+		+				
AD047															
AD048														+	
AD049			+												
AD050															
AD051											+				+
AD052		+	+												
AD055										+	+				
AD056															
AD057			+									+			
AD060			+		+						+	+			
AD061							+								
AD062			+		+						+				
AD063			+		+										
AD064															
AD065			+												
AD066			+								+	+			
AD067			+				+								
AD068	+		+												
AD069															
AD070															

4. Methods

4.1. Human specimens

Human samples were acquired via the DELCODE, DESCRIBE and DANCER studies at the DZNE. All studies have been approved by the ethics committee of the medical faculty of the Rheinische Friedrich-Wilhelms-Universität Bonn and are in line with national legal regulations and the ICH-GCP guidelines (local ethics vote 227/19). All patients provided written informed consent according to the Declaration of Helsinki before specimens were collected.

Clinicians completed exclusion criteria forms and provided CSF biomarker information wherever possible to allow us to classify patients into the AT(N) framework and place them in the correct condition cohort (Supplementary Figure 7). The exclusion criteria forms included information regarding comorbidities, medication and a list of pre-defined exclusionary criteria designed to prevent donors with known inflammatory or autoimmune comorbidities from being recruited (Tables 8 & 10). These exclusion criteria included individuals with a BMI>30, HIV, Diabetes Type I, recent infection, other autoimmune conditions, or currently receiving steroids, NSAIDs or chemotherapy.

PBMCs were obtained by the collection of 9 ml venipuncture blood into tubes containing EDTA (Ethylenediamine tetra-acetic acid). CSF samples were collected by lumbar puncture and transportation was handled via the clinical research biorepository team at the DZNE Bonn. Any CSF samples containing haemoglobin were discarded.

4.2. Isolation of PBMCs from whole blood

PBMC were isolated from anti-coagulated whole blood by density centrifugation (at 20°C and 800g for 20 min with centrifugation break off) over Pancoll (density: 1.077 g/ml; PAN-Biotech).

PBMC were extracted from the interphase and all further steps were conducted at 4°C. Subsequently, the PBMCs were prepared for scRNA-seq or cryopreserved and analyzed later. Cryopreserved samples were mixed with Resuspension Buffer (60% RPMI, 40% FBS) and 2X Freezing media (70% Resuspension Buffer, 30% DMSO) before transfer to cryotubes in a refrigerated cryostorage device and kept overnight at -80°C before liquid nitrogen tank storage.

4.3. Isolation of cells from cerebrospinal fluid

CSF cells were pelleted by centrifugation of CSF by the biorepository team and all but 1 ml supernatant was removed. On receipt of the samples, samples were centrifuged again (400g for 10 min) and directly prepared for scRNA-seq or cryopreservation.

4.4 Seq-Well

The Seq-Well method described by the Shalek lab (Gierahn et al., 2017) was used for the initial component of this work. Fresh PBMCs were collected from both patients and matching controls. Below we describe the specifics of array preparation and library generation for these 8 patients and eleven controls. The cohort was divided and sequenced in three independent sequencing runs: AD001-AD010 with sequencing data from donors 1 to 10, AD011-AD018 (donors 11 to 18) and AD019-AD020 (donors 19 and 20) (Table 7). The samples were fresh, however, stored frozen samples were also included for AD019-AD020. The datasets displayed a total of 24,963 genes across 60,027 cells before downstream analysis.

4.4.1. Preparation of Seq-Well arrays

The arrays used for Seq-Well were prepared following the published protocol (Gierahn et al., 2017). Base and crosslinker from the Sylgard kit were mixed (10:1), put under vacuum (15 minutes), poured into moulds and baked for 2 hours at 70^{o}C. After being removed and tidied up they were functionalized by adding and washing a sequence of chemicals designed to allow the sealing of a semi-permeable polycarbonate membrane and the interchange of lysis and RNA hybridization buffers. The complete process for this can be found in the published protocol (Gierahn et al., 2017).

4.4.2. Preparation of Seq-Well libraries and sequencing

The preparation and generation of Seq-Well libraries from isolated PBMCs were conducted as described by Gierahn *et al.* (Gierahn et al., 2017). Here we provide an overview of the process, for a more in-depth description refer to the original protocol (Seq-Well v1.7, (Gierahn et al., 2017)). Functionalized arrays were loaded with mRNA capture beads and 20,000 cells that had been sorted by flow cytometry with a DAPI stain to select for live cells. After loading, the process uses washing steps to remove any beads or cells that are not in microwells and then an incubation step in lysis buffer (5M guanidine thiocyanate, 1mM EDTA, 0.5% Sarkosyl and 1% β-mercaptoethanol in H_2O) is performed to lyse cells. Next, mRNA capture beads were collected from the arrays and reverse transcription was performed on the mRNA captured on the beads. After this, there were further washing steps and excess primers were digested in an exonuclease reaction. Then beads were resuspended and counted before being pooled (5,000 beads/pool) for PCR (95°C for 3 min, 4 cycles of 98°C for 20 s, 65°C for 45 s, 72°C for 3 min, 12 cycles of 98°C for 20 s, 67°C for 20 s, 72°C for 3 min and final extension of 72°C for 5 min). After PCR, 16,000-20,000 beads were combined and PCR products cleaned up with AMPure XP beads before cDNA was measured using a High Sensitivity D5000 assay for the Tapestation 4200 (Agilent). After tagmentation, these cDNA libraries went through a further PCR for barcoding with index primers and cleaned up again

with AMPure XP beads. After a final High Sensitivity DNA5000 assay on a Tapestation 4200 (Agilent), and quantification with the Qubit high-sensitivity dsDNA assay, the libraries were equimolarly pooled and prepared for sequencing in paired-end mode (2*75 cycles) with the NextSeq 500 System.

4.4.3. Processing of scRNA-seq raw data

For pre-processing, the fastq files generated from Seq-Well libraries were loaded into a data pre-processing pipeline based on the Drop-seq tools package developed by the McCarroll lab (Macosko et al., 2015). The human GENCODE reference genome and transcriptome hg38 release 27 (Harrow et al., 2012) were used for STAR alignment and produced datasets were imported into the R package ‘Seurat’ (v. 2.3.4) for downstream analyses.

4.4.4. Quality control and normalisation

Quality control was performed according to the Seurat Guided Clustering Tutorial from the Satija lab (Stuart et al., 2019). This includes filtering low-quality background cells. Cells with a gene count of <50 genes per cell and genes that were expressed in <3 cells were excluded from further analysis. We also set a threshold which excludes cells with more than 5% mitochondrial genes from analysis as high mitochondrial gene presence is indicative of stressed and apoptotic cells. Micro-clustering problems in the analysis caused us to later adjust the quality threshold to a gene count of more than 150 genes per cell.

The data was log-normalized with a scale factor of 10,000 and the 2,000 most variable features were calculated via the “vst” method included in Seurat.

4.4.5. Dimensionality reduction and clustering

The Seurat default clustering algorithm based on shared nearest neighbour (SNN)-graphs were used to cluster the data (Stuart et al., 2019). This considered 20 principal components (PCs) and a resolution of 0.5 respectively. The dimensionality of the data was then reduced with the Uniform Manifold Approximation and Projection algorithm (UMAP) (McInnes, Healy, Saul, et al., 2018) which provides two-dimensional data representation based on the 20 calculated PCs.

4.4.6. Integration

Individual datasets were separately log-normalized (default settings) and for each, the top 2,000 most variable genes were selected by the implemented Seurat function based on the “vst” method. These top 2,000 features were then used to integrate the data by the Seurat Integration Algorithm based on the intersection of all genes across the data as well as 30 PCs (Stuart et al., 2019). After scaling, the data dimensionality was reduced to 20 PCs, clustered with a resolution of 0.5 and represented via UMAP, taking the top 20 calculated PCs into account.

4.4.7. Cell Type Annotation based on transcriptomic marker genes

Expression profiles of cell types and prior knowledge of canonical markers (Table 11) were used for annotation. Correct annotations were verified by SingleR using the built-in references “MonacoImmuneData” and “BlueprintEncode” (Aran et al., 2019).

Table 11: Marker genes used for PBMC cell type annotation.

Cell type	Gene	Cell type	Gene
Naive CD4⁺ T	*IL7R, CCR7*	**NK**	*GNLY, NKG7*
Memory CD4⁺ T	*IL7R, S100A4*	**DC**	*FCER1A, CST3*
CD14⁺ Monocyte	*CD14, LYZ*	**Platelet**	*PPBP*
B	*MS4A1*	**pDCs**	*JCHAIN*
CD8⁺ T	*CD8A*	**Granulocytes**	*HBA, HBB*
CD16⁺ Monocyte	*FCGR3A, MS4A7*	**preDCs**	*AXL, CD123, IRF7*

4.4.8. Exclusion of AD008-AD010 and AD019-AD020

Data from four samples (AD008-AD010 and AD019-AD020) were excluded from the final analysis. While most of the samples were sequenced using the protocol Seq-Well v1.7, AD008-AD010 used an adapted experimental protocol (Seq-Well v3) which resulted in poor quality of data due to low gene counts and low unique molecular identifier (UMI) counts.

Samples AD019-AD020 used the protocol Seq-Well v1.7 but were excluded due to data quality issues. While the manual cell type annotation (Table 11) was sufficient for discriminating between all major PBMC types in the data, one cluster did not display any known cell type markers and originated solely from the AD019-AD020 dataset. We analysed the dataset AD019-AD020 independently from all the others and found that, unlike the other two Seq-Well datasets which included sequencing data for only fresh PBMCs, AD019-AD020 also included data from frozen PBMCs. The cluster was present in all pools but for donor AD020 depletion of monocytes was detected upon freezing.

As the anomalies outlined above may have been caused by problems in the alignment pipeline, we analysed the quality of intergenic and intronic bases for all datasets to rule out possible technical anomalies. Percentages of both intronic and intergenic bases per cell were higher in pools corresponding to AD019-AD020 compared to all the other samples. Consequently, we excluded AD019-AD020 from the further analysis.

After these exclusions were made, AD001-AD007 and AD011-AD018 were quality controlled and integrated using the same parameters described above. After scaling, the dimensionality of the data was reduced to 25 PCs and clustered with a resolution of 0.4. Based on the top 25 calculated PCs, UMAP was used for visualization purposes. Cell types were annotated as described above and the final dataset included 18,345 genes across 10,871 cells.

4.4.9. Differential Expression Analysis

Differentially expressed genes (DE genes) were globally calculated between AD and control samples based on the RNA assay and a Wilcoxon Rank Sum test implemented in Seurat (default settings are a logarithmic fold-change (log-FC) of 0.25, a minimum fraction of 0.1 cells in either of the two groups and a minimum difference (min.diff.pct) of –Inf). This is in line with the Seurat Guided Clustering Tutorial from the Satija lab (Stuart et al., 2019).

4.4.10. scRAD package

The heterogeneous expression differences between patients in the dataset were assessed by implementing the Single-Cell Reproducibility Across Donors package in R (scRAD) (Li et al., 2011). This aims to control the influence of individual patients on the DE analysis. One of the analyses scRAD provides is an irreproducible discovery rate (IDR) analysis, which evaluates “reproducible” differential expressions across donors and correlates their significance accordingly. First, we downsampled the data to have identical numbers of cells in the patient and control groups (4956 cells per group). We identified marker genes between every patient and every control individually by a Wilcoxon Rank Sum test in Seurat. We set the log-FC threshold for marker genes >0.01 and min.pct cells as 0.01, returning both positive and negative marker genes from the input RNA assay. Secondly, the list of significant scores

(p-values) for individual patient-control combinations was negative logarithmic transformed, which is a prerequisite for the IDR analysis. Besides, all NAs were excluded from the analysis. Thirdly, the IDR was estimated using a multivariate Gaussian copula mixture model, implemented in the “est.IDRm” function of scRAD (Li et al., 2011), and the following parameters: *mu* = 2, *sigma* = 2, *rho* = 0.5 and *p* = 0.01. The model assumes that each component follows a Gaussian copula, a multivariate cumulative distribution function, which describes the dependency between random variables. It is provided with a correlation matrix of each random variable, thereby taking each random component into account for the dependencies (Li et al., 2011; Marbac et al., 2017).

Finally, the results were filtered for an IDR threshold higher than 0.01 and a median log-FC across all patient-control combinations of higher than 0.2 and lower than -0.2 respectively. The filtered genes were visualized in a Heatmap. Moreover, genes with a high IDR value were visualized before log-FC filtering, signifying genes which might be reproducible across donors.

4.5 BD Rhapsody

The BD Rhapsody Single-Cell Analysis System (BD Biosciences) is a commercial platform that consists of a BD Rhapsody express instrument and a scanner for assessing cell and bead loading at several stages of the protocol. PBMCs and CSF immune cells were isolated from both patients and matching controls as described in sections 4.2 and 4.3. Below the specifics of sample preparation and library generation for the PBMCs and CSF immune cells collected are described. The datasets displayed a combined total of 46,174 genes across 115,000 cells before downstream analysis.

4.5.1. Preparation of cells for BD Rhapsody

PBMCs and CSF immune cells prepared as detailed above were processed with the BD Rhapsody Single-Cell Analysis System (BD Biosciences). The protocol followed for this was the *BD Rhapsody Single-Cell Analysis System Instrument User Guide* (Doc ID: 214062 Rev. 3.023-21336-01). Here, I give an overview of the process and refer to the manufacturer's protocol for further details. After isolation, cells were labelled with sample tags (BD Human Single-Cell Multiplexing Kit), washed and resuspended in BD Sample Buffer before counting using a Countess Cell Counter. Cells were then stained for viability (2 mM Calcein AM and DRAQ7) and the BD Rhapsody Single-Cell Analysis System scanner calculated pooling concentration for loading onto the cartridge. For every run, a cartridge was loaded with approximately 40,000 cells with an average of 10,000 cells for each sample. From here single cells were lysed, barcoded, washed, retrieved and underwent an exo-nuclease reaction according to the manufacturer's recommendations (BD Biosciences).

4.5.2. Preparation of Rhapsody WTA libraries and sequencing

cDNA libraries were prepared by following the *BD Rhapsody mRNA Whole Transcriptome Analysis (WTA) and Sample Tag Library Preparation Protocol* (Doc ID: 23-21712-00). Sample tag and cDNA libraries were prepared in parallel. Sample tags were denatured from the BD Rhapsody Cell Capture Beads and amplified through a series of PCR steps. The cDNA libraries were generated directly from the beads using a random priming approach and index PCR. Quantification of final libraries was done with the Qubit Fluorometer and Qubit dsDNA HS kit The Agilent high sensitivity D5000 assay on a TapeStation 4200 system was used to measure fragment size distribution. Libraries were equimolarly pooled and prepared for sequencing in paired-end mode (2*75 cycles) with the NovaSeq 6000 or NextSeq 500 System.

4.5.3. Processing of scRNA-seq raw data

After demultiplexing and quality control, paired-end scRNA-seq reads generated on the Rhapsody platform were filtered for valid cell barcodes using the barcode whitelist provided by BD. The Gencode v27 reference genome (Dobin et al., 2013) was used for STAR 2.6.1b alignment. The Drop-seq tools package developed by the McCarroll lab (Macosko et al., 2015) was used to quantify gene expression and hashtag-oligo based demultiplexing of single-cell transcriptomes and subsequent assignment of cell barcodes to their sample of origin based on the respective multiplexing tag sequences were added to the reference genome and quantified for downstream analyses in R package 'Seurat' (v. 2.3.4).

4.5.4. Quality control of scRNA-seq data

Quality control was performed according to the Seurat Guided Clustering Tutorial from the Satija lab (Stuart et al., 2019). This includes filtering low-quality background cells. The Rhapsody dataset used the same cut-offs that were used for the Seq-Well dataset, excluding cells with a gene count of <50 genes per cell and genes that were expressed in <3 cells from further analysis. We also set a threshold which excluded cells with more than 5% mitochondrial genes from the analysis.

4.5.5. Dataset integration and dimensionality reduction of scRNA-seq data

After demultiplexing following the *Demultiplexing with hashtag oligos (HTOs)* protocol from the Satija lab (Stoeckius et al., 2018), data from individual Rhapsody cartridges were merged into one collective Rhapsody dataset. The collective Rhapsody dataset then underwent QC as described above and doublet removal using the 'DoubletFinder' package (version 2.0.2, McGinnis et al., 2019). The data was log-normalized with a scale factor of 10,000 and the 2,000 most variable features were calculated via the 'vst' method from the

'FindVariableFeatures' function included in Seurat. Integration was completed using the 'Harmony' package in Seurat which integrates data based on 'anchors' across batches (Korsunsky et al., 2019; Stuart et al., 2019). This reduces the influence of batch effects which could be introduced at several stages of the sample pipeline. Next, we reduced the dimensionality of the dataset and visualised the data through UMAP representation. The parameters for this were different for the different Rhapsody datasets (Whole/PBMC/CSF) and individual values and settings are reported in the results section. More generally, Seurat and the ggplot2 package (version 3.3.6, (Wickham, 2016)) were used for data visualisation.

4.5.6. Cell-type annotation based on reference transcriptome datasets

Initially, we annotated the data through SingleR using the built-in references "Monaco Immune Data" (Monaco et al., 2019), "Blueprint Encode" (Aran et al., 2019), and "Human Primary Cell Atlas Data" (Mabbott et al., 2013) which provided a basic classification of cell types. Later we supplemented this using Azimuth annotation (Hao et al., 2021). It was then necessary to use prior knowledge of canonical markers from the literature to further annotate the datasets. This was especially true for CSF-specific cell types as the built-in references used are focused on peripheral immune cells and might not truthfully reflect the heterogeneity of CSF immune cells.

4.5.7. Marker gene identification of scRNA-seq data

Identification of DE genes between AD and control samples was done using a Wilcoxon rank sum test for differential gene expression implemented in Seurat. A significance threshold was set to an adjusted p-value < 0.001 and a logarithmic fold change cutoff of at least 0.25. Visualisation of DE genes was mainly achieved using Seurat functions, such as dot plot representation of cell types-/cluster-specific marker gene expression or heat map representation of marker genes across single cells. We also used the R package 'pheatmap' in which the genes were clustered according to the 'ward.D' agglomeration method.

4.5.8. scCODA statistical analysis

Statistical evaluation was carried out using the single-cell compositional data analysis (scCODA) package (Büttner et al., 2021). This detects statistically relevant changes in cell type composition and calculates the model inclusion probability for each covariate. The package was designed specifically to be used with scRNA-seq data and can cope with the low number of sample replications that are common with this data type, which made it a good choice for our dataset. It is also able to account for the proportional nature of cell type counts and the bias that can be introduced in a cell population when one type is depleted or inflated.

5. Results

5.1. Analysis of PBMC of AD donors using the Seq-Well approach revealed transcriptional changes but no inflammatory signature

As previously detailed, the Seq-Well data gathered in this project is a combination of PBMCs from a total of eight patients and eleven matching controls, which yielded three datasets. After analysis of the ten donors for the preliminary dataset (AD001-AD010), I integrated all datasets and jointly analysed them to compare the transcriptome across donors.

5.1.1. Analysis of the preliminary Seq-Well dataset (AD001-AD010) resulted in an adapted analysis approach for all subsequent data

To explore cellular differences between the first ten donors of the preliminary data set (AD001-AD010), I analysed this data set independently from the other data. Therefore, the data dimensionality was reduced by the Seurat UMAP algorithm (McInnes, Healy, Saul, et al., 2018) revealing a complex topology of approximately 10 main clusters and over 25 micro-clusters (Figure 7A). These micro-clusters were not specific for any cell type, diagnosis, donor, pool, age, or gender (Figure S1A-E) and contained substantially lower numbers of reads compared to the main clusters. Furthermore, cellular marker genes were detectable in both the main and several sub-clusters with a similar expression level (Figure 7B). As the number of reads for duplicated barcodes indicated an adequate sequencing depth, we can rule out insufficient sequencing depth as cause for the unexpected distribution of marker genes over the dataset. Thus, there was no inherent reason to re-sequence these pools to increase data quality.

The pools associated with AD008-AD010 displayed a very low unique molecular identifier (UMI) count as well as a low feature count. These pools were sequenced according to the protocol Seq-Well v.3, while all the others were sequenced according to Seq-Well v.1.7. As a

consequence, we excluded AD008-AD010 from further analyses. However, the micro-clusters were still present and were only removable by increasing the cut-off for cells to be further included in the analysis to 150 expressed genes per cell (Supplementary Figure 1F).

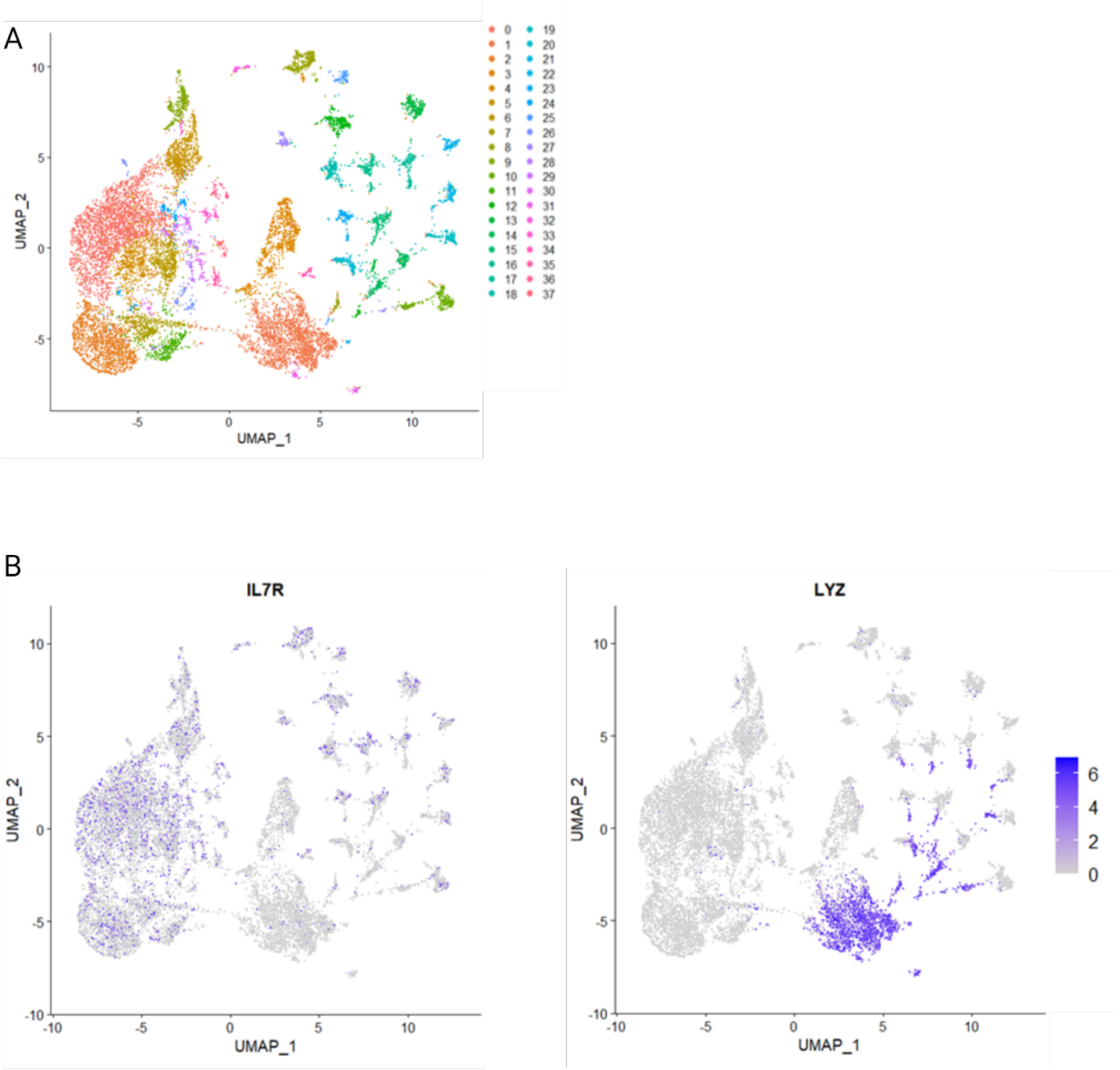

Figure 7. Characterisation of the dataset from donors AD001-AD010. (A) Uniform Manifold Approximation and Projection (UMAP) representation of cells in the dataset AD001-AD010, displaying micro-clustering. (B) UMAP representation of IL7R and LYZ expression, marker genes for T cells and monocytes respectively. The gene expression in the micro-clusters is mirrored in the main clusters.

5.1.2. Integration of additional samples allowed to establish QC criteria to exclude AD019-AD020 from the further analysis

Afterwards, we integrated AD001-AD007 and the remaining datasets AD011-AD018 and AD019-AD020 into a joint dataset, before visualising and evaluating the data. While manual cell type annotation allowed to discriminate between all major PBMC types in the data (Figure 8A), cluster 7 did not display any known cell type markers (Figure S2A) and originated solely from the AD019-AD020 dataset (Figure 8B).

To further investigate the nature of cluster 7, we analysed the dataset AD019-AD020 independently from all the others using the same Seurat pipeline we already implemented for the analysis of AD001-AD007. In contrast to the other two datasets which included sequencing data for only fresh PBMCs, AD019-AD020 also included sequencing data from frozen PBMCs. The cluster in question was present in all pools (Figure 8C, purple) and depletion of monocytes was observed upon freezing (Figure 8C, * frozen, Figure S2B), especially for donor AD020. Note that AD020 accounted for 4410 cells in total, while AD019 included 614 cells.

Since the anomalies outlined above might arise from problems with the alignment pipeline, we analysed the quality of intergenic and intronic bases for all datasets. As depicted in Figure 8D, the percentage of both intronic and intergenic bases per cell was much higher in pools corresponding to samples AD019-AD020 compared to all the others (Figure 8D, red boxes). Consequently, we excluded samples AD019-AD020 from further analysis and re-aligned the data for subsequent downstream processing and analysis.

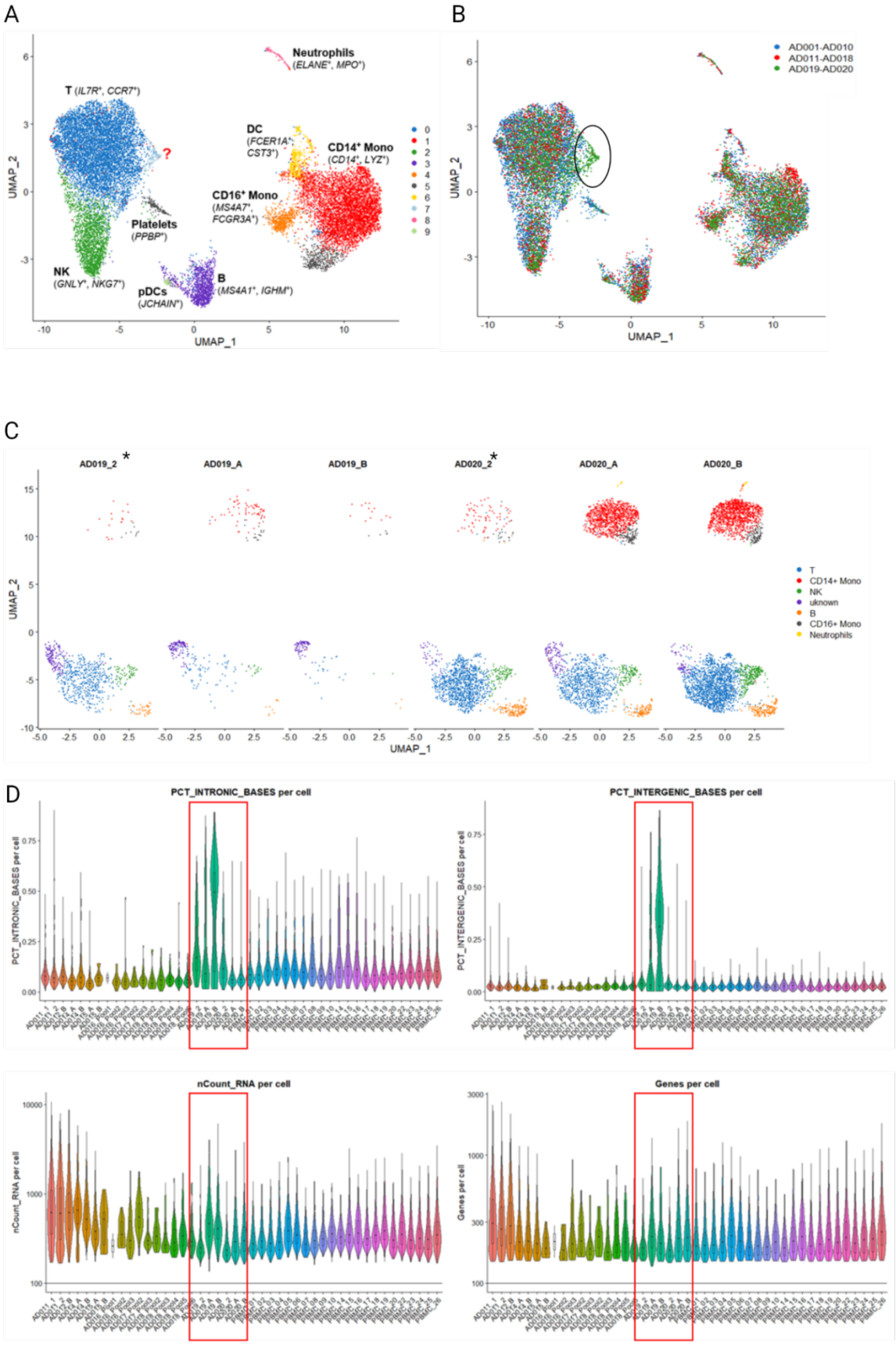
A
Neutrophils
(ELANE+, MPO+)
T (IL7R+, CCR7+)
DC
(FCER1A+,
CST3+)
CD14+ Mono
(CD14+, LYZ+)
CD16+ Mono
(MS4A7+,
FCGR3A+)
Platelets
(PPBP+)
NK
(GNLY+, NKG7+)
pDCs
(JCHAIN+)
B
(MS4A1+, IGHM+)
UMAP_1
UMAP_2
B
AD001-AD010
AD011-AD018
AD019-AD020
C
AD019_2
AD019_A
AD019_B
AD020_2
AD020_A
AD020_B
T
CD14+ Mono
NK
uknown
B
CD16+ Mono
Neutrophils
D
PCT_INTRONIC_BASES per cell
PCT_INTERGENIC_BASES per cell
nCount_RNA per cell
Genes per cell

Figure 8. Visualisation of AD001-AD020 integration and AD019-AD020 separately. (A) UMAP representations of cell types in the integrated dataset AD001-AD020. The red question mark highlights the cluster in question (cluster 7), which does not display known cell type markers (Figure S2A) (marker genes given in brackets). (B) UMAP representation of (A), grouped by the input dataset. Circle highlights cluster 7, originating solely from dataset AD019-AD020. (C) UMAPs for dataset AD019-AD020, visualising each sequencing pool separately. Fresh samples, an asterisk indicates frozen samples. (D) Violin plots of each sequencing pool for AD001-AD020 showing percentages of intronic bases and intergenic bases per cell or number of UMIs and genes per cell, respectively. Red box highlighting the sequencing pools for AD019-AD020.

5.1.3. Analysis of the final dataset demonstrated minor transcriptional differences in AD

The final dataset for Seq-Well included AD001-AD007 as well as AD011-AD018, containing 18,345 expressed genes across 10,871 cells. Figure 9A displays the UMAP visualisation of the clustered final dataset, identifying all major PBMC cell types. Besides, it exhibits distinct clusters for erythrocytes and proliferating cells that were not present before. The frequency of AD and control donors was balanced across all clusters except for cluster 6, which comprises a second CD14+ monocyte cluster. Here, cells from control donors were more frequent than cells from AD patients; however two single control donors contributed largely to this fraction (Figure 9B). These observations were confirmed by splitting the UMAP visualisation between AD and control (Figure 9C). Although the total number of cells varied largely across individual donors (Figure 9D), cell types were similarly distributed amongst donors with low and high cell numbers (Figure S3A). The frequency of T cell and monocyte subsets varied slightly between AD and control but displayed a large variability between donors (Supplementary Figure 3B).

Therefore, we evaluated transcriptional differences between control and AD patients first globally, instead of analyzing several cellular subsets individually. Visualisation of the global DE genes we identified over the complete dataset, indicated only very slight differences

between the two groups, representing very few significant genes and no group-specific clustering (Figure 10A). To control for inter-donor heterogeneity, we implemented the irreproducible discovery rate (IDR) analysis from the scRAD package (Li et al., 2011). Upon calculating marker genes for every control across every patient, we determined IDR values for every significant score and filtered them accordingly. Unfortunately, the visualization of reproducible gene expression differences across multiple donors did not improve compared to the standard Seurat pipeline, displaying no defined clusters and only slight gene expression changes between patients and controls (Figure 10B).

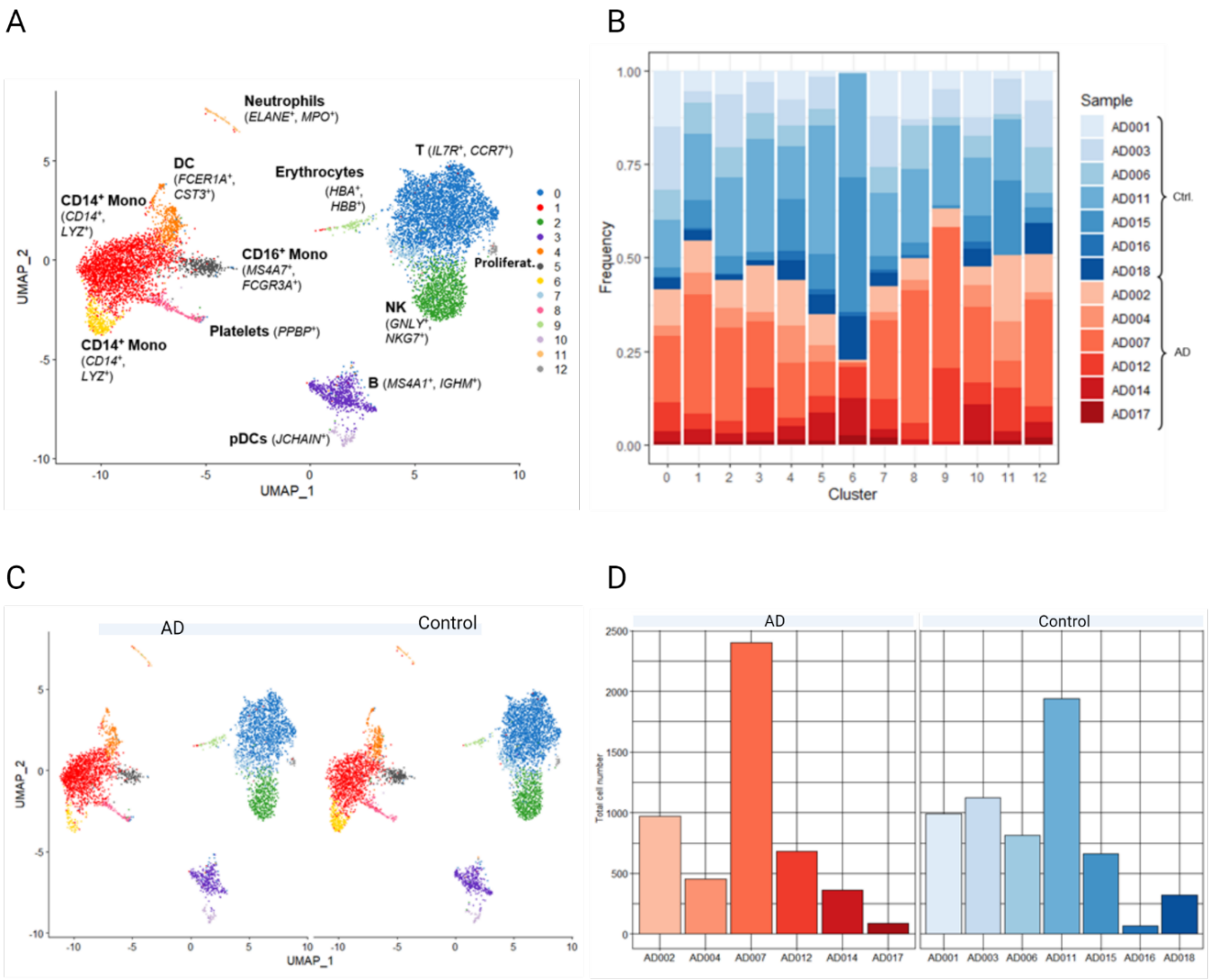

Figure 9. Characterisation of integrated final Seq-Well dataset . (A) UMAP representation of the integrated datasets AD001-AD008 and AD011-AD018, including 18,345 genes across 10,871 cells (marker genes given in brackets). (B) Stacked bar plot visualizing the frequency of donors and AD vs. control across all clusters in (A). (C) UMAP representation of (A), divided into AD vs. control. (D) Bar plot highlighting the total number of cells for each donor, grouped by AD and control respectively.

By filtering identified DE genes for top IDR outliers, we were able to detect genes which were consistently up or downregulated across donors (Figure 10C). Among these genes, we found *LYZ*, *MALAT1,* and *HLA-DRA*, while *FTH1* and *SNHG5* were downregulated in AD patients (Figure 10C). Except for *SNHG5*, all of these genes are known to be associated with AD, contributing directly or indirectly to AD risk (Dunne et al., 2020; J. L. Liu et al., 2018; Ma et al., 2019; Mansouri et al., 2015; Sandin et al., 2016; Steele et al., 2017; P. Wang & Wang, 2017; J. Xu et al., 2020). Moreover, *SNHG5* represents a snoRNA host gene, and an aberrant expression of snoRNAs has been associated with disease development for a range of diseases (Steinbusch et al., 2017; Stepanov et al., 2015).

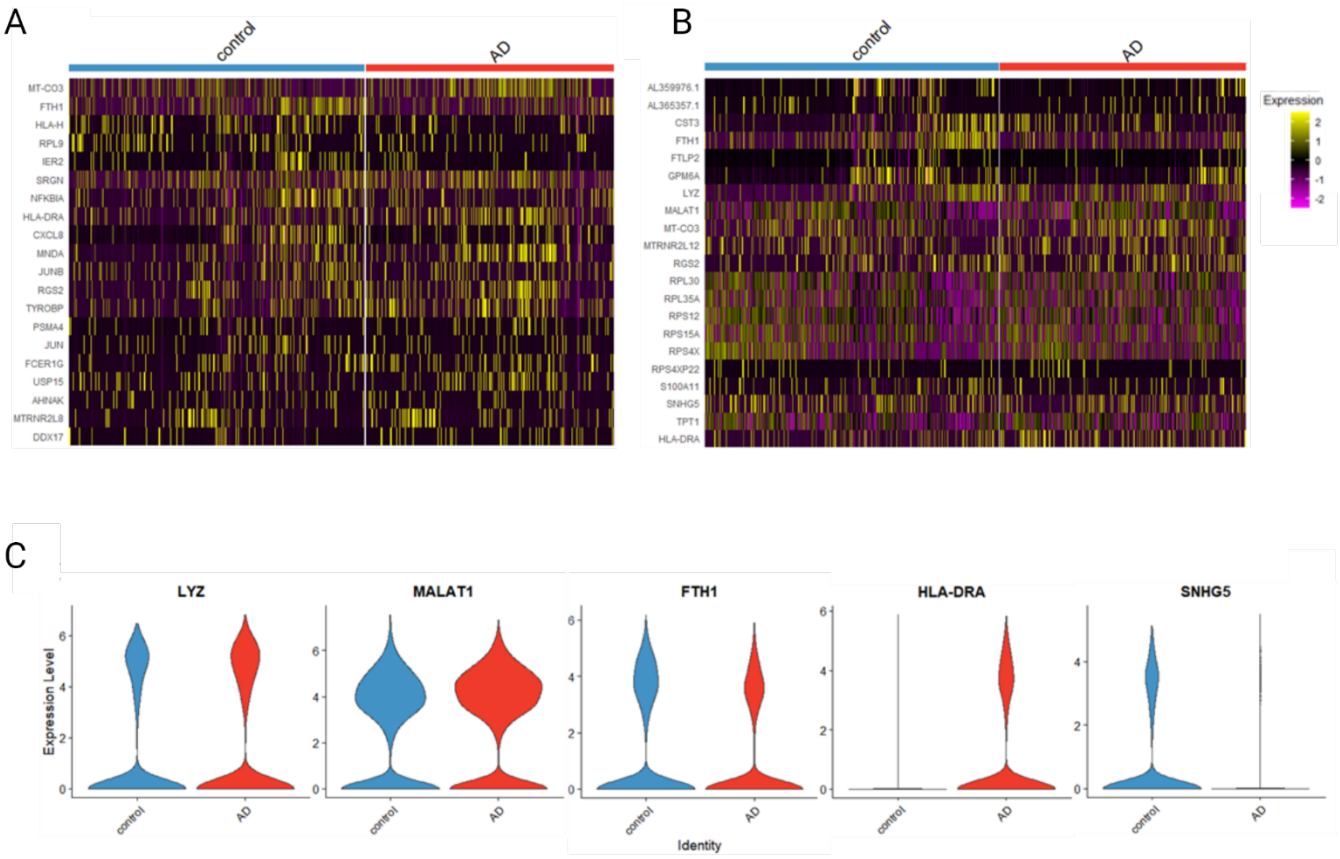

Figure 10. Differentially expressed genes in final Seq-Well dataset. (A) Heat map of marker genes differing between control and AD, using Seurat (source). The marker gene expression is represented by a z-transformed value. (B) Heat map of marker genes differing between control and AD using the irreproducible rate (IDR) analysis by scRAD (source). IDR values are calculated based on marker gene significant scores, comparing every patient against every control separately. Genes are filtered for IDR values > 0.01 and logarithmic fold-changes (logFC) > 0.2 and < -0.2 respectively. Finally, they are displayed in the heat map by a z-transformed value. (C) Violin plots of gene expression levels between AD and control, displaying genes with high consistency across donors as determined by IDR analysis.

In summary, data sparsity and heterogeneity across donors negatively impacted the data analysis leading to the discovery of only minute transcriptional changes. However, the genes that passed rigorous filtering criteria raise interesting links with immune dysfunction on the

basis of which we postulated the hypothesis that an elevated inflammatory signature might be present in the blood of AD patients.

5.2. A holistic analysis of CSF and PBMC in AD donors using the BD Rhapsody approach revealed cell population changes in the former

Because of these short-comings of the SeqWell technology we switched to a newly developed commercial platform for the generation and assessment of single-cell transcriptomes. The Rhapsody system employs a very similar approach as the SeqWell technology as both rely on cell capture in microwells, however side-by-side comparisons revealed significantly improved gene coverage and cell recovery for the Rhapsody system. Therefore, the dataset generated using the Rhapsody platform is the more extensive dataset collected in this study and combines CSF and PBMC samples across five conditions: AD, AD Pathological Change, Non-AD Pathological Change, Control, and Non-Biomarker Controls (Figure 11). These five conditions were defined using clinical protein biomarkers to classify donors according to the AT(N) framework. The Non-Biomarker Control group contains donors for which no biomarker information was available. We kept this group in the analysis in a limited capacity to support the biomarker-validated Control group. The complete Rhapsody dataset comprises 46,174 genes across 115,000 cells.

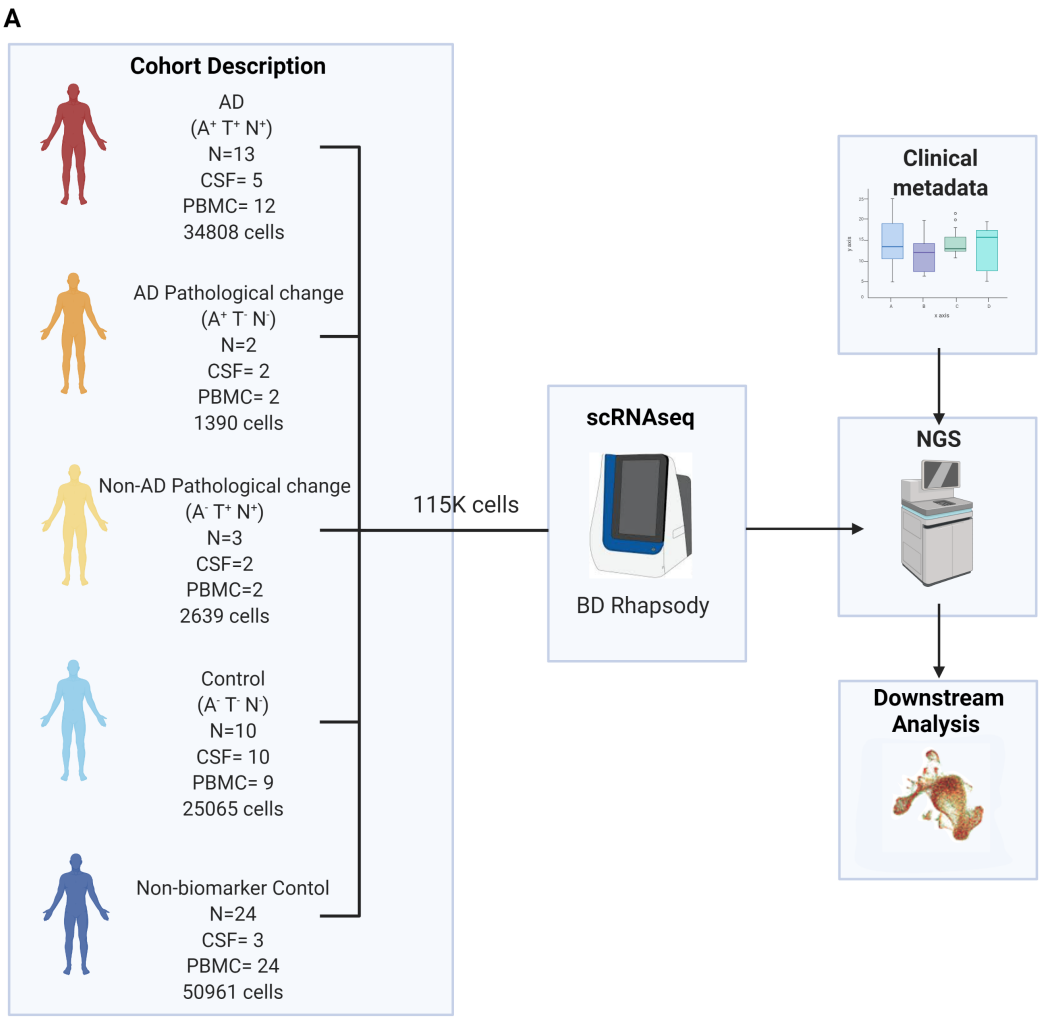
A
Cohort Description
AD
(A+ T+ N+)
N=13
CSF= 5
PBMC= 12
34808 cells
AD Pathological change
(A+ T- N-)
N=2
CSF= 2
PBMC= 2
1390 cells
Non-AD Pathological change
(A- T+ N+)
N=3
CSF=2
PBMC=2
2639 cells
Control
(A- T- N-)
N=10
CSF= 10
PBMC= 9
25065 cells
Non-biomarker Contol
N=24
CSF= 3
PBMC= 24
50961 cells
115K cells
scRNAseq
BD Rhapsody
Clinical metadata
NGS
Downstream Analysis

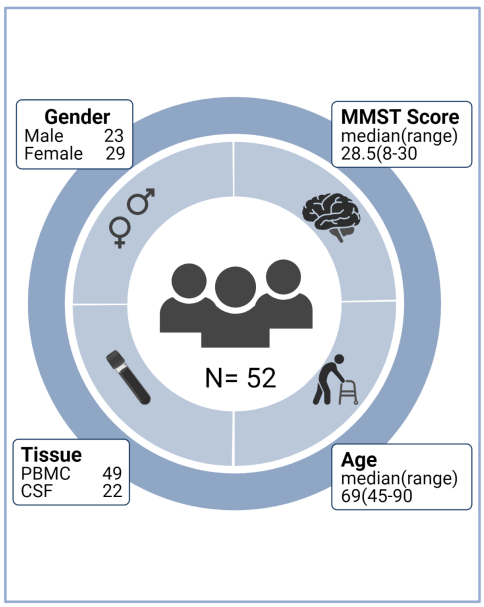
B
Gender
Male 23
Female 29
MMST Score
median(range)
28.5(8-30
N= 52
Tissue
PBMC 49
CSF 22
Age
median(range)
69(45-90

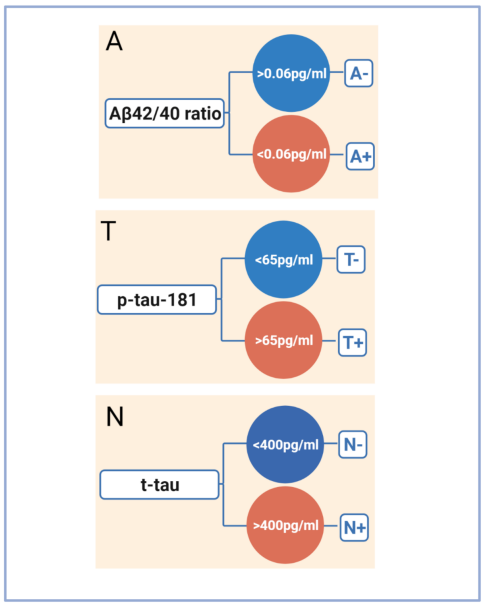
C
A
Aβ42/40 ratio
>0.06pg/ml
A-
<0.06pg/ml
A+
T
p-tau-181
<65pg/ml
T-
>65pg/ml
T+
N
t-tau
<400pg/ml
N-
>400pg/ml
N+

Figure 11 Overview of the Rhapsody cohort (A) Study workflow including cohorts for CSF and PBMC donors. (B) Characteristics of the study cohort. (C) AT(N) cut-offs used for cohort classification.

5.2.1. An overview of the combined PBMC and CSF dataset

After sequencing, alignment and demultiplexing, data from individual Rhapsody cartridges were merged into one collective Rhapsody dataset combining cells from peripheral blood and CSF. Quality control checks were used to remove low-quality background cells and doublets (McGinnis et al., 2019) prior to integration (Korsunsky et al., 2019; Stuart et al., 2019) to create an object that would allow an overview of all donors and tissue types (Figure 12).

At a clustering resolution of 0.9. the whole dataset forms 18 clusters (Figure 12A). Next, we performed cell type annotation and identified cell types across these clusters (Figure 12B) and assessed donor heterogeneity across clusters, revealing that donors are well distributed with no cluster dominated by a single donor (Figure 12C). This further supports that a successful integration of the data across donors was feasible. Distribution of the different disease conditions was evaluated, which also revealed a sufficient distribution of the individuals, independent of disease over the different cell clusters (Figure 12D). Following this, we assessed how the different tissue types were distributed and found a large amount of overlap, with many clusters in common (Figure 12E). Only clusters 11 and 15 are unique to the CSF, and cluster 12 is more highly represented in the CSF though it still contains some PBMC samples. While the distribution of conditions across the clusters is generally heterogeneous as described above, the CSF-specific clusters 11 and 15 mainly present in CSF are visibly dominated by the AD cohort. Finally, we determined the top 5 characteristic marker genes for each cell type, which allowed us to manually validate the computer-based annotations and identify subtypes (Figure 12F).

Taken together, these data demonstrate that over a series of samples from 52 individuals collected over a 2.5 year period, the Rhapsody technology was able to generate scRNA-seq data that could be successfully integrated and yielded sufficient data depth to allow for further analysis. Based on the identification of CSF-specific subpopulations of cells, we decided at

this point that a joint analysis of both types of biomaterial could potentially obscure more subtle findings and therefore analysed both sources of biomaterial separately.

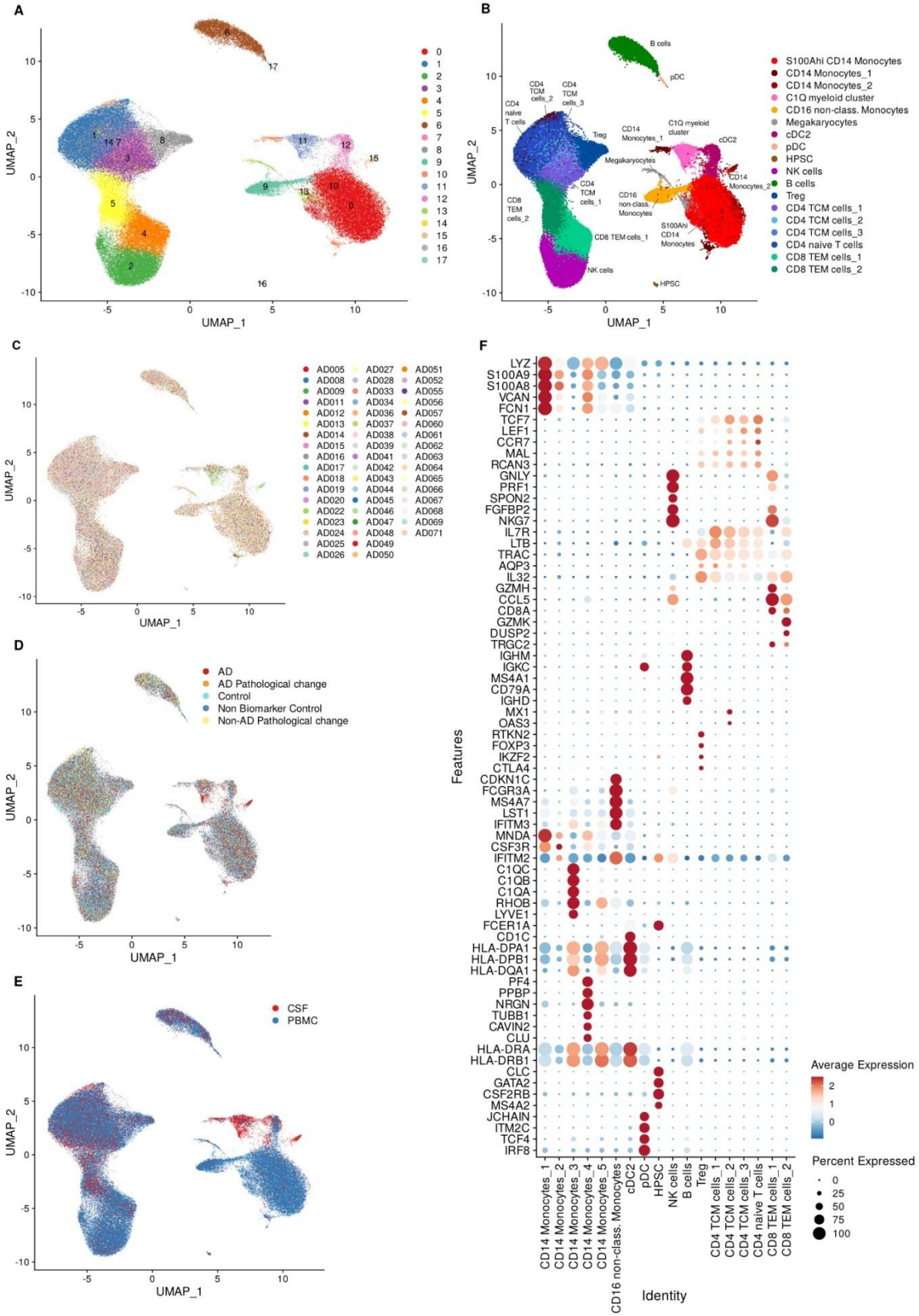
A
B
C
D
E
F
UMAP_1
UMAP_2
S100Ahi CD14 Monocytes
CD14 Monocytes_1
CD14 Monocytes_2
C1Q myeloid cluster
CD16 non-class. Monocytes
Megakaryocytes
cDC2
pDC
HPSC
NK cells
B cells
Treg
CD4 TCM cells_1
CD4 TCM cells_2
CD4 TCM cells_3
CD4 naive T cells
CD8 TEM cells_1
CD8 TEM cells_2
AD
AD Pathological change
Control
Non Biomarker Control
Non-AD Pathological change
CSF
PBMC
Features
Identity
Average Expression
Percent Expressed

Figure 12 Summary of the combined PBMC and CSF dataset (A) UMAP representation and clustering of cells contained in main clusters 0-17. (B) UMAP showing cell types in the whole dataset. (C) UMAP showing donors in the whole dataset. (D) UMAP showing conditions in the whole dataset. (E) UMAP showing tissue types in the whole dataset. (F) Dotplot of characteristic marker expression of the top 5 genes sorted by average log fold change assigned to each cell type.

5.2.2. Analysis of CSF in AD donors using the Rhapsody approach revealed an expanded myeloid cell compartment and reduced lymphocyte compartment in AD

Prior to recent improvements in NGS and the popularisation of single-cell RNA-seq, the characterisation of cell types in the CSF has been modest relative to sample types such as PBMCs or brain tissues. Factors such as accessibility and sparsity of cells in CSF samples (1-5 cells/µL) mean that they require robust technology with high sensitivity to yield reliable data (Esaulova et al., 2020).

To investigate our Rhapsody CSF dataset we took the data object produced during the processing and analysis of the Rhapsody whole dataset and subsetted this by tissue type to produce separate data objects for the CSF and PBMC samples. The CSF dataset reported here is made up of 14,046 cells from 20 donors. The mean number of cells contributed per donor was 702.3 and samples contributing <50 cells were excluded from the analysis. These numbers are in line with published CSF single-cell RNA-seq datasets which often contain only a few donors and similar cell numbers (Esaulova et al., 2020; Gate et al., 2020; Schafflick et al., 2020), with the exception of a recent study which sampled a much larger cohort of 57 individuals (Roostaei et al., 2021).

For demonstration purposes, the analysis of the CSF dataset has been split into two parts: firstly we analysed the data across all conditions to provide an overview of the different groups. Secondly, we analysed only the AD and Control groups, as the other groups contained low sample numbers (two donors for AD Pathological Change, one for Non-AD Pathological Change, and three donors for the Non-Biomarker Control group, respectively) which would not withstand robust statistical testing.

5.2.2.1. Defining a ground truth about the distribution of cell types in healthy CSF

As discussed in the introduction, the ChP not only produces CSF but also acts as a blood-CSF-barrier which can also be an entry point for immune cells into the CSF (Lun et al., 2015). Despite traditionally being thought of as an immune-privileged site, there are an increasing number of studies that detail the trafficking and entry of peripheral immune cells into the CSF. Infiltrating immune cells migrating from the blood via the ChP must cross the fenestrated outer endothelial layer into the stromal space before crossing the basolateral epithelium into the ventricles of the brain (Ransohoff & Engelhardt, 2012). For lymphocytes, the ChP facilitates a route into the CSF through the expression of adhesion molecules and chemokines (Schwartz & Baruch, 2014). For monocyte-derived macrophage recruitment, the route is still debated, with some studies favouring the damaged BBB as a path (Sweeney et al., 2018) and others suggesting monocytes transit via the ChP as demonstrated in the context of spinal cord injuries where it was described that monocytes are recruited via the ChP into the CSF to resolve lesion sites (Shechter et al., 2013).

According to a review by Ranshoff and Engelhardt (2012), immune cells traffic into the CSF in the following approximate proportions: 90% T cells, 5% B cells, 5% monocytes, and <1% dendritic cells. However, as they do not cite a source for this estimate and only give broad cell types, we did not take this as our CSF baseline. Some studies also include a small number of NK cells (<2%) and cite slightly lower B cell numbers (<1%) (Farhadian et al., 2019). To establish a baseline of healthy immune cell types in CSF we first determined the percentages of immune cells in our dataset. This analysis revealed that 61.8% of the cells from our AD cohort were classified as monocytes compared to 12.4% in our healthy control (HC) cohort. Meanwhile, percentages of T cells were reduced in the AD cohort, $CD4^+$ effector memory cells decreased from 11.2% to 4.3%, and $CD4^+$ central memory dropped from 37.2% to 10.5%.

To compare these findings with prior knowledge we integrated a baseline study for cell type numbers in CSF into our analysis (De Graaf et al., 2011). This study used 6-colour flow cytometry on fresh CSF samples from 84 individuals. These individuals showed no signs of neurological disease, cancer, or treatment with immunosuppressive or cytostatic drugs (except for spinal anaesthesia for patients undergoing surgery). They also had normal CSF glucose and protein levels and a normal WBC count. Whilst not all cell types present in the De Graaf dataset were present in our CSF dataset (and visa versa), we were able to compare the percentages of cell types we identified using the Azimuth package (Hao et al., 2021) during our initial round of annotation.

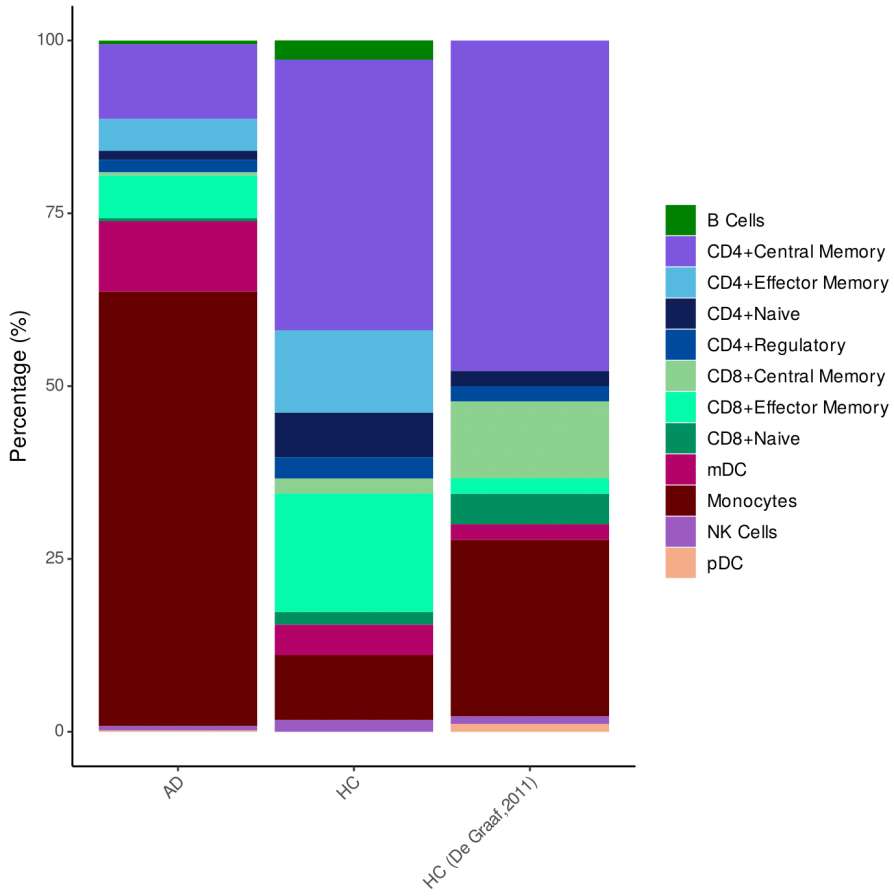

Figure 13. Establishing a healthy CSF baseline using published data. Barchart depicting a comparison of immune cell type percentages from AD and Control groups in CSF data collected in this study, and CSF data from healthy donors in De Graaf et al., 2011.

This analysis showed a reasonable comparability between our control samples and the healthy samples described in De Graaf (Figure 13). In fact, the percentages shown by our healthy controls more closely resemble the broad estimates published by Ranshoff and Engelhardt than those from the De Graaf study which cites a higher percentage of monocytes (25%).

Next, we compared the cell type distribution in healthy donors to the biomarkers positive AD cases and observed that our AD samples have an expanded monocyte compartment compared to either the De Graaf controls, our controls, or the percentages suggested by Ranshoff and Engelhardt. Having established that our control samples matched prior knowledge, we were able to move on to further elucidate the CSF cell types in our samples and investigate differences between the conditions in our study.

5.2.2.2. Characterisation of the immune cell compartment in the CSF of all conditions reveals two CSF specific clusters

To investigate the cell types detected in our CSF dataset we used the CSF object described in 5.2.1. A second integration was carried out with the Harmony package (Korsunsky et al., 2019) and the dimensionality of the data was reduced to 10 PCs which served as an input for UMAP visualisations. The harmonised data was clustered using the Seurat default Louvain algorithm based on shared nearest neighbour (SNN)-graphs, considering the 10 principal components (PCs) established in Harmony and a resolution of 0.5. Afterwards, the reduced dimensionality was represented in a UMAP, allowing a two-dimensional representation based on the 10 calculated PCs from the Harmony data reduction.

Initial annotation through SingleR using the built-in references “Monaco Immune Data” (Monaco et al., 2019), “Blueprint Encode” (Aran et al., 2019), and “Human Primary Cell Atlas Data” (Mabbott et al., 2013) provided a basic classification of cell types which was later supplemented by Azimuth annotation (Hao et al., 2021). The “Blueprint Encode” reference identified the cells found exclusively in CSF (clusters 3 and 9, Figure 14A) as macrophages,

however, on closer inspection they expressed only low levels of canonical macrophage markers.

Overall, the cell-type annotation showed that we could identify all the major immune cell types that were suggested by Ranshoff and Engelhardt (2012) plus two microglia-like myeloid cell subclusters (clusters 3 and 9) that are CSF specific (Figure 14B) and cluster with a mixed signature that did not carry any of the canonical immune or CNS marker genes (cluster 8). The microglial-like clusters 3 and 9 have been annotated as Microglia-like myeloid subset and FTL^{hi} microglia subset respectively, and are subsequently referred to by these names. The rationale for their classification is explored in the subsequent section (*5.2.2.4. Characterisation of the immune cell compartment in the CSF of AD donors*).

Visualising proportions of cell types across all conditions (Figure 14C) showed that the AD cohort dominated the CD14+ monocyte, mDC, and microglia-like cell clusters. Meanwhile, the mixed, B cell and T cell clusters were mostly comprised of the other conditions. However, the inclusion of conditions with low donor numbers makes it difficult to fully assess the actual cell type changes beyond the comparison of AD and healthy donors.

The reference datasets were mostly immune-based and do not cover the CSF-specific cell types, therefore further validation, and adjustment of cell type classifications was required. The annotations were augmented by a comparison of top cluster gene markers (Figure 14D) with gene expression profiles gathered from current CSF literature *(*Supplementary Figure 4).

Cluster 4 is a CD14+ monocyte group which has been annotated as $S100A^{hi}$ CD14+ monocytes due to the high expression of alarmins *S100A8/9* (Figure 14D). They also show low expression of human leukocyte antigen genes (*HLA-DPA1/B1, HLA-DQA1/B1*) which is reminiscent of CD14+ monocytes from PBMCs observed in patients of severe COVID-19 which were high in alarmins and low in HLA-DR genes (*HLA-DRA* and *HLA-DRB)* (Schulte-Schrepping et al., 2020).

The CSF T cell compartment in our data was characterised by four T cell subsets. Two of these belong to the CD4+ central memory T (TCM) cell subsets (clusters 0 and 1) and two are CD8+ effector memory T (TEM) cell subsets (clusters 2 and 5). This is in line with published literature which suggests that the CSF contains very few naïve T cells but contains

primarily effector and memory CD8+ T cells and CD4+ T cells (Ransohoff & Engelhardt, 2012). These T cells can sometimes carry characteristics of both TCM and TEM cells often making it difficult to distinguish between them using classical approaches but also scRNA-seq (Ransohoff & Engelhardt, 2012).

Next, we calculated the percentage of cells that the different conditions contributed to each cell type (Supplementary Figure 5). This highlighted the variation introduced to the dataset by the conditions with only a few donors (AD Pathological Change, Non-AD Pathological Change, and Non-Biomarker Control). To further investigate this, we plotted a separate UMAP for each condition accompanied by bar charts of cell type percentages in CSF samples, split by individual and condition (Figure 15). Here we could observe that for the AD Pathological Change and Non-AD Pathological Change groups the number of donors is not sufficient to draw conclusions based on biology rather than individual differences. While the Non-Biomarker Control group shows more homogeneity, with three donors it is unlikely that any finding will be statistically robust. Whilst no further analysis has been made including these groups for this reason, it can be noted that their cell type distribution is broadly similar to the control group.

The increase in the microglial-like cell clusters that was noted before (Figure 14C) when assessing the integrated dataset can be pinpointed to only three out of the five AD donors (Donors AD046/47/50) (Figure 15). However, as a caveat to this, these three donors with a higher percentage of microglial-like cells are samples that were processed on different Rhapsody cartridges on different days, while the remaining two AD donors (Donors AD062 and AD064) who showed percentages of microglial-like cells more similar to the control group were donated on the same day and processed on the same Rhapsody cartridge. While this does not completely rule out any technical variability affecting the results, it supports that this is not a batch effect but underlying biological differences.

This cell type variation within conditions could be caused by the severity of the condition and disease stage. However, whilst metadata includes cognitive tests, e.g. MMST scores, we were unable given the timeframe to obtain more detailed severity information such as Braak stages for our donor cohort. Unfortunately, the MMST scores between individuals are variable and

do not explain the differences we see between these AD individuals on a cellular level (*Materials:* Table 9).

In summary, these data demonstrate that our CSF samples contained all expected CSF cell types listed in Ransohoff and Engelhardt (2012) plus two additional CSF specific clusters, the classification of which is fully explored in the subsequent section (5.2.2.4.). The cell type variation within conditions suggested that AD donors have an expanded myeloid compartment compared to healthy donors. We decided to explore this further by investigating differential gene expression in the myeloid compartment.

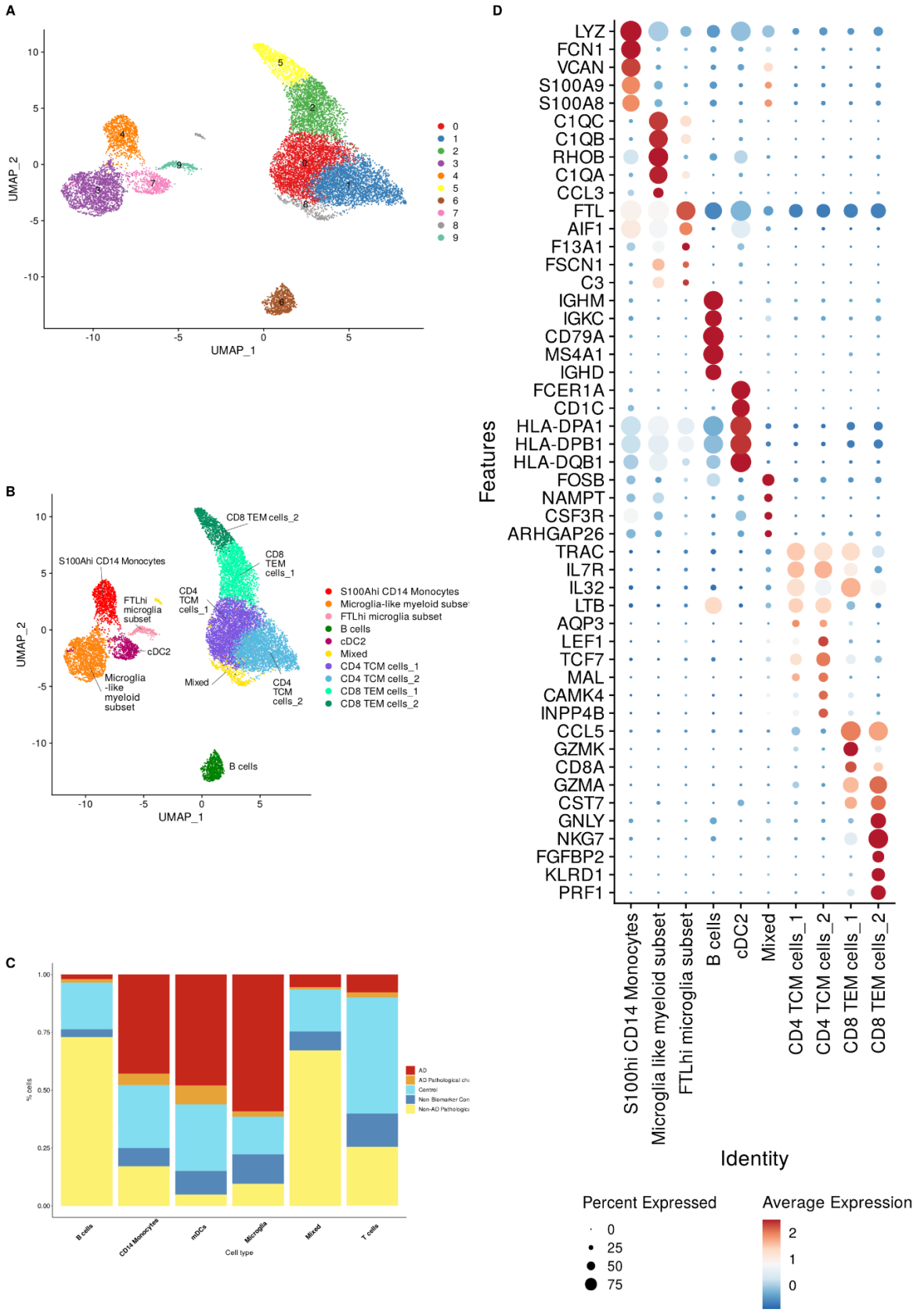
A
UMAP_2
UMAP_1
0
1
2
3
4
5
6
7
8
9
B
S100Ahi CD14 Monocytes
FTLhi microglia subset
cDC2
Microglia -like myeloid subset
CD8 TEM cells_2
CD8 TEM cells_1
CD4 TCM cells_1
Mixed
CD4 TCM cells_2
B cells
Microglia-like myeloid subset
CD8 TEM cells_1
C
% cells
Cell type
B cells
CD14 Monocytes
mDCs
Microglia
Mixed
T cells
D
Features
LYZ
FCN1
VCAN
S100A9
S100A8
C1QC
C1QB
RHOB
C1QA
CCL3
FTL
AIF1
F13A1
FSCN1
C3
IGHM
IGKC
CD79A
MS4A1
IGHD
FCER1A
CD1C
HLA-DPA1
HLA-DPB1
HLA-DQB1
FOSB
NAMPT
CSF3R
ARHGAP26
TRAC
IL7R
IL32
LTB
AQP3
LEF1
TCF7
MAL
CAMK4
INPP4B
CCL5
GZMK
CD8A
GZMA
CST7
GNLY
NKG7
FGFBP2
KLRD1
PRF1
S100hi CD14 Monocytes
Microglia like myeloid subset
FTLhi microglia subset
B cells
cDC2
Mixed
CD4 TCM cells_1
CD4 TCM cells_2
CD8 TEM cells_1
CD8 TEM cells_2
Identity
Percent Expressed
0
25
50
75
Average Expression
2
1
0

Figure 14. CSF analysis of all conditions. (A) UMAP representation and clustering of cells contained in main clusters 0-9. (B) UMAP showing cell types in CSF. (C) Cell proportions in the CSF according to condition. (D) Dotplot of CSF characteristic marker expression of top 5 genes sorted by average log fold change assigned to each cell type.

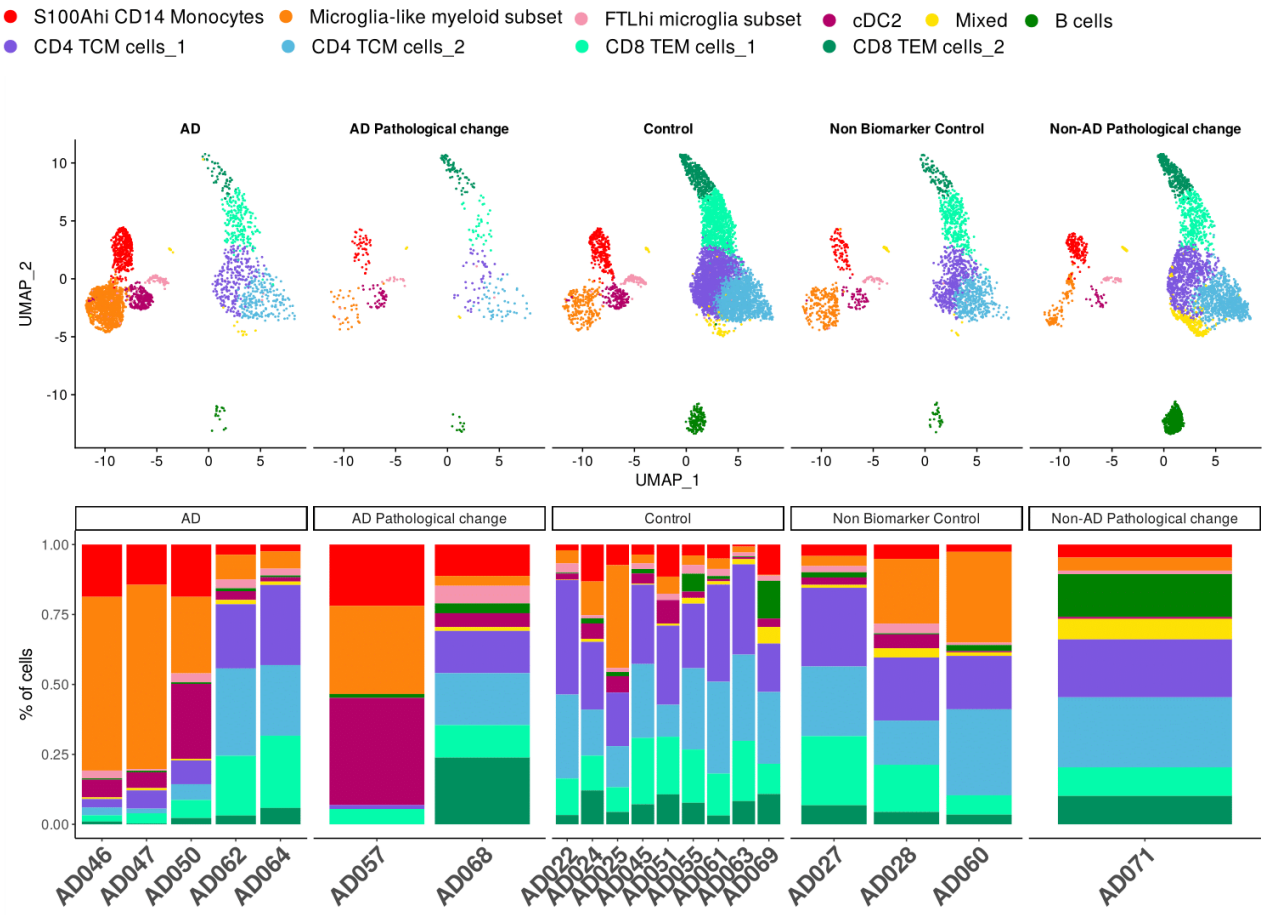

Figure 15. Comparison of cell type percentages in CSF samples. UMAPs showing cell types in CSF by condition and corresponding cell types proportions from individual donors.

5.2.2.3. Differential gene expression analysis shows upregulation of chemokine genes in the Microglia-like myeloid cell subset

We calculated differential gene expression for the CSF AD cohort and removed any genes with an adjusted p-value above 0.05. This filtering identified only seventeen genes that were

being differentially expressed. One of these, Inhibitor of DNA Binding 2 *(ID2),* was upregulated in the CD8 TEM_1 subset. Pseudogene *AL365357.1* is upregulated in both CD4 TCM subsets, as well as the Microglia-like myeloid cell subset.

Pseudogene *AL365357.1* and the remaining fifteen differentially expressed genes can be observed in the Microglia-like myeloid cell subset (Figure 16). In the Microglia-like myeloid cell subset the expression of inflammatory C-C motif chemokine genes *CCL4, CCL3, CCL4L2,* and *CCL3L3* is upregulated. Pre-microglia and activated microglia clusters identified in murine glioma environments have been shown to upregulate orthologues of human *CCL3* and *CCL4* genes (Ochocka et al., 2021). These genes were formerly known by the names macrophage inflammatory protein 1-alpha and beta respectively (*MIP-1α* and *MIP-1β*) (Guan et al., 2001). The CC chemokine family is known for encoding proteins that play a role in the migration of leukocytes (Menten et al., 2002). Up-regulation of these genes in the Microglia-like myeloid subset could suggest peripheral immune recruitment into the CSF through the expression of chemokines. Increased expression of these genes has been demonstrated before in both microglia and macrophages when stimulated *in vitro* with Aβ (El Khoury et al., 2003). Whilst research into the role of these two chemokines in AD is sparse, we know that both act on the receptor CCR5. This receptor is expressed on microglia and monocytes and is suggested to be involved in peripheral monocyte recruitment into the CNS and movement of microglia towards Aβ plaques (Guedes et al., 2018).

The significant upregulation of *CCL3*, *CCL4* and *C3AR1* in Microglia-like myeloid cells in the AD cohort is further associated with disease pathology by a study that described several microglial subpopulations from cerebral cortex samples (Olah et al., 2020). Interestingly, the cluster that was enriched for *CCL3*, *CCL4* and *C3AR1* in this microglial study was also found to be associated with Aβ.

The key point in this analysis was the suggestion that the presence of chemokine genes in the Microglia-like myeloid cell subset could indicate peripheral immune recruitment into the CSF, alongside the identification of other genes which may have been linked with Aβ. We decided the next step was an in depth look at the AD cohort versus the control cohort to elucidate AD links in the myeloid cell compartment. As insufficient donor numbers in the other

three condition cohorts would be a limiting factor in any further analysis of these datasets, we excluded them to allow an unbiased comparison.

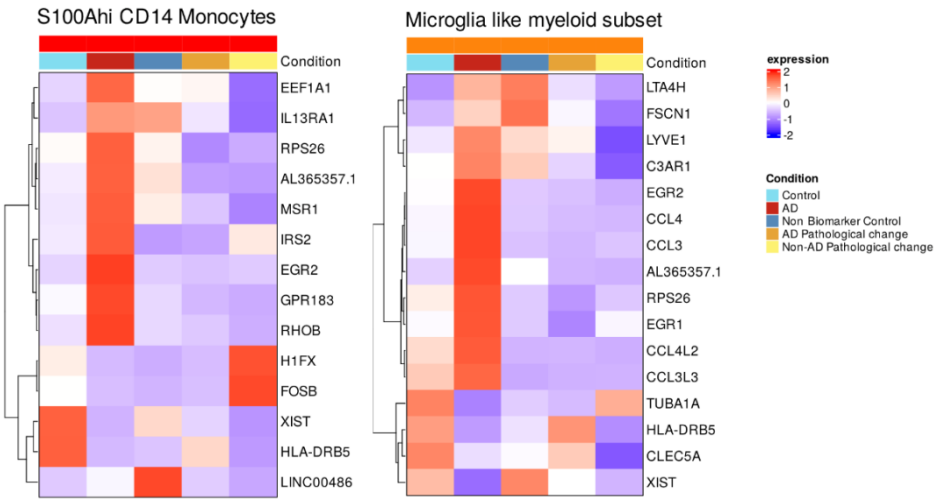

Figure 16. **Comparison of AD DEG in the CSF myeloid cell compartment against expression in the same genes in other conditions**. Heatmaps of DEG with an adjusted p-value <0.05 in the AD cohort CSF cell type clusters S100A^{hi} CD14+ monocytes and Microglia-like myeloid cell subset. Scaled per cell type and also showing expression levels of these genes across all other conditions.

5.2.2.*4*. Characterisation of the immune compartment in the CSF of AD donors

Next, we performed a more focused analysis of cells from AD patients and healthy controls only to further identify changes in cell populations between these groups. The input of cells from these two conditions is variable, with more cells in the control group due to their higher number of donors (AD=2730; control= 5603). To be able to conduct comparisons between the two conditions we downsampled the cells in each condition so that both subsets contributed 2730 cells to the analysis.

An overview of the cell types (Figure 17A) revealed that none were lost by excluding the three other conditions. To simplify assessment of CSF cell proportions across conditions and donors, annotated cell types were integrated into six groups: B cells, CD14+ monocytes, mDCs, microglia, a mixed group, and T cells (Figure 17B). This analysis decision was supported by the expression of marker genes that characterised individual cell types, which were clearer in the myeloid compartment than in the T cell groups (Figure 17C). The comparison in figure 17B shows that the AD condition represents lower proportions of cells in the B cell, T cell and mixed groups.

In the comparison of individual donors on the more fine-grained level (Figure 17D), there were marked changes in several compartments that are not removed by the downsampling. Firstly, in both the myeloid and dendritic cell compartments there is an increased percentage of cells being contributed by the AD cohort. The Microglia-like myeloid cell subset is strongly represented in three out of the five AD donors, whereas in all control donors they constitute less than 25% of any sample. In contrast, the FTL^{hi} microglia-like subset is more consistent across conditions and shows little variation between individuals. CD14+ monocytes and cDC2's appear only slightly augmented in three out of the five AD donors compared to the control group. The donor identified as AD050 is an exception here and has a 4-fold increase in cDC2's compared to the other donors. This may be overcontributing to the difference shown for the cDC2 in both Figure 17B and the cDC2 cell cluster in the UMAP in Figure 17D.

Further analysis of the comparison of the individual donors (Figure 17D) revealed that the control donors all show high percentages of T cells (>75%) made up of a mixture of CD4 TCM cells and CD8 TEM cells. In contrast, three out of the five AD donors have a smaller T cell compartment (<75%). The remaining two AD donors once again appear much more like the control group with a T cell compartment constituting >75% of the cells in their samples. We theorise that differences between AD and control conditions in the proportions of B cells, T cells and mixed cells may be a relative decrease in response to the expanded myeloid group.

Taken together these data show a higher percentage of cells belonging to AD patients within the myeloid groups: CD14+ monocytes, mDC and microglia. This pattern can be seen on a more granular level when we looked at the donors as individuals, with the Microglia-like myeloid cell subset showing the most pronounced difference from the control group.

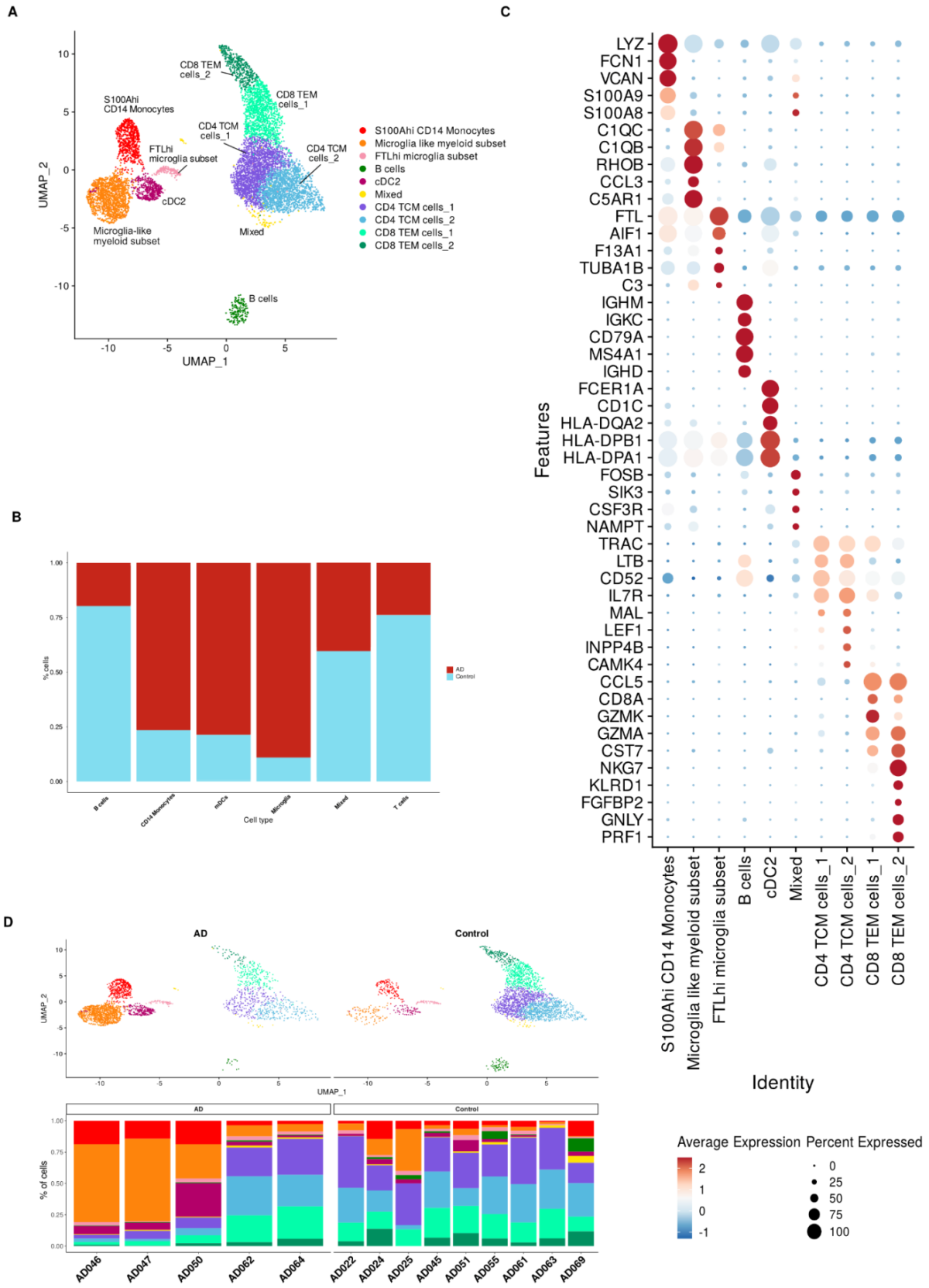
A
UMAP_2
UMAP_1
S100Ahi CD14 Monocytes
CD8 TEM cells_2
CD8 TEM cells_1
CD4 TCM cells_1
CD4 TCM cells_2
FTLhi microglia subset
cDC2
Microglia-like myeloid subset
Mixed
B cells
S100Ahi CD14 Monocytes
Microglia like myeloid subset
FTLhi microglia subset
B cells
cDC2
Mixed
CD4 TCM cells_1
CD4 TCM cells_2
CD8 TEM cells_1
CD8 TEM cells_2
B
% cells
Cell type
AD
Control
C
Features
LYZ
FCN1
VCAN
S100A9
S100A8
C1QC
C1QB
RHOB
CCL3
C5AR1
FTL
AIF1
F13A1
TUBA1B
C3
IGHM
IGKC
CD79A
MS4A1
IGHD
FCER1A
CD1C
HLA-DQA2
HLA-DPB1
HLA-DPA1
FOSB
SIK3
CSF3R
NAMPT
TRAC
LTB
CD52
IL7R
MAL
LEF1
INPP4B
CAMK4
CCL5
CD8A
GZMK
GZMA
CST7
NKG7
KLRD1
FGFBP2
GNLY
PRF1
S100Ahi CD14 Monocytes
Microglia like myeloid subset
FTLhi microglia subset
B cells
cDC2
Mixed
CD4 TCM cells_1
CD4 TCM cells_2
CD8 TEM cells_1
CD8 TEM cells_2
Identity
Average Expression
Percent Expressed
D
AD
Control
UMAP_2
UMAP_1
% of cells
AD046
AD047
AD050
AD062
AD064
AD022
AD024
AD025
AD045
AD051
AD055
AD061
AD063
AD069

Figure 17. CSF analysis of AD and Control donors. (A) UMAP showing cell types in CSF. (B) CSF donor cell proportions by cell group. (C) Dotplot of CSF characteristic marker expression of top 5 genes sorted by average log fold change assigned to each cell type (D) Comparison of cell type percentages in CSF samples split by individual and condition. (Downsampled to 2730 per condition).

5.2.2.5. Analysis of the CSF myeloid cell compartment shows that FTL^{hi} microglia and Microglia-like myeloid cell subsets are distinct from monocytes

To gain a better understanding of the CSF myeloid cell compartment we calculated the marker expression for the top fifteen genes sorted by average log fold change assigned to each of its three clusters, annotated as S100A^{hi} CD14+ monocytes, microglia-like myeloid cells and FTL^{hi} microglia-like cells (Figure 18A). These clusters were all initially annotated as CD14+ monocytes when first identified using annotation packages such as SingleR (Aran et al., 2019) and Azimuth (Hao et al., 2021). Following a closer inspection of the marker genes, it was apparent that the microglia-like myeloid cell and FTL^{hi} microglia-like cell subset did not express a typical CD14+ monocyte signature. Each displayed a gene expression signature that shared insufficient overlap with any of the other myeloid cell clusters. Most canonical CD14+ monocyte markers such as *LYZ, VCAN, CD36, and FCN1* were expressed at low levels or absent from both clusters. However, the microglia-like myeloid cell subset expressed other typical markers for monocytes or monocyte-derived cells, e.g. *CD14* while retaining also *LYZ* expression.

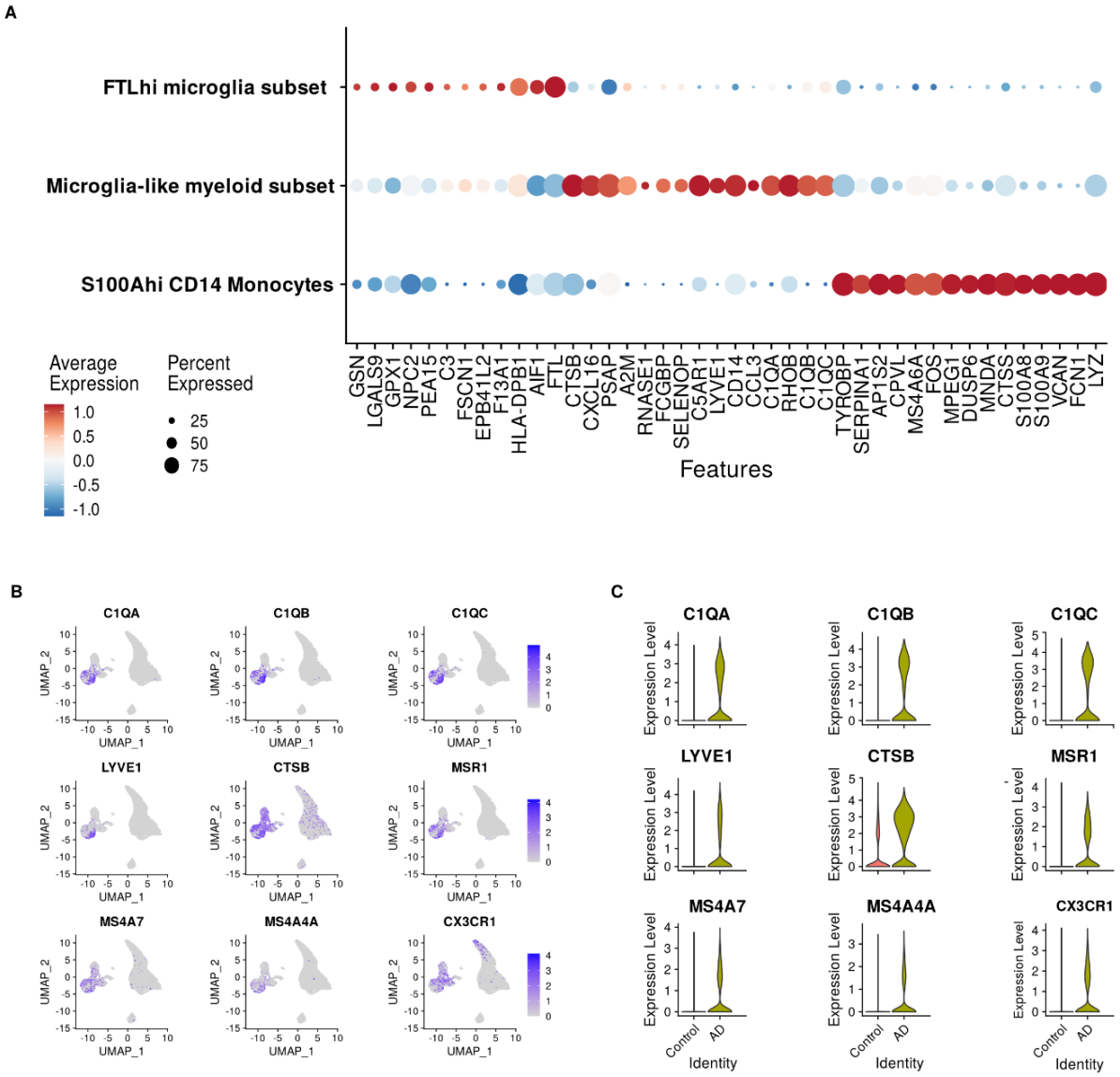

Figure 18. **Analysis of the CSF myeloid cell compartment in AD and control cohort.** (A) Dotplot depicting expression for top 15 genes of gene marker of the myeloid compartment sorted by average log fold change assigned to each cell type. (B) Feature maps for CSF myeloid cell genes of interest in the Microglia-like myeloid subset. (C) Violin plots for CSF myeloid genes of interest in the Microglia-like myeloid subset.

To correctly annotate these myeloid cell clusters we cross-referenced gene expression in these subsets with previously published scRNA-seq CSF datasets to determine gene markers that were present in these clusters. One study, which was used for cell type annotation, performed scRNA-seq of CSF cells from patients with inflammatory demyelinating diseases (anti-MOG disorder and RRMS) and described cell clusters within the myeloid cell compartment containing what the authors described as microglia-specific genes: *LYVE1, TREM2, C1QB, GPR34, OLR1, and C3* (Esaulova et al., 2020). The obvious similarities with one of our myeloid cell clusters lead us to assess expression of this signature in our data set (Supplementary Figure 4). The signature shared some similarities with our microglia-like myeloid cell subset, with prominent expression of complement components (*C1QA-C*) and *LYVE1* as well as moderate expression of *TREM2, GPR34,* and *OLR1.*

Another scRNA-seq study using CSF from adults with and without HIV found two CSF-specific myeloid cell subsets (Farhadian et al., 2019). One of these subsets expressed genes that the study identified from previous literature (Keren-Shaul et al., 2017) as enriched in neurodegenerative disease-associated microglia in mice. The CSF-associated microglia-like cells found in that study represented <5% of all CSF cells analysed and were significantly expanded in the CSF of individuals with HIV compared to the controls, which they attribute to chronic immune activation in the CNS. Once again, we identified similarities with our myeloid cell clusters and assessed expression of this CSF-associated microglia-like expression signature in our data (Supplementary Figure 4). Key similarities included the strong expression of complement components (*C1QA-C*), *LYVE1, CD14, CTSB* and *MSR1,* (Figure 18B/C) as well as moderate expression of *OLR1, SELENOP, AXL, MARCO, CTSL, SLC2A5, HAVCR2* and *FCGBP*. The expression of typical macrophage signature genes *MSR1* and *MARCO* caused us to assess enrichment of a macrophage signature in this cluster. I used the signature from (Baßler et al., 2020) and observed that only *MSR1* and *FCGR3A* were expressed in >50% of cells in the cluster (Supplementary Figure 4). As *FCGR3A* is also a known marker of CD16+ monocytes and *MSR1* can be expressed in DCs (Herber et al., 2010) and microglia (Farhadian et al., 2019), we can exclude from this analysis that this cluster is enriched in macrophage genes but is expressing transcripts in line with the acquisition of microglia-like features.

Unlike microglia which originate from the fetal yolk sac and populate the CNS in early development, CNS-infiltrating monocyte-derived macrophages originate from blood-borne myeloid cells and only enter the CNS under neuroinflammatory conditions (Ginhoux et al., 2010). Despite sharing morphological and phenotypical features with activated microglia, these monocyte-derived macrophages are not similarly limited in their self-renewal capacity (Hanisch & Kettenmann, 2007). This, alongside increased phagocytic capacity and anti-inflammatory characteristics, means that these cells are potentially beneficial in neurodegenerative diseases (Shechter & Schwartz, 2013).

Recently a study demonstrated the bone-marrow-derived origin of CSF microglia-like cells taken from a human donor (Roostaei et al., 2021). The donor was female and had chronic progressive multifocal leukoencephalopathy (PML) after an infection of the brain with the John Cunningham (JC) virus following a bone marrow transplant for lymphoma a decade earlier. The bone marrow transplant had come from a male donor and when CSF samples from the female recipient were assessed, the authors observed expression of sex chromosome genes that strongly suggested a male origin. This confirmed that the CSF microglia-like cells identified in this study were bone-marrow-derived. Similar to our own Microglia-like myeloid subset, the CSF microglia-like cells identified in Roostaei et al. expressed high levels of *C1QA-C* and *APOE* suggesting that also the microglia-like cells we observe are bone-marrow derived.

Next, we assessed the Microglia-like myeloid subset (clusters 3) for the expression of marker genes for CNS-infiltrating monocyte-derived macrophages using a gene signature from a scRNA-seq study investigating phenotypes of myeloid cell subpopulations in murine gliomas which profiled microglia, infiltrating monocyte-derived macrophages and CNS border-associated macrophages (Ochocka et al., 2021). The gene signature contained murine-specific genes which were replaced with known human orthologues or excluded from the signature where no orthologue exists. The Microglia-like myeloid cell subset expressed strong levels of *MS4A7* (Figure 18B/C), and *MRC1*, as well as moderate levels of *APOE*, which are all known border-associated macrophage (BAM) genes (Supplementary Figure 4) (Ochocka et al., 2021; Van Hove et al., 2019). However, they also highly expressed *MS4A4A*, a human orthologue of *Ms4a4c*, which has been reported as a novel monocyte-derived macrophage

marker (Ochocka et al., 2021). The annotation of cluster 3 is further complicated by its high expression of microglial marker *CX3CR1* (murine orthologue *Cx3cr1*) (Figure 18B/C) and moderate expression of CST3 and IFITM3 which are low specificity markers for both microglia and monocyte-derived macrophages (Ochocka et al., 2021). In summary, the markers from this study do not clearly identify the Microglia-like myeloid subset as BAMs, monocyte-derived macrophages or microglia, as the subset carries marker genes for all three groups.

The FTL^{hi} microglia subset is named in reference to the high expression of the Ferritin Light Chain gene (*FTL*) observed as the top marker for this cluster (Figure 18A). Another highly expressed gene in this cluster is Allograft inflammatory factor 1 (*AIF1,* alias *Iba1*), which is known as a marker of homeostatic microglia and macrophages and is upregulated after activation of both cell types (Kenkhuis et al., 2021). An AD-specific dystrophic microglia phenotype has been identified in the human middle temporal gyrus (MTG) (Kenkhuis et al., 2021) and is characterised by increased *FTL* and *Iba1* expression, and decreased *TMEM119* and *P2RY12* expression. This matches the expression profile of our FTL^{hi} microglia subset (Supplementary Figure 4). Furthermore, the expression of major histocompatibility complex (MHC) Class II DP Beta 1 (*HLA-DPB1*) together with the above markers, could suggest a DAM-like microglia phenotype. *HLA-DPB1* encodes one of the beta chains of the HLA-DP complex and studies have shown that the HLA-DP complex is present on the surface of microglia and plays a role in antigen recognition and presentation, particularly in the context of neuroinflammation and neurodegenerative diseases such as AD (Forabosco et al., 2013; Masuda et al., n.d.).

The genes used to characterise enrichment of a macrophage signature (Baßler et al., 2020) were not enriched in the FTL^{hi} microglia subset (Figure 18A), which would suggest that this cluster is not a typical macrophage cluster. However, this is questioned by the expression of *F13A1*, a marker highly and specifically expressed by BAMs (Ochocka et al., 2021). In summary, the gene expression markers for the FTL^{hi} microglia subset share some similarities with one of the microglial subpopulations identified in an scRNA-seq study of the human cerebral cortex, which further validates their classification as microglia.

The gene signature for CSF-associated microglia-like cells in HIV patients (Farhadian et al., 2019) that we used earlier to characterise the Microglia-like myeloid subset also contained

marker genes that were exclusively expressed by the FTL^{hi} microglia subset, supporting the notion that the two microglia subsets are distinct. The top markers expressed by the FTL^{hi} microglia subset (Figure 18A) include *EPB41L2, F132A1* and *C3*, which are all genes that appear in the CSF-associated microglia-like cell signature from these HIV patients (Farhadian et al., 2019). This means that while our two microglial subclusters express markers that are distinct from one another, they do both express genes found in this literature-defined CSF-associated microglia-like cell signature. This implies that both clusters contain some degree of microglial differentiation.

Taken together this analysis of the gene expression data of the CSF myeloid cell compartment suggests that the subsets we call FTL^{hi} microglia and Microglia-like myeloid cells are distinct from monocytes and each other. An examination of the literature has excluded the possibility that these subsets are macrophages and instead both subsets have different gene markers that suggest each could be a distinct type of dysregulated microglia.

5.2.2.*6*. The Microglia-like myeloid cell subset is upregulated in CSF of AD donors

As outlined before (5.2.2.4), this Microglia-like myeloid cell subset appears to be upregulated in the CSF of the AD cohort (Figure 15/17). To substantiate this observation we used the single-cell compositional data analysis (scCODA) package (Büttner et al., 2021), which detects statistically relevant changes in cell type composition and calculates the model inclusion probability for each covariate. We chose to use this package because it was designed specifically to be used with scRNA-seq data and can cope with the low number of sample replications that are common with this data type. It also accounts for the proportional nature of cell type counts and the bias that can be introduced in a cell population when one type is depleted or inflated. In short, whilst inflation of one cell type may appear to decrease the relative frequencies of differential cell types, this is unlikely to be a real effect and instead represents negative correlations between the cell types. This is important in our CSF data as

it will help us to differentiate between real cell type changes and relative decreases occurring only in response to the expanded myeloid cell group.

After initially visualising the data across all conditions to obtain an overview of changes in all cohorts (Figure 19A), we subsetted the data to AD and control donors to determine how AD influences the cell composition. From this, we could observe a large increase in the Microglia-like myeloid subset in the AD samples compared to the Control group (Figure 19B). Concomitantly, there is a slight increase in the $S100A^{hi}$ CD14+ monocytes and minimal increases in the FTL^{hi} microglia subset and cDC2s. All other cell types show minimal decreases in AD, except the T cell subsets (CD4 TCM cells and CD8 TEM cells) which appear strongly depleted in AD. To establish whether this depletion is real or relative to the increase in the Microglia-like myeloid cell subset we modelled inclusion probability for each covariate. To achieve this we first selected a reference cell type that has a nearly constant relative abundance. In this case, we use the Mixed cell type as a reference. The model returns two analysis parameters: “intercept” showing cell types distribution without active covariates, and “effect” which indicates if a statistically credible effect is detected. Here, we observed a statistically credible effect for the Microglia-like myeloid subset and all four T cell groups. The reporting of credible effects is based on inclusion probability which are depicted for each cell type (Figure 19B). The cutoff is defined by the FDR which we set at a level of 0.1. Setting a smaller FDR would give a more conservative result, however having reviewed the author’s recommendations in the paper the chosen cut-off of 0.1 is in line with the study's example datasets (Büttner et al., 2021).

To surmise, we find a statistically credible effect for five cell types: the Microglia-like myeloid subset, the two CD4 TCM cell subsets and the two CD8 TEM cell subsets. This implies firstly that the increase in the Microglia-like myeloid subset in AD patients is genuine and secondly that the depletion of the T cells groups in AD patients is also a biologically relevant finding.

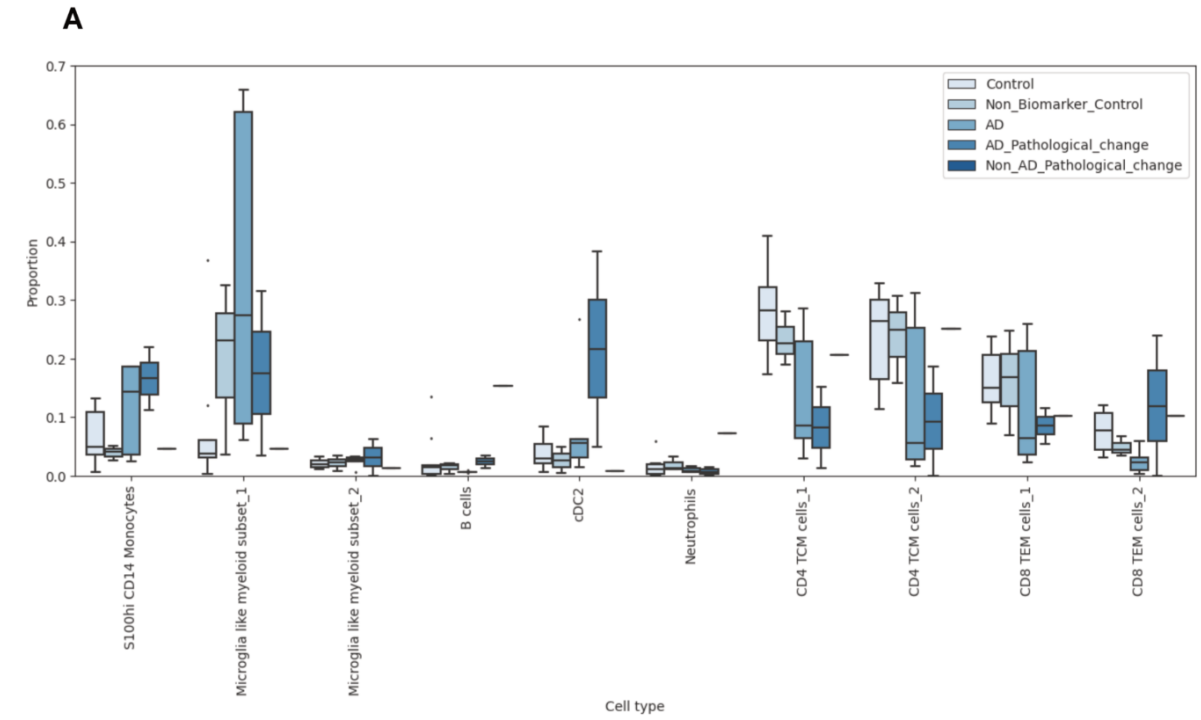
A
Control
Non_Biomarker_Control
AD
AD_Pathological_change
Non_AD_Pathological_change
Proportion
0.0
0.1
0.2
0.3
0.4
0.5
0.6
0.7
S100hi CD14 Monocytes
Microglia like myeloid subset_1
Microglia like myeloid subset_2
B cells
cDC2
Neutrophils
CD4 TCM cells_1
CD4 TCM cells_2
CD8 TEM cells_1
CD8 TEM cells_2
Cell type

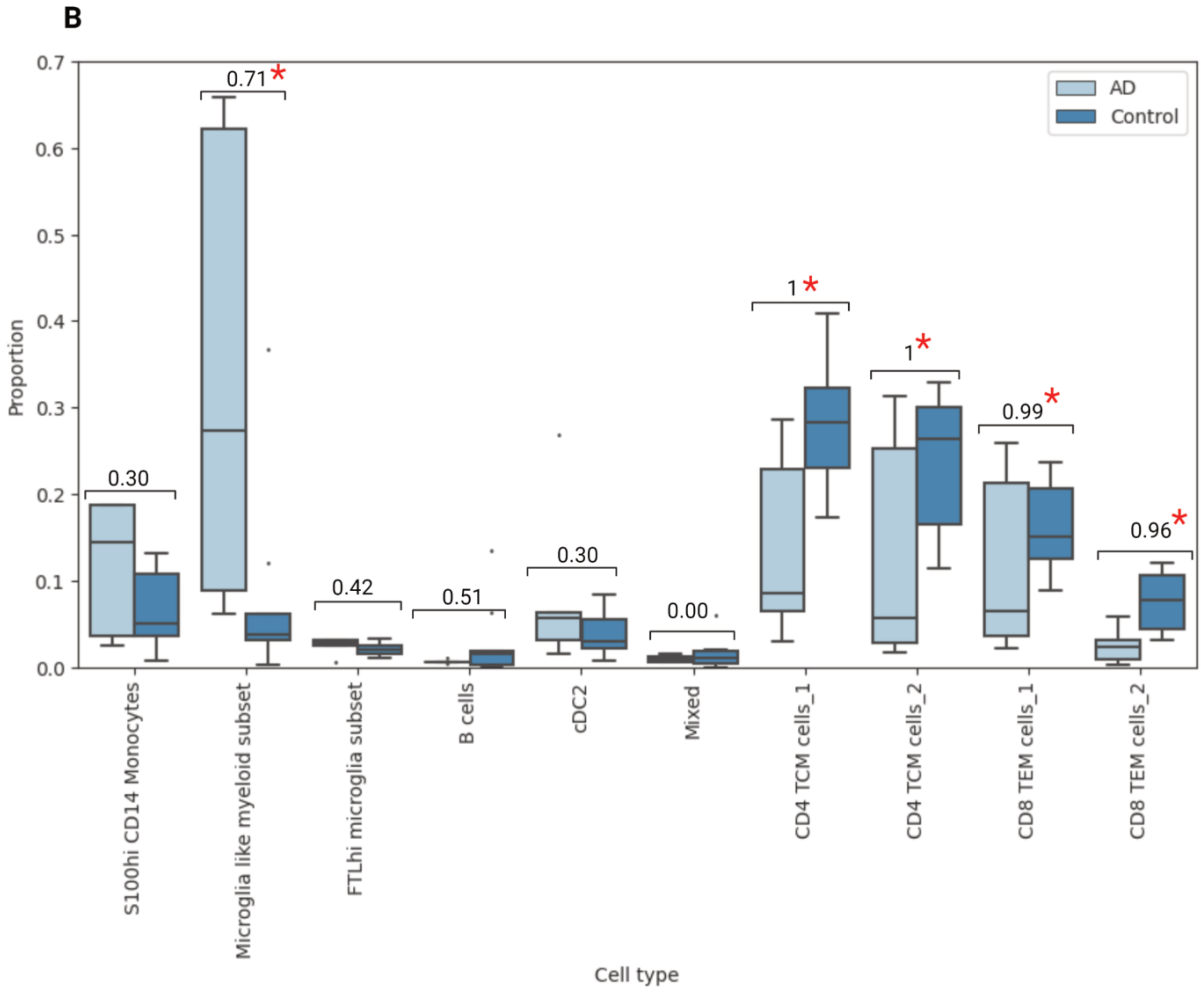
B
AD
Control
Proportion
0.0
0.1
0.2
0.3
0.4
0.5
0.6
0.7
0.30
0.71*
0.42
0.51
0.30
0.00
1*
1*
0.99*
0.96*
S100hi CD14 Monocytes
Microglia like myeloid subset
FTLhi microglia subset
B cells
cDC2
Mixed
CD4 TCM cells_1
CD4 TCM cells_2
CD8 TEM cells_1
CD8 TEM cells_2
Cell type

Figure 19. CSF analysis with scCODA. (A) scCODA results on all CSF cell types (B) scCODA comparison of AD and control samples in CSF. Cell types are marked with inclusion probability values and statistically credible changes in cell type compositions are highlighted with a red asterisk. (FDR =0.1).

5.2.3. Analysis of pB in AD donors using the Rhapsody approach found no statistically verifiable change between AD and control donors

While CSF is more closely connected to the brain parenchyma and as such a higher impact of neurodegenerative processes directly affecting cell composition in the CSF can be envisioned, the peripheral blood, circulating constantly also within the vessels of the CNS, could be exposed to secretory mediators affecting also peripheral blood cells and the hematopoietic system. To study the impact of neurodegeneration on the peripheral blood, we also assessed PBMCs by scRNA-seq.

Therefore, our Rhapsody PBMC dataset was generated by subsetting the data object produced in the Rhapsody whole dataset analysis by tissue type (see section *5.2.1. An overview of the combined PBMC and CSF dataset*). PBMC samples are more easily accessible and contain far more cells per ml than CSF and so the PBMC dataset is comparatively well-populated, containing 97,046 cells from 48 donors. The mean number of cells contributed per donor is 2022 and the median is 1497.

Just like the CSF analysis, the PBMC dataset analysis was split into two parts: firstly we analysed the data across all conditions to provide an overview of the different groups then secondly, we analysed only the AD and Control groups. The AD Pathological Change and Non-AD Pathological Change cohorts contain only two PBMC donors each, which prohibited a statistically robust full analysis. The Non-Biomarker Control groups contained 24 PBMC donors, and whilst this would withstand robust statistical testing we cannot fully characterise these individuals as a healthy control group without the full biomarker information that has been used to classify the other groups. For this reason, we include them only for the overview analysis of all conditions where they support the data provided by the nine control donors.

5.2.*3.1*. Characterisation of the PBMC immune cell compartment across all conditions

Once generated, the PBMC object was prepared in the same way as previously described in the CSF and methods sections. During the Harmony integration (Korsunsky et al., 2019), the dimensionality of the data was reduced to 10 PCs and later clustered with a resolution of 0.9. This resolution resulted in the identification of twenty-four clusters which included a higher number of subclusters than is optimal (Figure 20A). However, any reduction in resolution led to hybrid clusters containing markers for both monocytes and T cells, and so it was necessary to maintain the resolution at 0.9 to form biologically likely clusters.

The twenty-four clusters generated were first annotated through SingleR references (Monaco (Monaco et al., 2019), Blueprint/Encode (Aran et al., 2019), HPCA (Mabbott et al., 2013)), then supplemented with annotations from the Azimuth PBMC atlas (Hao et al., 2021).

The annotated clusters identified immune cell groups in the blood (Figure 20B) that fit with published single-cell RNA-seq PBMC data (Bassler et al., 2019; Kapellos et al., 2019; Schulte-Schrepping et al., 2020). Multiple subsets were identified in the myeloid, NK and T cell compartments that were later investigated through comparison of their top cluster marker genes with previously published gene expression profiles (Figure 20D).

The myeloid cell compartment was characterised by seven subsets (clusters 2, 3, 10, 12, 13, 19 and 20) (Figure 20A/B). One of these subsets (cluster 10) was marked in the references and by its canonical genes to be non-classical monocytes (CD16+ monocytes). Low expression of *HLA-DRB1 and HLA-DRA* alongside high expression of alarmins *S100A8/9/12* in cluster 3 led us to annotate it as S100A^{hi} CD14+ monocytes. A recent COVID-19 PBMC study (Schulte-Schrepping et al., 2020) observed a similar expression profile in their monocyte subsets (*HLA-DR^{lo}S100A^{hi}*). Cluster 12 also expressed low levels of *HLA-DRB1 and HLA-DRA* alongside high levels of *S100A8/9/12* markers (though not as high as cluster 3). Once again we noted similarities with another monocyte subset in the COVID-19 PBMC study defined as *HLA-DR^{lo}CD163^{hi}* (Schulte-Schrepping et al., 2020). However, our cluster 12 did not contain *CD62L* and *CD163* used to characterise *HLA-DR^{lo}CD163^{hi}* as its top markers.

Instead, cells from this cluster shared a strong expression of *MX1, APOBEC3A* and moderate expression of *IFITM3,* all of which are genes associated with IFN type I (Taura et al., 2022). The study noted that low expression of HLA-DR genes, such as we see in clusters 3 and 12, is a sign of dysfunctional monocytes with reduced response to stimuli (Schulte-Schrepping et al., 2020; Veglia et al., 2018; Venet et al., 2021).

We identified a myeloid cell subcluster (cluster 20: C1Q myeloid cluster) that contained cells which moderately expressed *CD14* but otherwise showed little expression of CD14+ monocyte-associated genes. Instead, this cluster demonstrated high expression of complement components (*C1QA-C*) and HLA class II genes (HLA-DPA1, HLA-DPB1, HLA-DQA1, HLA-DQB1, HLA-DRA and HLA-DRB1). This suggested that the cells from this cluster have a stronger capacity for antigen presentation. Cells from this cluster also showed a moderate expression of Fc gamma binding protein (FCGBP), Alpha-2-Macroglobulin (A2M), and MSR1. These last two markers could suggest monocyte-to-macrophage differentiation in this cluster as both genes are expressed by macrophages (Bassler et al., 2019; Vandooren & Itoh, 2021).

The remaining myeloid clusters 2, 13 and 19 contained enough myeloid-specific marker genes to place them in this compartment, but it was not possible to further describe these clusters based on these genes.

The NK compartment was split into two subsets: NK cells_1 and NK cells_2 (clusters 1 and 16 respectively) (Figure 20A/B). Cells from these clusters had canonical markers in common (*NKG7, GNLY, IL2RB, KLRF1, KLRD* and *NCAM1*) but each additionally displayed a distinct set of marker genes. The NK cells_1 subset was distinguished by the expression of *PRF1*, *GZMB* and *SPON2*. These last two markers were amongst the demarcating genes for a subset of NK cells in a scRNA-seq study of human bone marrow NK cells (Crinier et al., 2020). The second NK subset (NK cells_2) expressed EOMES, *DUSP2* and *GZMK*, again the latter two genes here are listed in the annotation for another NK subset identified in human bone marrow by the same study (Crinier et al., 2020).

The T cell compartment was characterised by four CD4+ naïve T cell subsets (clusters 0, 7, 9 and 18), three CD4+ TCM cell subsets (clusters 4, 14 and 23), two CD8+ TEM cell subsets (clusters 5 and 8) and one cluster of Regulatory T cells (Treg) (cluster 11) (Figure 20A/B). The CD4+ naïve T cell subsets (clusters 0, 7, 9 and 18) are all marked by canonical marker genes *TCF7, LEF1, CCR7* and *ILR7*. However, this signature is strongest in cluster 7 which also includes expression of *FHIT, TSH22, MAML2* and *INPPB4*. The CD4+ TCM cell subsets (clusters 4, 14 and 23) are difficult to annotate and are separating due to their very low marker gene expression. However, from the markers present and SingleR references, they appear best characterised as CD4+ TCM cells. Finally, the two CD8+ TEM cell subsets (clusters 5 and 8) are marked by canonical markers *CCL5* and *CD8A*. This classification is slightly complicated by the expression of TRGC2 in both subsets as this is normally a marker of gamma delta T-cells (γδ T-cells) (Zakeri et al., 2022) and which could indicate that this cluster contains a fraction of contaminating gamma-delta T cells.

When we visualised proportions of cell groups across all conditions (Figure 20C), we observed that the cell percentages contributing to the cell type groups were homogenous across cohorts. This is especially true when we compare this data to the changes previously seen in the CSF dataset (Figure 14B and 17C). We calculated the percentage of cells that the different conditions contributed to each cell type (Supplementary Figure 6) which mostly showed variation in the AD Pathological Change and Non-AD Pathological Change groups that we mainly attribute to high variance because of the low donor numbers.

Next, we generated a UMAP for each condition accompanied by bar charts of cell type percentages in PBMC samples, split by individual and condition (Figure 21). Whilst all the conditions show minimal differences and are mostly homogenous between individuals and conditions, the AD Pathological Change donors have a larger myeloid compartment that takes up around 75% of their cells compared to around 25% in other conditions. Once again the low donor number in this cohort makes it difficult to rely on this result – which is not observed in the AD group. The Control and Non-Biomarker Control groups appear similar despite the individual variation that we see across all donors.

In summary, these data demonstrate that our PBMC samples contained all expected PBMC cell types identified in published single-cell RNA-seq PBMC data. We observed only minor cell type variations within conditions and cell type percentages were homogenous across condition cohorts. However, due to the myeloid cell changes observed in CSF data, we decided to investigate differential gene expression in the myeloid compartment.

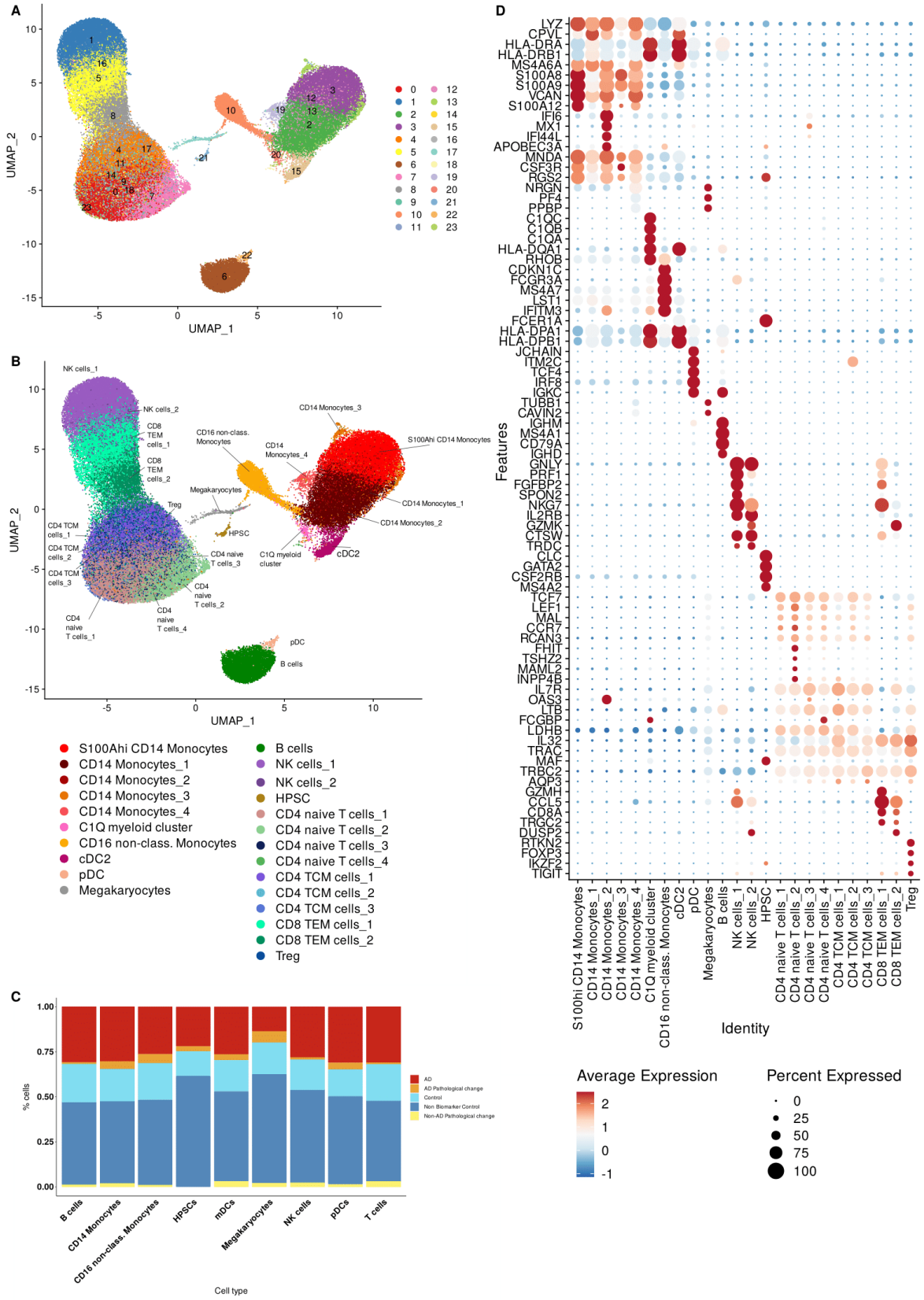
A
UMAP_2
UMAP_1
B
NK cells_1
NK cells_2
CD8 TEM cells_1
CD8 TEM cells_2
CD16 non-class. Monocytes
CD14 Monocytes_3
CD14 Monocytes_4
S100Ahi CD14 Monocytes
CD14 Monocytes_1
CD14 Monocytes_2
Megakaryocytes
Treg
HPSC
CD4 TCM cells_1
CD4 TCM cells_2
CD4 TCM cells_3
CD4 naive T cells_3
C1Q myeloid cluster
cDC2
CD4 naive T cells_2
CD4 naive T cells_1
CD4 naive T cells_4
pDC
B cells
S100Ahi CD14 Monocytes
CD14 Monocytes_1
CD14 Monocytes_2
CD14 Monocytes_3
CD14 Monocytes_4
C1Q myeloid cluster
CD16 non-class. Monocytes
cDC2
pDC
Megakaryocytes
B cells
NK cells_1
NK cells_2
HPSC
CD4 naive T cells_1
CD4 naive T cells_2
CD4 naive T cells_3
CD4 naive T cells_4
CD4 TCM cells_1
CD4 TCM cells_2
CD4 TCM cells_3
CD8 TEM cells_1
CD8 TEM cells_2
Treg
C
% cells
AD
AD Pathological change
Control
Non Biomarker Control
Non-AD Pathological change
B cells
CD14 Monocytes
CD16 non-class. Monocytes
HPSCs
mDCs
Megakaryocytes
NK cells
pDCs
T cells
Cell type
D
Features
Identity
Average Expression
Percent Expressed

Figure 20. PBMC analysis of all conditions. (A) UMAP representation and clustering of cells contained in main clusters 0-23. (B) UMAP showing cell types in PBMCs. (C) Plot of top 5 genes sorted by average log fold change assigned to each cell type.

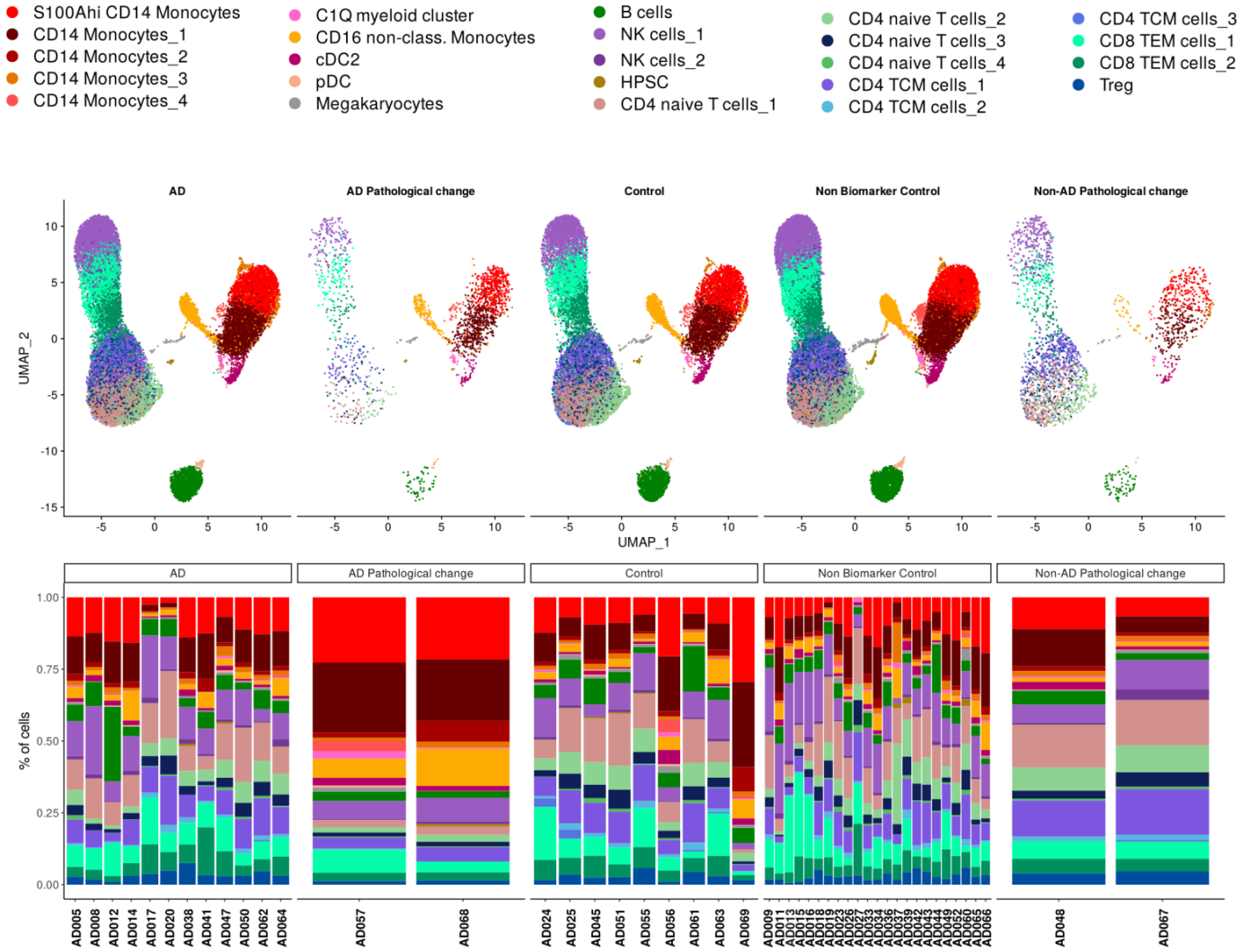

Figure 21. Comparison of cell type percentages in PBMC samples split by individual and condition.

5.2.3.2. Differential gene expression in PBMCs

To investigate the possibility that PBMCs in the AD cohort may contain DEGs which could indicate inflammatory pathways linked with AD, we subsetted cells from the myeloid cell clusters for the PBMC AD cohort and calculated differential gene expression against the control group. After removing any genes with an adjusted p-value above 0.05 we were left with ninety-five downregulated genes and only one upregulated gene.

We visualised the significantly expressed genes in the myeloid cell types (Figure 22) and despite the low numbers of DEG made several interesting observations. Firstly that there was only one upregulated gene (*AL365357.1),* but this was upregulated in four out of the seven myeloid clusters: S100A^{hi} CD14+ monocytes, CD14+ monocytes_1, CD14+ monocytes_4 and non-classical monocytes. This gene was previously identified in the CSF as upregulated in the Microglia-like myeloid subset and both CD4 TCM subsets. The gene is one of several pseudogenes for *RPS14* which encodes human ribosomal protein S14 (I. T. Chen et al., 1986). While the literature does not specifically link *AL365357.1* to AD, there are studies linking AD to other pseudogenes. One such study (Q. Liu et al., 2021), found high expression of the Pseudogene ACTBP2 in a murine AD model, increased KHDRBS2 transcription which in turn promoted HEY2 expression in cerebral microvascular endothelial cells and increased BBB permeability.

Another observation was the significant downregulation in the expression of 2'-5'-oligoadenylate synthetase 1 (*OAS1*) in the CD14+ monocytes_4 subset from the AD cohort. This is unexpected as *OAS1* is implicated as a risk gene for AD and transcripts of this gene increase in response to amyloid deposition in the brain tissue of transgenic mice (Salih et al., 2019). However, we did note that expression of this gene was upregulated ($p>0.05$) in the CD14+ monocytes_2 cells from the AD Pathological Change cohort (Figure 22). The *OAS1* gene is involved in the regulation of interferon response and the activation of viral RNA-degrading ribonucleases (Donovan et al., 2013; Lee et al., 2019). Interferon-related genes have been linked with ageing in murine studies and ‘interferon response microglia’ populations have been described in murine brain tissue (Sala Frigerio et al., 2019), however, their exact role in AD is not yet fully understood (Salih et al., 2019). Whilst we previously made

observations in the CSF regarding the expression of genes in our microglial subset related to inflammatory responses (see *5.2.2.3. Differential gene expression analysis shows upregulation of chemokine genes in Microglia-like myeloid subset*), it is not plausible to link this with the expression of *OAS1* in the PBMCs.

The C1Q myeloid cluster shows significant downregulation of the expression of Cathepsin B encoding gene *CTSB* in AD donors. The increased expression of the protein cathepsin B is associated in the CNS with cognitive dysfunction in AD (Hook et al., 2020). This doesn't fit with the downregulation we see in our C1Q myeloid cluster, however, altered levels of cathepsin B protein in the serum and PBMCs have been correlated with AD which may suggest that while there appears to be an association the exact nature of this is not yet clear (Morena et al., 2017; Sundelöf et al., 2010).

Taken together, it is difficult to present a unified picture of gene expression from this data. The upregulation of pseudogene *AL365357.1* in AD is not enough by itself to suggest a neurodegeneration linked inflammatory pathway, especially without any established precedent linking this specific pseudogene to any function or disease phenotypes. Meanwhile, expression of other significantly expressed genes such as *OAS1* and *CTSB* did not correspond with AD in line with published data.

As a result of low donor numbers in the AD Pathological Change, Non-AD Pathological Change, and the lack of full biomarker information in Non-Biomarker Control groups we decided to exclude these groups from all subsequent analyses. Instead, we placed our focus on identifying differences between the AD and Control groups in the cells of the peripheral immune system.

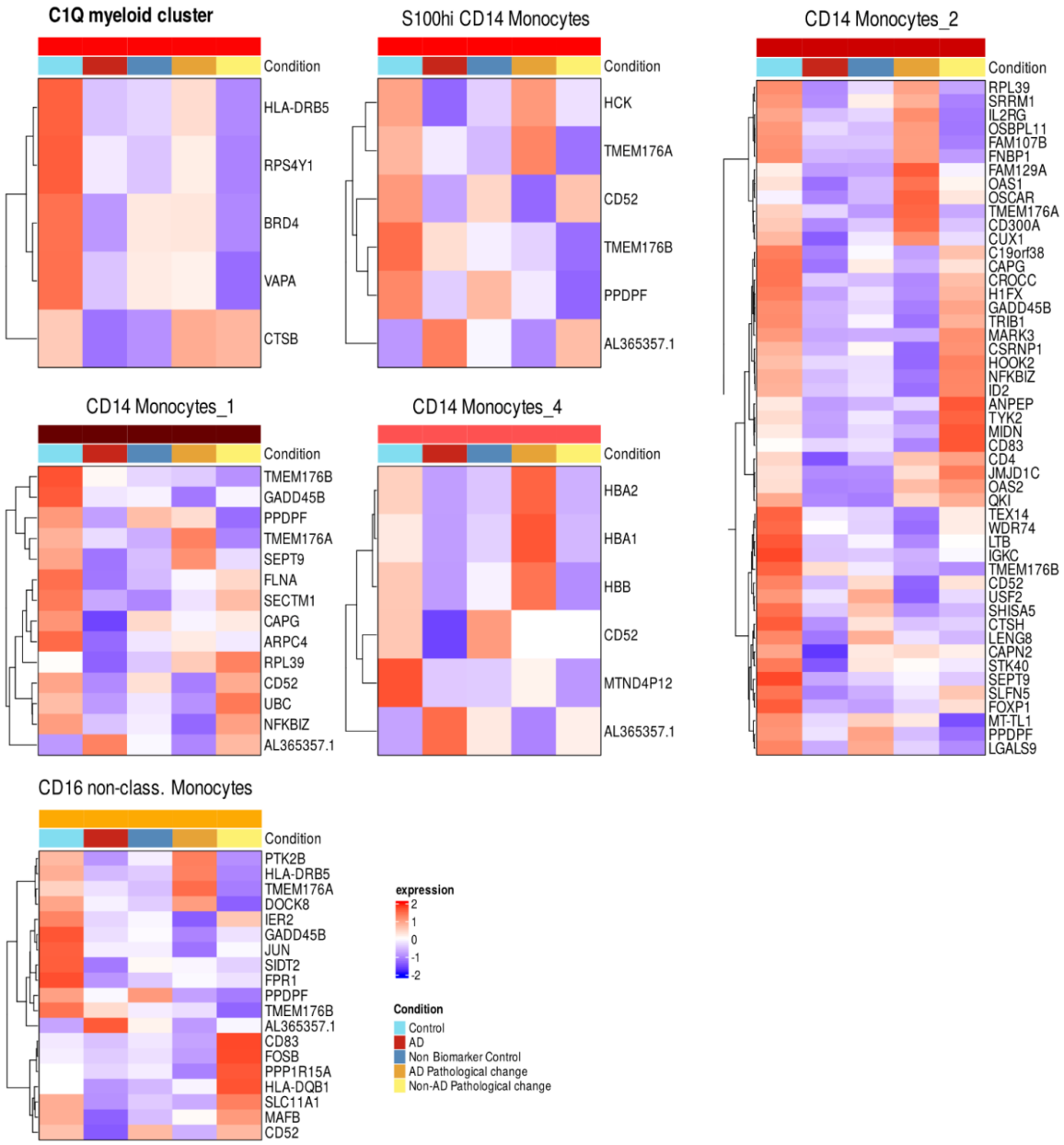

Figure 22. Heatmaps of DEG with an adjusted p-value <0.05 in the AD cohort PBMC myeloid clusters. Significantly expressed genes in AD cohort including expression levels of the same genes across all other conditions for comparison.

5.2.*3.3*. Characterisation of the immune cell compartment in the peripheral blood of AD donors

After excluding all conditions except the AD and Control groups, we ran a further analysis to identify if the two were transcriptionally distinct. The cell types remained the same 24 clusters as before, with the same annotation (Figure 23A/B). Visualisation of PBMC donor cell proportions between these conditions showed homogeneity across all cell type groups (Figure 23C).

A direct comparison of the AD and control groups shows minimal differences between the donors of the two groups (Figure 23D). The input of cells from these two conditions is variable, with more cells in the AD group due to their higher number of donors (AD= 29174; control= 18504).

The myeloid cell compartment fluctuates in size across all donors, but for most remains within the range of 25-30%. There are a few donors that are outside of this range: two control donors (AD056 and AD069) have a myeloid compartment expanded to 50-75% and two AD donors (AD017 and AD020) have a reduced compartment of <10%. Despite steps taken during the analysis to remove batch effects, this could still potentially be caused by technical bias introduced in the lab. Another possible explanation is that this could be a result of undetected conditions in these donors. Whilst we used a predetermined list of exclusion criteria (See *Methods: 4.1. Human specimens*) to exclude donors with known immune system alterations, some donors may have conditions that have not yet been detected in the clinic.

In summary, the reduction of the dataset to two conditions did not affect the number of cell types in the dataset or their annotations. However, it has also not revealed a clear difference between the cell type proportions which remain constant in both conditions. A closer look at the contributions of individual donors revealed minor fluctuations in the myeloid compartment of AD donors and two control donors with an expanded myeloid compartment. It was unclear whether this was due to a technical bias or unknown donor comorbidities which were not filtered by our clinical exclusion criteria. Overall, we did not observe strong hints pointing towards a distinct AD group. To validate this we decided to perform a more detailed statistical analysis.

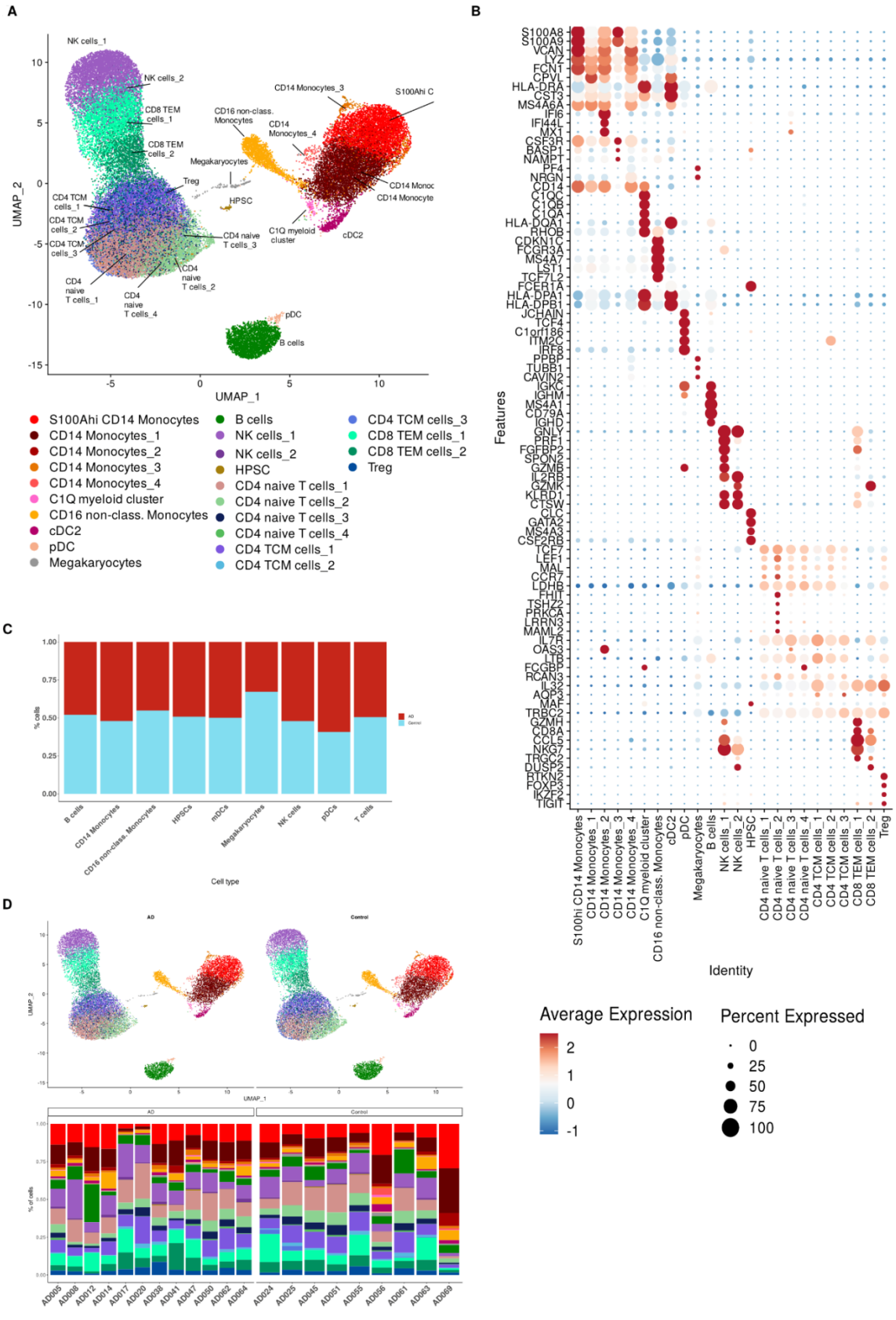
A
B
C
D
UMAP_1
UMAP_2
S100Ahi CD14 Monocytes
CD14 Monocytes_1
CD14 Monocytes_2
CD14 Monocytes_3
CD14 Monocytes_4
C1Q myeloid cluster
CD16 non-class. Monocytes
cDC2
pDC
Megakaryocytes
B cells
NK cells_1
NK cells_2
HPSC
CD4 naive T cells_1
CD4 naive T cells_2
CD4 naive T cells_3
CD4 naive T cells_4
CD4 TCM cells_1
CD4 TCM cells_2
CD4 TCM cells_3
CD8 TEM cells_1
CD8 TEM cells_2
Treg
Features
Identity
Average Expression
Percent Expressed
% cells
Cell type
AD
Control
% of cells

Figure 23. scRNA-seq analysis of PBMCs from AD and Control donors did not demonstrate differences in AD. (A) UMAP showing cell types in PBMCs. (B) Dotplot of the expression of top 5 marker genes for each cluster sorted by average log fold change assigned to each cell type. (C) PBMC donor cell proportions. (D) Comparison of cell type percentages in PBMC samples split by individual and condition.

5.2.3.*4*. Absence of significant cell type changes in PBMCs between control and AD donors

To verify the lack of cell type changes observed between the AD and control cohort in the PBMC dataset (Figure 23D) we used the single-cell compositional data analysis (scCODA) package (Büttner et al., 2021).

We first visualised the data across all conditions to get an overview of changes in all cohorts (Figure 24A). This again reflects the variation introduced by having low donor numbers in the AD Pathological Change and Non-AD Pathological Change cohorts. Whilst the AD Pathological Change shows a higher proportion of myeloid cells than the other conditions it isn't possible to statistically prove this without more donors in this group.

When we subsetted the data to AD and control donors to determine how AD influences the cell composition we observed that whilst visually there appears to be a slightly higher percentage of cells in the AD cohort for the S100A^{hi} CD14+ monocytes and CD14+ monocytes_1 cell types (Figure 24B), there is no statistically credible effect for any of the cell types. We used an FDR of 0.1 (the same as with the CSF dataset) and used the pDCs as the reference cell type. Even when we checked the data with a less conservative FDR of 0.3 there were still no credible effects in any of the cell types. This statistically confirms the lack of cell type changes in the PBMC dataset that has been observed so far. However, it is possible that an increased number of donors may be able to discern a trend that is not clear at this level.

A

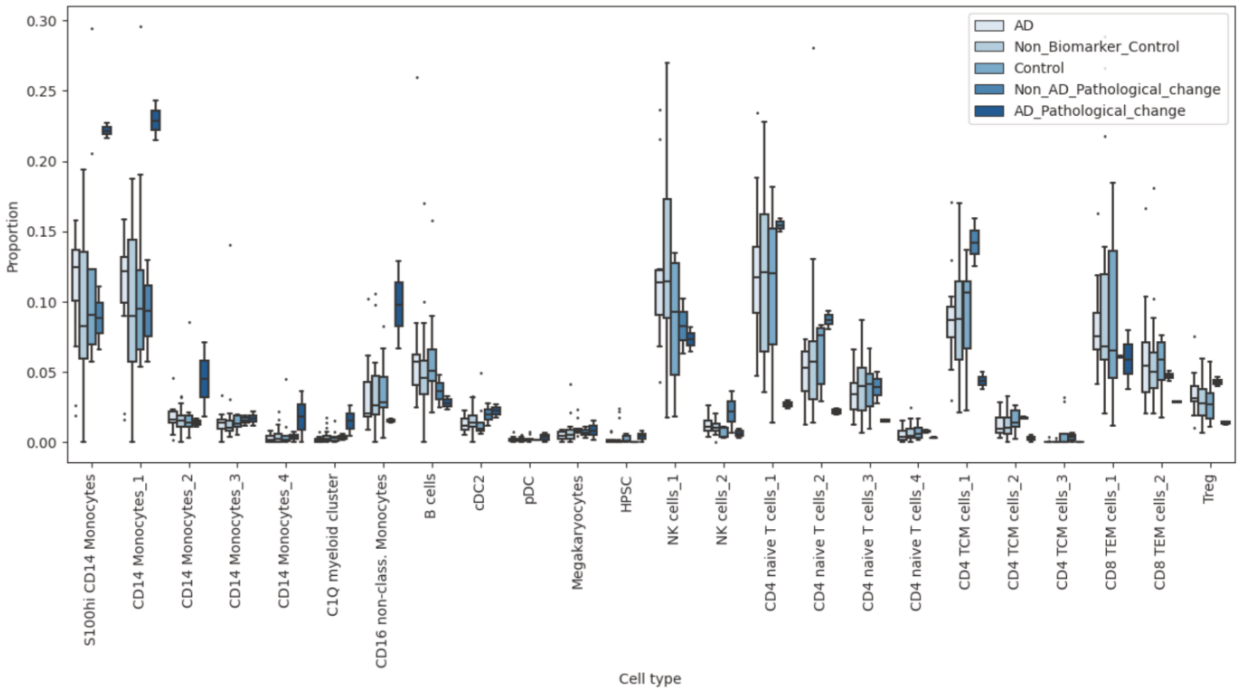
AD
Non_Biomarker_Control
Control
Non_AD_Pathological_change
AD_Pathological_change
Proportion
0.30
0.25
0.20
0.15
0.10
0.05
0.00
S100hi CD14 Monocytes
CD14 Monocytes_1
CD14 Monocytes_2
CD14 Monocytes_3
CD14 Monocytes_4
C1Q myeloid cluster
CD16 non-class. Monocytes
B cells
cDC2
pDC
Megakaryocytes
HPSC
NK cells_1
NK cells_2
CD4 naive T cells_1
CD4 naive T cells_2
CD4 naive T cells_3
CD4 naive T cells_4
CD4 TCM cells_1
CD4 TCM cells_2
CD4 TCM cells_3
CD8 TEM cells_1
CD8 TEM cells_2
Treg
Cell type

B

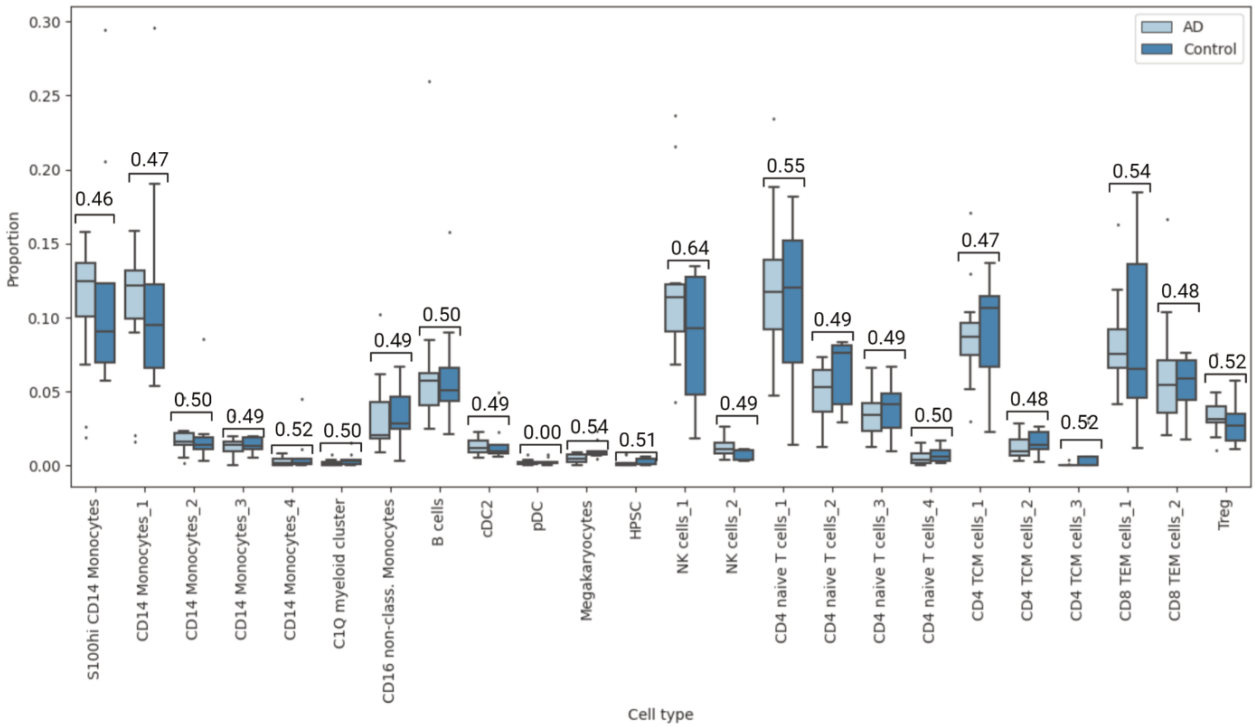
AD
Control
Proportion
0.30
0.25
0.20
0.15
0.10
0.05
0.00
0.46
0.47
0.50
0.49
0.52
0.50
0.49
0.50
0.49
0.00
0.54
0.51
0.64
0.49
0.55
0.49
0.49
0.50
0.47
0.48
0.52
0.54
0.48
0.52
S100hi CD14 Monocytes
CD14 Monocytes_1
CD14 Monocytes_2
CD14 Monocytes_3
CD14 Monocytes_4
C1Q myeloid cluster
CD16 non-class. Monocytes
B cells
cDC2
pDC
Megakaryocytes
HPSC
NK cells_1
NK cells_2
CD4 naive T cells_1
CD4 naive T cells_2
CD4 naive T cells_3
CD4 naive T cells_4
CD4 TCM cells_1
CD4 TCM cells_2
CD4 TCM cells_3
CD8 TEM cells_1
CD8 TEM cells_2
Treg
Cell type

Figure 24. PBMC analysis with scCODA. (A) scCODA results on all PBMC cell types (B) scCODA comparison of AD and control samples in PBMCs. (FDR =0.1).

6. Discussion

This project set out to investigate the relationship between the CNS and PIS in patients with AD. Specifically, we are interested in what can be learnt from scRNA-seq analysis of circulating immune cells in these systems and if a pathological event in the CNS such as AD can initiate detectable change in the PIS. Current interest in blood-borne biomarkers for AD suggests that there is potential for detectable biomarkers of PIS change (Fandos et al., 2017; Janelidze et al., 2021; Mielke et al., 2018). However, this work is mostly focused on measuring circulating levels of AD-associated proteins Aβ and tau-181, while a few recent studies focused also on inflammatory soluble markers (Brosseron et al., 2022) and only few have approached this at a single-cell level using flow cytometry or scRNA-seq. Where this has been approached at a single-cell level, the number of samples collected has been prohibitively low (H. Xu & Jia, 2021).

The analysis of existing scRNA-seq data on the peripheral immune response to AD (H. Xu & Jia, 2021) centred around T cells, with AD patients showing a significantly higher proportion of CD4+ T cells but a lower proportion of CD8+ T cells. The authors suggested their data implies adaptive PIS dysfunction in AD and that this could lead to worsening of conditions in the CNS. To some extent, this fits with existing work in the area of neuroinflammation such as spinal cord injuries where lymphocyte recruitment to the CNS has previously been observed with mixed effects (Kunis et al., 2013; Lun et al., 2015; Schwartz & Baruch, 2014).

The approach of profiling immune cells from the PIS and CNS side by side through the collection of CSF and PBMCs is also reasonably novel in AD. Gate *et al.* profiled PBMC and CSF immune cells from AD patients in a lymphocyte–orientated study that found increased CD8+ T_{EMRA} cells with enhanced T cell receptor (TCR) signalling in the PBMCs and clonally expanded CD8+ T_{EMRA} cells in the CSF (Gate et al., 2020). However, it is worth noting that the CSF and PBMC samples in this study were derived from different clinical cohorts and not observed in parallel from the same donors which could have provided a more holistic view. A murine study took a combined approach to elucidate links between the PIS and CNS when they modelled the effects of peripheral immune stimulation on the brains of mice with AD

pathology (Wendeln et al., 2018). Samples from the blood and cortex tissue were investigated with FACS and RNA-seq alongside other methods to show that inflammation in the PIS can shape the brain's immune response and reprogramme microglia for six months or potentially longer.

Therefore, the parallel collection of CSF and PBMC samples in humans is a novel approach to elucidating the relationship between the CNS and PIS in AD. The data we have gathered using this approach has offered new insight to the nuance of the myeloid cell compartment but has also highlighted some of the challenges of comparing data across sample types.

6.1. Preliminary data show transcriptional changes suggesting a dysfunctional PBMC compartment in AD

The Seq-well datasets in this study (both preliminary and final) showed all the major expected PBMC cell types but did not display robust cell type changes between the AD and control cohorts. When we explored transcriptional changes in this analysis only a handful of genes were highlighted as interesting but all of these could be linked with immune cell dysfunction. *HLA-DRA* was upregulated and encodes an HLA class II alpha chain paralogue which is part of the MHC (Dunne et al., 2020; J. Xu et al., 2020). Polymorphisms of *HLA-DR* genes have previously been cited as contributing to AD risk (Mansouri et al., 2015; Steele et al., 2017) and could suggest an elevated inflammatory signature in the PIS of these AD patients. This is supported by the other upregulated genes *LYZ* and *MALAT1. LYZ* encodes an enzyme called lysozyme which is mainly expressed in myeloid cells and upregulated in brain tissues and CSF of AD patients. Drosophila models suggest that this enzyme binds Aβ(1–42), reducing its toxicity (Sandin et al., 2016). *MALAT1* is part of the body's response to AD including the promotion of neurite growth and has been shown to play an anti-inflammatory role through the reduction of the pro-inflammatory cytokine TNF-α and induction of the anti-inflammatory mediator IL-10 (Ma et al., 2019). Meanwhile, *FTH1* and *SNHG5* were downregulated in AD compared to the control group. *SNHG5* is not related to AD but has

been linked with tumours (Pang et al., 2019) and pro-inflammatory roles in chronic obstructive pulmonary diseases (COPD) (Shen et al., 2020; W. Tang et al., 2016). *FTH1* encodes Ferritin Heavy Chain 1 which is a protein normally associated with intracellular iron storage (Rucker et al., 1996). Disrupted iron metabolism in the brain is a hallmark of AD (J. L. Liu et al., 2018; P. Wang & Wang, 2017) and causes oxidative stress reactions damaging both cells and their genetic material which in turn contributes to the formation of Aβ and NFT. The translation of *FTH1* is triggered by pro-inflammatory cytokines interleukin-1α (IL-1α) and interleukin-1β (IL-1β), which again links the inflammatory response to AD (Lumsden et al., 2018; Thomson et al., 2005). The dysregulation of iron metabolism is a theme we will return to later as it is something we also saw in the CSF-specific FTL^{hi} microglia subset in our Rhapsody dataset.

Based on this preliminary analysis and the concurrent technical improvements, we switched at this point in time to a commercial microwell system with higher sensitivity to confirm the observations we had made using the SeqWell-technology.

6.2. Blood monocytes trafficking through the CSF differentiate into microglia-like cells

The Rhapsody dataset was designed to collectively investigate the changes induced by AD from two perspectives: firstly through the CSF samples of the CNS and then peripherally from the PBMC samples of the PIS. The CSF samples demonstrated a baseline cell type composition that in healthy control samples matched data from the literature (De Graaf et al., 2011; Farhadian et al., 2019; Ransohoff & Engelhardt, 2012). Once a baseline composition was established it was possible to determine deviations from this that came from an expanded myeloid compartment and reduced lymphocyte compartment in AD. The driving force behind these changes appeared to be the CSF-specific Microglia-like myeloid cell subset which was significantly expanded in the AD patients. Next, we compared the gene signature from this subset with a range of myeloid cell expression signatures from the CNS gathered from current literature. The range of similar cell types included CSF-specific microglia (Esaulova et al.,

2020; Farhadian et al., 2019), AD-specific disease-associated microglia (DAM) (Keren-Shaul et al., 2017) and to a lesser extent monocyte-derived macrophages (Ochocka et al., 2021) and border-associated macrophages (Ochocka et al., 2021). However, the absence of well-expressed canonical macrophage genes as well as the knowledge that BAMs share transcriptional overlap with microglia suggested that this was not a macrophage cluster but is more likely to be a microglial cluster (Brioschi et al., 2020). Strong similarities with the CSF-specific microglia-like subsets described by Esaulova *et al.* and Farhadian *et al*., as well as the expression of canonical classical monocyte markers such as *CD14*, led us to speculate whether our CSF-specific Microglia-like myeloid cell subset could be "replacement microglia" derived from PBMC myeloid progenitors. Whilst homeostatic microglia in the brain parenchyma are widely known to originate from the fetal yolk sac (Ginhoux et al., 2010), recent work has developed a hypothesis for an alternative source under inflammatory conditions (Esaulova et al., 2020; Shemer et al., 2018). This hypothesis suggests that under stress conditions disruption of the BBB may allow the entry of blood-derived myeloid progenitors into the CNS where they take on the characteristics, morphology and to some extent the gene expression profiles of the native microglia. However, on this last point, Shemer *et al.* state that the transcriptional signature of these cells is still always distinguishable from the native microglia (Shemer et al., 2018). The migration of PIS immune cells through the BBB may be initiated by chemokine signalling from cells in the CNS. Esaulova *et al.* found chemokine receptors *CCR1, CCR5, CXCR4,* and *CX3CR1* on their CSF-specific microglia-like subsets (Esaulova et al., 2020). We found inflammatory C-C motif chemokine genes *CCL4, CCL3, CCL4L2,* and *CCL3L3* significantly upregulated in our Microglia-like myeloid subset. Unlike in Esaulova *et al.,* these genes encode chemokine ligands, not receptors. However, ligands encoded by *CCL3* and *CCL4* (aliases *MIP-1α* and *MIP-1β*) are known to act on receptor CCR5 which is expressed by microglia and monocytes and involved in both peripheral monocyte recruitment into the CNS and microglial migration towards Aβ plaques (Guedes et al., 2018). Meanwhile, *CCL3* expression is known to be increased by exposure of microglia to Aβ 1–42 aggregates (Heneka et al., 2015). Another perspective comes from a recent publication which found that individuals with AD or MCI exhibited CSF monocyte signalling to clonal CD8+ T cells via CXCL16-CXCR6 (Piehl et al., 2022). The study cites this as a possible mechanism for antigen-specific T cell entry into the CSF, which is different from our theory of monocyte

trafficking through the BBB but nonetheless provides another example of chemokines being used to attract peripheral cells into the CSF in cognitively impaired individuals. In summary, the Microglia-like myeloid cell subset in our data appears to be strongly implicated in the stress-induced recruitment of peripheral immune cells into the CNS.

Another parallel between the Microglia-like myeloid cell subset and the CSF microglia highlighted in Esaulova *et al*. is that both are characterised by strong expression of complement components genes (*C1QA-C*). As discussed in the introduction C1q genes encode the C1q subcomponent of the classical complement pathway (Gani, 2021; Schäfer et al., 2000) which becomes activated in response to antibody-antigen complexes binding with C1q to form a C1-complex (Gani, 2021). The presence of C1q genes does not reveal the origin of these cells as the complement system is active in both the CNS and PIS. However, it does support the idea that these cells are fulfilling an immune role linked to AD. For example, C1q proteins are localised in close proximity to Aβ plaques and in a murine study deletion of C1q genes resulted in reduced neuron damage from Aβ plaques possibly because complement-activated inflammation can exacerbate neuronal degeneration (Fonseca et al., 2004).

Whilst the increase in CSF S100A^{hi} CD14+ monocytes did not yet reach statistical significance, they do show an interesting marker expression profile which is distinct from the one seen in PBMC S100A^{hi} CD14+ monocytes. This signature has the typical markers of classical CD14+ monocytes but also contains the genes *TYROBP* and *CTSS.* These two genes are found in an AD-associated activated microglial signature (Keren-Shaul et al., 2017) and are also identified as having a high number of connections to other genes in the innate immune network expressed by amyloid-responsive microglia (Salih et al., 2019). If our "replacement microglia" theory is correct and our CSF-specific Microglia-like myeloid cell subset is derived from PBMC myeloid progenitors, then it might also be possible that the crossover we see between our CSF S100A^{hi} CD14+ monocytes and published AD-associated activated microglial signatures (Keren-Shaul et al., 2017) could represent an early transitory phase of these blood-derived monocytes towards microglia-like cells.

6.3. FTL^{+}Iba1^{+}TMEM119^{-}P2RY12^{-} microglia in CSF suggest dysregulated iron metabolism

The other microglial subset we found was transcriptionally distinct from the Microglia-like myeloid cell subset and was characterised by high expression of *FTL,* which encodes an iron storage protein, and *Iba1,* which is a marker of activated microglia. These FTL^{hi} microglia showed a marked similarity to a dysfunctional parenchymal microglia subtype in AD (Kenkhuis et al., 2021). Both our FTL^{hi} microglia and the published AD-associated microglial subtype have raised *FTL* and *Iba1* expression and lower *TMEM119* and *P2RY12* expression than homeostatic microglia. The expression of *FTL* in these microglia is interesting as ferritin has frequently been linked with AD (Bulk et al., 2018; Kenkhuis et al., 2021; J. L. Liu et al., 2018; Lumsden et al., 2018; Ward et al., 2014). This includes also our Seq-Well PBMC dataset, where we observed possible dysregulation of iron metabolism through the downregulation of *FTH1.* Here in the CSF, the mechanism is different as *FTL* is being expressed by microglia. Dysfunctional *FTL^{+}Iba1^{+}TMEM119^{-}P2RY12^{-}* microglia have a higher prevalence in AD patients and are thought to infiltrate Aβ plaques (Kenkhuis et al., 2021). To date, several theories have been put forward to explain FTL expression in these cells. Firstly, as *FTL* encodes a protein used in the cellular storage of iron, any increase in its expression is likely to indicate a change in intracellular levels of iron (Kenkhuis et al., 2021). The brain uses iron for a range of processes including metabolism, oxygen transportation, mitochondrial respiration and synthesis of DNA, myelin and neurotransmitters (Ward et al., 2014). Even in healthy brains accumulation and binding of iron via ferritin have been shown to occur with age, the difference in neurodegenerative pathologies like AD is that this accumulation is reported to be more substantial and region-specific (Ward et al., 2014). In AD intracellular iron increases may occur in response to increased blood-brain barrier permeability or misformation of myelin sheaths around axons (Bulk et al., 2018; Ward et al., 2014). Another hypothesis for the expression of FTL may be as a response to inflammation as ferritin is recognised as an acute-phase reactant (APR) and *FTL* could be part of a stress response after the microglia have interacted with Aβ (Streit et al., 2018). In the context of our dataset, this would imply that these microglia have already encountered a stress event in the parenchymal tissues, become

activated and are afterwards found in the CSF. The issue with this theory is that our subset of these cells shows no change between condition groups and is present in the CSF of our control cohort at similar levels to the AD cohort. Furthermore, only one instance of significant differential gene expression occurred in this cell type, which was the downregulation of human leukocyte antigen gene *HLA-DRB5* in AD. If these cells are, as speculated, responding to an inflammatory stimulus then it seems counterintuitive that a key inflammatory gene responsible for antigen-presentation is being significantly downregulated. This is also incongruous with the subset's expression of complement component 3 gene (*C3*) which is a central part of all three complement system activation pathways (Gani, 2021). *C3* is also one of the genes this subset has in common with a signature for CSF-associated microglia-like cells in HIV patients (Farhadian et al., 2019), which helps confirm the identity of this subset as CSF microglia with links to neuroinflammation.

6.4. Depletion of lymphocytes in the CSF of AD patients

Beyond the changes in the myeloid cell type composition, the CSF data also exhibited significant decreases in the two CD4+ TCM cell subsets and the two CD8+ TEM cell subsets. However, significant differential expression in these groups was limited to upregulation of the pseudogene *AL365357.1* in the CD4+ TCM subsets and Inhibitor of DNA Binding 2 *(ID2)* in the CD8+ TEM_1 subset. Initially, we speculated that this cell type depletion in AD was only occurring relative to increases in the myeloid compartment, yet scCODA confirmed the statistical robustness of these changes. If they represent real biological change this would be a direct contrast with current literature, which comprehensively describes T cell recruitment and trafficking into the CNS in AD and other neurological conditions (Gate et al., 2020; Heneka et al., 2015; Kunis et al., 2013; Lun et al., 2015; Pietronigro et al., 2016; Schwartz & Baruch, 2014).

A flow cytometry-based study into the distribution of immune cells in the CSF reported reductions in CD8+ and CD4+ TCM cells in all dementia types investigated, bhut increased numbers of CD8+ and CD4+ TEM cells in patients with AD compared to age-matched healthy

controls (Busse et al., 2021). However, what they suggest is a transition from central memory T cells to effector T cells, which still does not align with our findings of total lymphocyte depletion in AD CSF, and so a technical or biological explanation for this observation is still needed.

6.5. No statistically verifiable changes in the cell type composition of the PBMC compartment of AD donors

The collection of circulating peripheral immune cells for the purpose of investigating neurodegenerative disease through scRNA-seq analysis presents significant challenges. Firstly, the volume of cells found in the five litres of blood that circulate through the PIS of the average human is vast in comparison to the average volume of cells within the CNS circulating CSF. This makes the task of identifying crosstalk between these two systems much easier in the CSF than in the PIS. Secondly, the trafficking of immune cells from the PIS into the CNS is a well-documented phenomenon (Kunis et al., 2013; Lun et al., 2015; Ransohoff & Engelhardt, 2012; Schwartz & Baruch, 2014; Shechter & Schwartz, 2013), however, travel in the other direction is more difficult to show. There are some accounts of memory T cells crossing into the CSF and then returning to the PIS via the subarachnoid space and deep cervical lymph nodes if no antigen is detected (Ransohoff & Engelhardt, 2012), but most pathology-driven research focuses on entry into the CNS.

Overall, we found no statistically significant changes in cell type composition between AD and healthy controls. And whilst there were hints of cell type changes occurring in the myeloid and T cell compartments of the AD Pathological Change cohort, the size of our study means that we did not have sufficient numbers of AD Pathological Change donors to make a statistically valid comparison. This lack of statistically verifiable cell type change in AD does not necessarily mean that these changes are not occurring, as the number of current studies to identify blood-borne protein biomarkers for AD certainly suggest that this is possible. However, our data suggest that identifying gene markers for this in the blood requires a very

large cohort with comprehensive metadata in order to control for the high individual variation that comes with this type of human dataset.

Despite this absence of statistically verifiable change, we did observe several changes that whilst they did not meet the threshold for significance, may hint at future areas of interest. For example, the small increase in S100A^{hi} CD14+ monocytes in the PBMCs of the AD cohort could be interesting as their low expression of HLA-DR genes could be a sign of dysfunctional monocytes with reduced response to stimuli (Schulte-Schrepping et al., 2020; Veglia et al., 2018; Venet et al., 2021). However, it should be kept in mind that this study recruited patients with a median age of sixty-nine, so there are many possible causes for inflammation and dysfunction in the PBMC compartment. A high threshold of evidence is required to directly link this to neurodegeneration, which we do not have here. This is also true for our finding of a C1Q myeloid cluster in the PBMCs. Whilst this cluster suggests a strong capacity for antigen presentation through the high expression of complement components (*C1QA-C*) and HLA class II genes (*HLA-DPA1, HLA-DPB1, HLA-DQA1, HLA-DQB1, HLA-DRA* and *HLA-DRB1*), it shows no change in AD patients and so cannot yet be directly linked to AD. Especially as an increase in background inflammation is expected in an elderly cohort in accordance with the theories of immunosenescence and inflammaging (Alberro et al., 2021; Barbé-Tuana et al., 2020; Furman et al., 2019).

In summary this scRNA-seq analysis presented significant challenges in terms of signal sensitivity in large blood volumes and a lack of prior work documenting immune cell trafficking from the CNS to the PIS. Overall, we saw no statistically significant change in cell type composition between AD and healthy controls. However, it is possible that further, more comprehensive study of an AD Pathological Change cohort could uncover myeloid and T cell disease related-variation.

6.6. Comparison of PBMC and CSF data suggests crosstalk between these systems

Evidence of crosstalk between the CNS and PIS in our datasets is limited to one direction: PIS to CNS. Arguably any presence of peripheral immune cells in the CNS represents crosstalk between the two systems because these cells are not native to this environment (Ransohoff & Engelhardt, 2012). However, we can go further than this and speculate that the expression of chemokines we see from the CSF-specific Microglia-like myeloid cell subset could be suggestive of peripheral immune cell recruitment into the CNS. Especially, when we combine this information with the presence of S100A^{hi} CD14+ monocytes in the CSF which show expression of genes which are normally found in AD-associated activated microglia (Keren-Shaul et al., 2017).

The cell types found in these compartments are not identical and we observed key cell type differences in line with what has been reported in the literature. The PBMC compartment has a much higher variety of immune cells than the CSF, where cell types such as naïve T cells, non-classical monocytes, megakaryocytes and NK cells are absent. Meanwhile, the CSF includes CNS-specific cells such as microglia and contains an S100A^{hi} CD14+ monocyte group which is transcriptionally distinct from the one seen in PBMCs.

Transcriptional changes in the PBMC compartment relating to AD have been difficult to elucidate. However, the data has possible clues for a peripheral inflammatory component of AD which may be worth further investigation. The minor increase ($p>0.05$) in S100A^{hi} CD14+ monocytes in the PBMCs of the AD cohort would be a good starting point for this. A larger AD cohort size is key here, but it would also be beneficial to expand the AD Pathological Change cohort as the limited data we have here hinted at a higher proportion of myeloid cells than the other conditions. If this were to be validated it could point to an early peripheral inflammatory response. A murine study that used peripheral immune stimuli to trigger long-term immune training and tolerance in the brain suggests that this training can worsen the Aβ burden in AD (Wendeln et al., 2018). If this model were also valid in humans then prodromal and MCI groups could offer valuable insight into the contribution of the PIS to AD.

6.7. Comparison of BD Rhapsody and Seq-Well technology suggests a choice between sensitivity and cost

During the course of this study, we utilised two different scRNA-seq technologies, transitioning from preliminary data collection via the Seq-Well technique (Gierahn et al., 2017) to the commercial BD Rhapsody platform (Chang et al., 2019) where we collected a more extensive dataset. These methods are both microwell-based and use UMI barcoded beads to capture RNA from individual cells in picolitre wells. Neither technique produces full-length transcripts, Seq-Well captures only the 3'-end whilst the Rhapsody protocol BD gets fragment cDNA by priming at random points along the length of synthesised first-strand cDNA. The time required for the initial capture and transcription of RNA is less with the Rhapsody. Especially when you take into account the isolation steps prior to this which are greatly reduced in the Rhapsody workflow as flow cytometric enrichment is not a prerequisite to the process. This is especially an advantage when working with CSF samples where cell populations are smaller than in peripheral blood and the increased stress on cells during flow cytometry can greatly reduce cell numbers available for scRNA-seq. The time required for library preparation is similar in both technologies.

Detection of cell types was assessed through a comparison of PBMC data as this was collected on both technologies. Both methods reliably detected the major cell types in the PBMC compartment, and it should be taken into account that differences in cell types identified may also be due to the different sensitivity of the technologies or the subsequent analysis strategies as e.g. the clustering resolutions that were set in Seurat during the analysis of these datasets were different (Seq-Well = 0.5 and Rhapsody = 0.9). There are two key differences in cell types detected, firstly Seq-Well identified a neutrophil cluster that was not seen in the Rhapsody data and secondly the Rhapsody identified a C1Q myeloid cluster that was absent in the Seq-Well data. The loss of a granulocyte compartment in our Rhapsody data may however be explained by the frozen storage of samples used in Rhapsody experiments. In general, the Rhapsody was able to detect more UMIs and genes per cell, however, Seq-Well technology has lower costs per cell.

6.8. Summary

The work performed in the scope of this study aimed to advance our understanding of the relationship between the CNS and PIS on a transcriptional and single-cell level. With this in mind, we investigated the immune cell compartments of blood and CSF from different healthy and pathological cohorts both independently and, where possible, in parallel. This investigation occurred across two single-cell technologies providing different perspectives which were largely in agreement yet still highlighted the unique advantages and disadvantages of these methods. The datasets generated describe shifts in the CSF myeloid compartment of AD suggestive of inflammation-triggered recruitment from the PIS into the CSF. Here, blood-borne myeloid progenitors transition into a Microglia-like myeloid cell subtype that imitates the characteristics, and to some extent the gene expression profiles of native microglia. This is supported by existing studies into AD-specific disease-associated microglia, CNS immune stimulation and neuroinflammatory conditions and which have observed transcriptionally similar cells (Esaulova et al., 2020; Keren-Shaul et al., 2017; Shemer et al., 2018). We speculate that the final destination of these migrating “replacement microglia” is the brain parenchymal tissues where their assistance is required in the clearance of toxic Aβ plaques. Determining the entry points for these cells is difficult as whilst the literature records several routes into the CNS for peripheral immune cell recruitment (Kunis et al., 2013; Lun et al., 2015; Ransohoff & Engelhardt, 2012; Schwartz & Baruch, 2014; Shechter & Schwartz, 2013), this can only be definitively confirmed through analysis of CNS barrier structures which was outside the scope of this study.

We also identified a subset of potentially dysfunctional CSF-specific microglia (*FTL*$^{+}$*Iba1*$^{+}$*TMEM119*$^{-}$*P2RY12*$^{-}$), that appear to be strongly linked to iron metabolism which is known to be dysfunctional in AD (Bulk et al., 2018; Ward et al., 2014). However, we were not able to link this subset directly with our AD cohort and observed no change in cell type composition in relation to this.

Concomitantly, we observed a depletion of lymphocytes in CSF of AD patients and validated this through statistical analysis. This was contradictory as the established literature describes T cell recruitment and trafficking into the CNS in AD and other neurological conditions (Gate et al., 2020; Heneka et al., 2015; Kunis et al., 2013; Lun et al., 2015; Pietronigro et al., 2016; Schwartz & Baruch, 2014).

Furthermore, we found no statistically verifiable changes in cell type composition between AD and healthy controls in the PBMC compartment. However, given that current research interest in elucidating blood-borne biomarkers is high, we suggest that AD-related changes in the PIS are possible but in this instance, transcriptional identification is limited by cohort size and insufficient metadata collection.

6.9. Future perspectives

On the whole, this study adds to our understanding of the involvement of the immune system in AD on a systemic level, by providing single-cell information on immune cells in two major compartments, the CSF and peripheral blood. However, through this study, we also learned more about the challenges and limitations involved in this task. Elucidating PIS change related to CNS pathologies requires the generation of datasets with a much larger number of samples to find statistically robust patterns. Which in turn is expensive and time-consuming and produces datasets that contain challengingly high background variation and require enormous computing power. These challenges are not insurmountable, current developments in machine learning are opening up novel analysis pathways and the rise of memory-driven computing represents a future-driven approach to computational power that could help overcome these hurdles. High sample number requirements can be fulfilled through studies such as the Rhineland study which aims to recruit a large cohort of donors (>10,000) and a wide array of data including PBMC samples over a long time period. Similarly, many researchers are taking a collaborative approach and working in multi-country consortia to accumulate larger datasets. A recently published GWAS study used samples from almost

800,000 participants across 15 European countries by bringing together ten different European GWAS consortia (Bellenguez et al., 2022).

The increasing capacity of scRNA-seq technologies to take a varied multi-omics approach offers fresh opportunities to expand datasets like the one we present here. Possibilities include BD AbSeq which would add protein expression using the same platform already in use here, or epigenetic techniques like scNMT-seq which combines chromatin accessibility, DNA methylation and scRNA-seq (Clark et al., 2018). Meanwhile, the analysis of CNS barrier structures and parenchymal tissues with spatial technologies could help determine peripheral immune cell entry points into the CNS and advance our understanding of the relationship between these environments.

In summary, this study found that scRNA-seq offers a unique perspective on the immune landscape in AD. The relationship between the PIS and CNS is much closer than originally thought and thorough characterisation of this in early AD stages could be the key to deciphering the progression and pathogenesis of this disease.

7. Supplementary figures

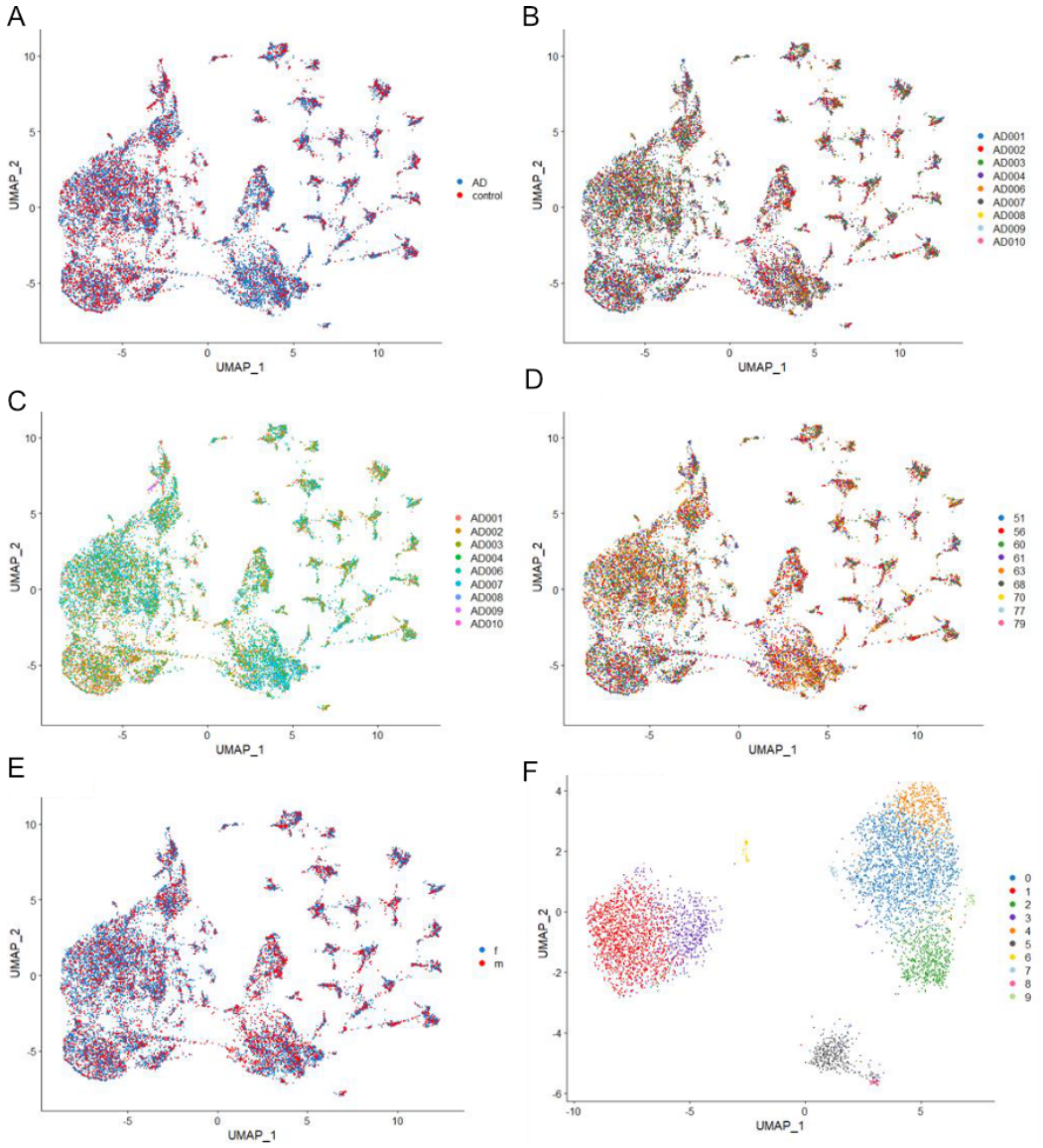

Supplementary figure 1. Further characterization of the dataset AD001-AD010. UMAP representations of cells in the dataset AD001-AD010 (A) Alzheimer's Disease (AD) and Controls; (B) Donors; (C) Sequencing pools; (D) Age of each donor [years]; (E) Gender: F = Female, M = Male (F) UMAP representation of AD001-AD010 after increasing Seurat's feature threshold to a minimum of 150 features per cell.

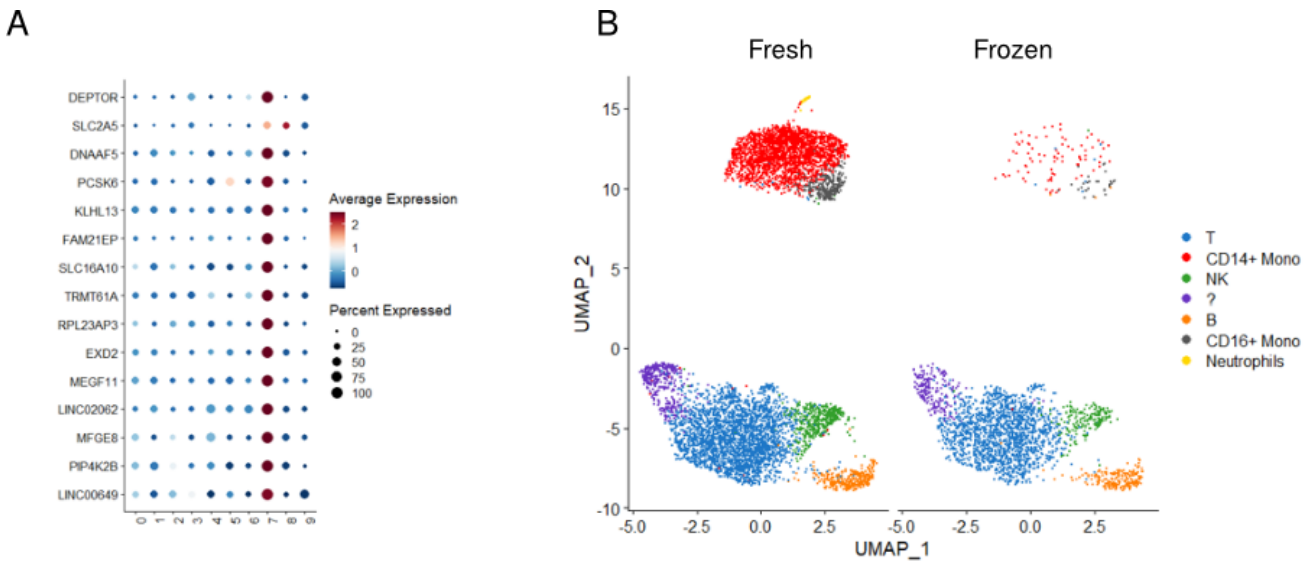

Supplementary figure 2. Investigation of AD019-AD020 (related to Figure 8). (A) Dotplot displaying the marker genes of cluster 7, part of UMAP visualization of the integrated datasets AD001-AD020 (Figure 2A). (B) UMAP representation of AD019-AD020, divided into the state of the sample: fresh vs. frozen.

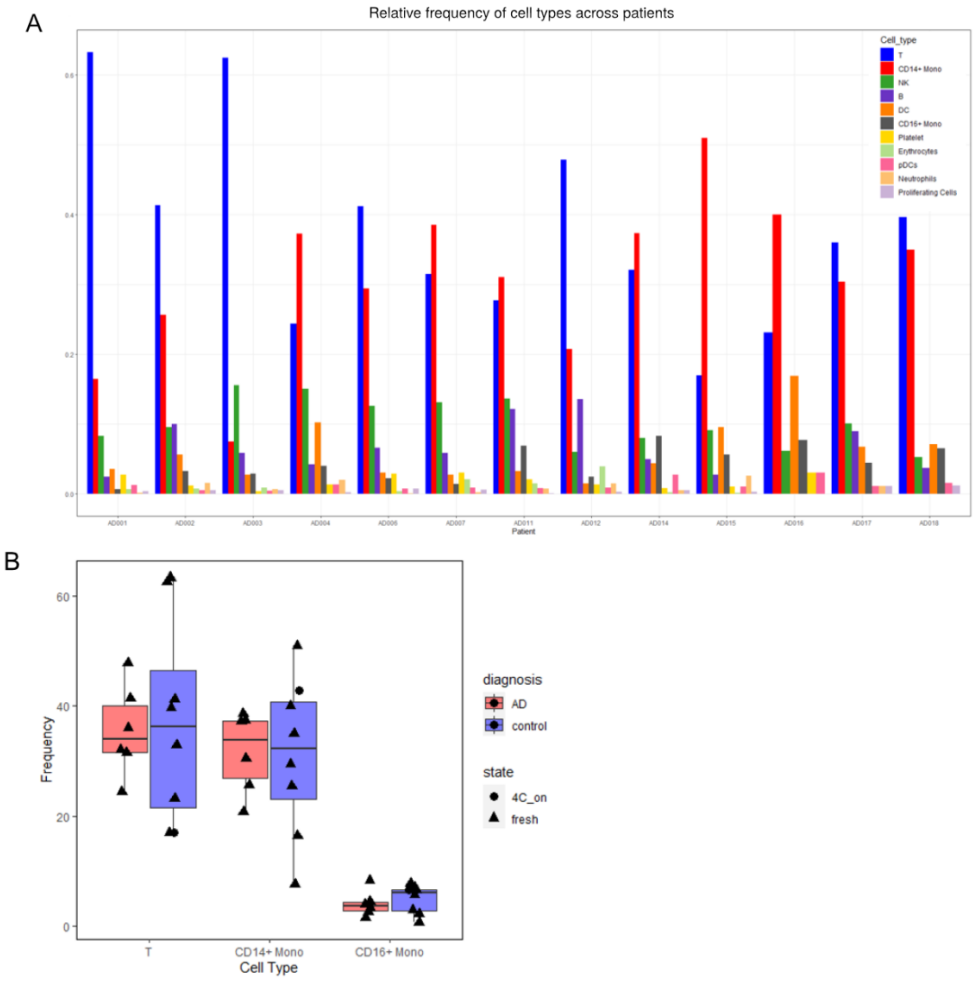

Supplementary figure 3. Cell type frequencies of the final dataset. Frequency of cell types in the integrated dataset AD001-AD008 and AD011-AD018. (A) Bar plot displaying the relative frequency of cell types across all donors. (B) Box plot highlighting the frequency [%] of T cells, CD14+ Monocytes and CD16+ Monocytes in AD and control. Each triangle represents a donor PBMC sample, which was sequenced fresh, each dot represents a donor PBMC sample which was stored at 4°C overnight.

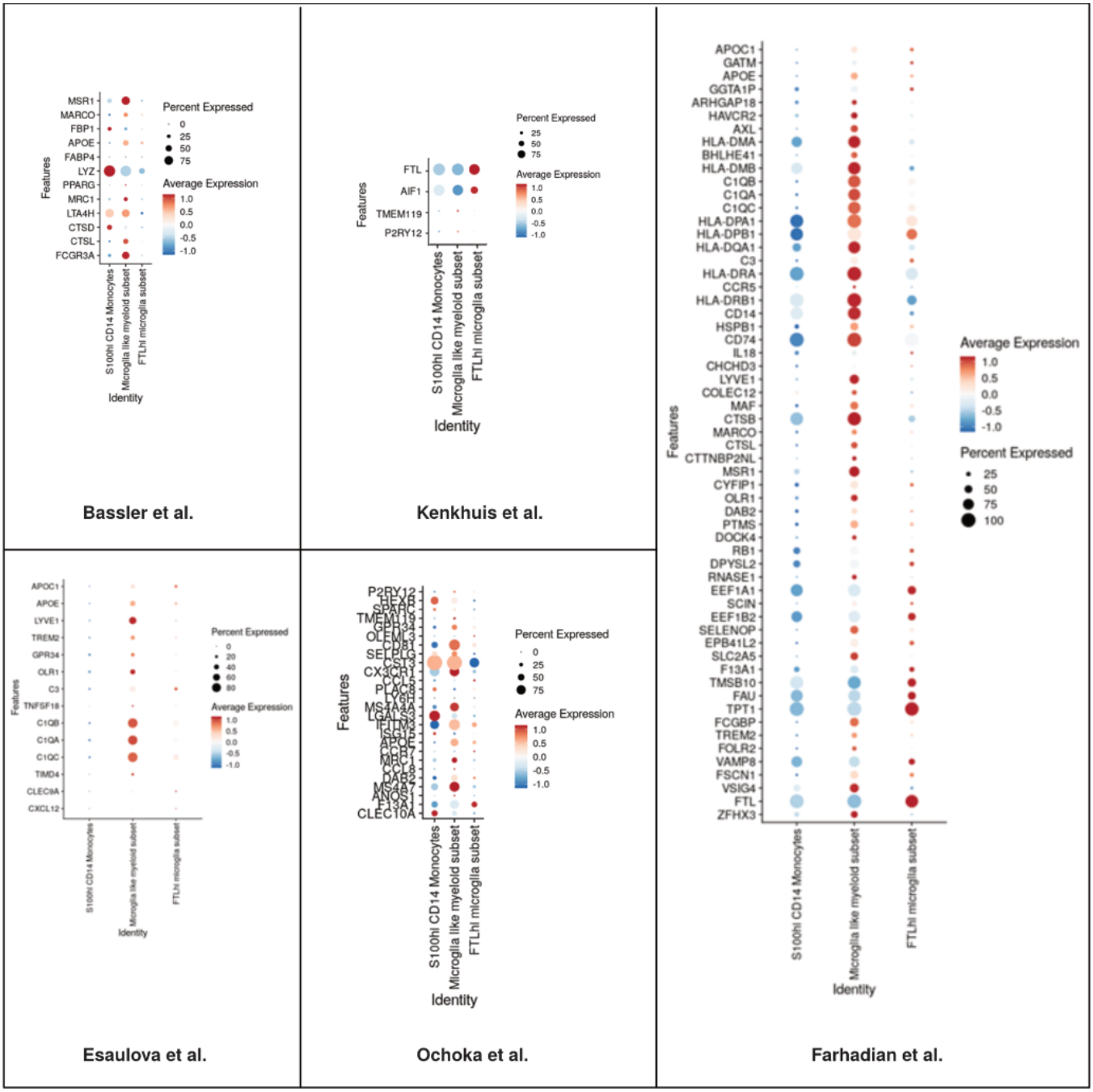

Supplementary figure 4. Identifying myeloid clusters through comparison with genes in literature. CSF based cell type marker genes taken from five publications and analysed for their expression in three CSF data myeloid clusters.

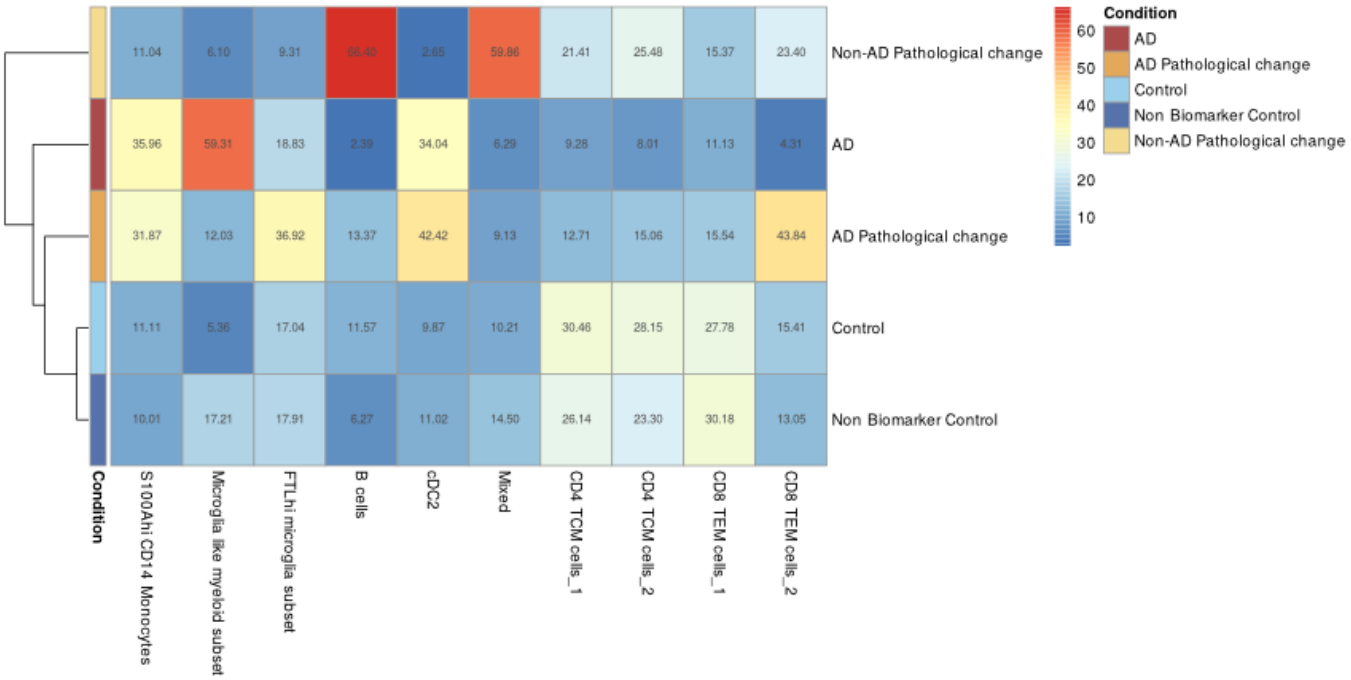

Supplementary figure 5. CSF percentage of cells per cohort. Percentage of cells contributed to each cell type by each condition in the CSF dataset.

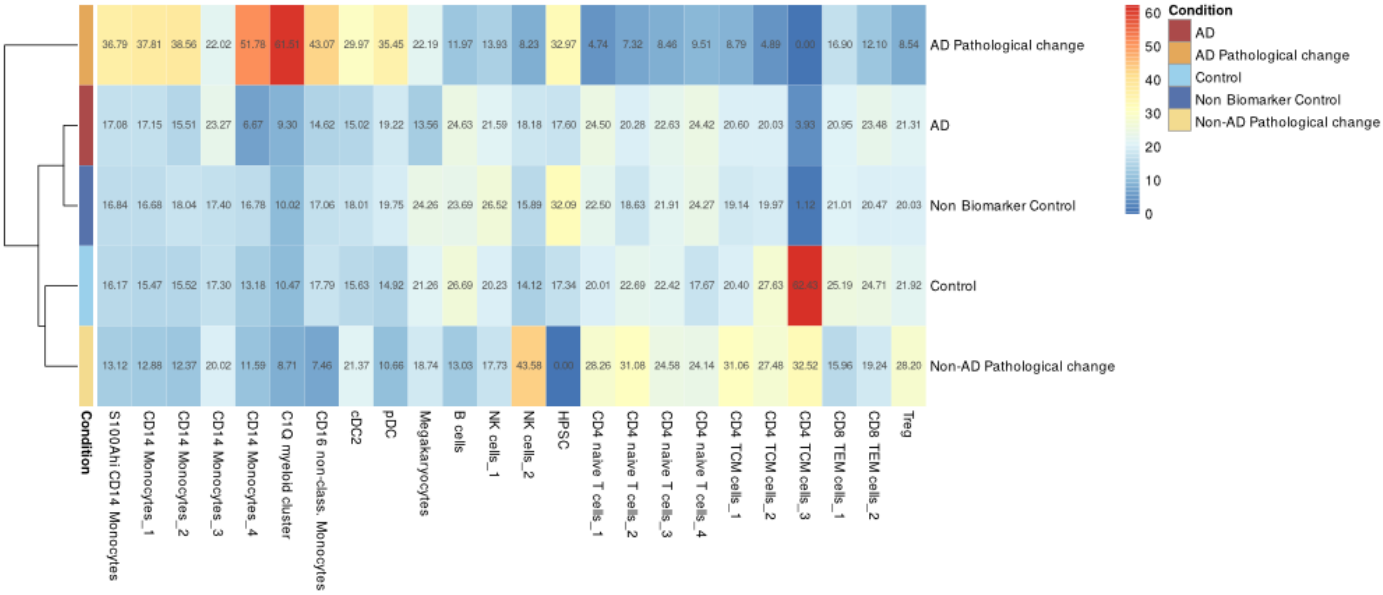

Supplementary figure 6. PBMC percentage of cells per cohort. Percentage of cells contributed to each cell type by each condition in the PBMC dataset.

Supplementary figure 7. Biomarkers for AT(N) classification of all donors

Internal ID	Information from Clinic						AT(N) Classification					
	Aß	Aß42/40-ratio	tau	p-Tau	Aß42/pTau	Diagnosis	**A** Aß42/40	**T** p-tau-181	**N** t-tau	ATN status	Biomarker category	AD Continuum
AD001												
AD002	n	p	p	p	p	AD	+	+	+	ATN	AD	Yes
AD003												
AD004	n	p	p	p	p	AD	+	+	+	ATN	AD	Yes
AD005	n	p	p	p	p	AD	+	+	+	ATN	AD	Yes
AD006												
AD007	p	p	p	p	p	AD	+	+	+	ATN	AD	Yes
AD008	n	p	p	p	n	AD	+	+	+	ATN	AD	Yes
AD009												
AD010												
AD011												
AD012	n	p	p	p	p	AD	+	+	+	ATN	AD	Yes
AD013												
AD014	n	p	p	p	p	AD	+	+	+	ATN	AD	Yes
AD015												
AD016												
AD017	p	p	n	p	p	AD	+	+	-	ATn	AD	Yes
AD018												
AD019												
AD020	p	p	n	p	p	AD	+	+	-	ATn	AD	Yes
AD022	n	n	n	n	n	Not AD	-	-	-	atn	Normal AD Biomarkers	No
AD023												
AD024	p	n	n	n	n	Not AD	-	-	-	atn	Normal AD Biomarkers	No
AD025	n	n	n	n	n	Not AD	-	-	-	atn	Normal AD Biomarkers	No
AD026												
AD027												
AD028												
AD029												
AD030												
AD031												
AD032												
AD033												
AD034												
AD035												
AD036												
AD037												

AD038	p	p	p	p	p	AD	+	+	+	ATN	AD	Yes
AD039												
AD040												
AD041	p	p	p	p	p	AD	+	+	+	ATN	AD	Yes
AD042												
AD043												
AD044												
AD045	p	n	n	n	n	Not AD	-	-	-	atn	Normal AD Biomarkers	No
AD046	n	p	p	p	p	AD	+	+	+	ATN	AD	Yes
AD047	n	p	p	p	p	AD	+	+	+	ATN	AD	Yes
AD048	n	n	p	p	p	Not AD	-	+	+	aTN	Non-AD Pathological change	No
AD049												
AD050	n	p	p	p	n	AD	+	+	+	ATN	AD	Yes
AD051	p	n	n	n	n	Other dementia	-	-	-	atn	Normal AD Biomarkers	No
AD052												
AD055	n	n	n	n	n	Not AD	-	-	-	atn	Normal AD Biomarkers	No
AD056	n	n	n	n	n	Not AD	-	-	-	atn	Normal AD Biomarkers	No
AD058	p	p	n	n	n	Other dementia	+	-	-	Atn	AD Pathological change	Yes
AD059												
AD060												
AD061	n	n	n	n	n	Not AD	-	-	-	atn	Normal AD Biomarkers	No
AD062	p	p	p	p	p	AD	+	+	+	ATN	AD	Yes
AD063	p	n	n	n	p	AD	-	-	-	atn	Normal AD Biomarkers	No
AD064	-	p	p	p	p	AD	+	+	+	ATN	AD	Yes
AD065												
AD066												
AD067	p	n	p	p	n	Not AD	-	+	+	aTN	Non-AD Pathological change	No
AD068	p	p	n	n	p	AD	+	-	-	Atn	AD Pathological change	Yes
AD069	n	n	n	n	n	Not AD	-	-	-	atn	Normal AD Biomarkers	No
AD070	p	p	p	p	p	AD	+	+	+	ATN	AD	Yes
AD071	p	n	p	n	n	Not AD	-	-	+	atN	Non-AD Pathological change	No
AD072	p	p	p	p	p	AD	+	+	+	ATN	AD	Yes
AD073	p	n	p	p	n	AD	-	+	+	aTN	Non-AD Pathological change	No

8. Acknowledgments

First and foremost I am extremely grateful to my supervisors, Prof. Joachim Schultze and Priv.-Doz. Dr. Marc Beyer for their invaluable advice and continuous support during my PhD study. Both of them have cultivated cutting-edge working groups and it has been my privilege to work in this fantastic and innovative environment for the last few years.

A special thank goes to Dr. Anna Drews for supervising me through the final year of my PhD and supporting me through the thesis writing process. I would also like to thank Dr. Elena De Domenico, Dr. Kristian Händler, Dr. Humberto Ferreira and Dr. Simone Picelli for their support along the way.

Furthermore, I would like to thank all present and past members of the Schultze and Beyer labs for their kind help and support which have made my studies in Bonn such a positive time. In particular, Dr. Maren Büttner for her help setting up scCODA analysis, Marius Jentzsch for his excellent work on the Seq-Well analysis and Jonas Schulte-Schrepping for his constant bioinformatics advice. Thanks also to the PRECISE team whose amazing technical support solved many problems along the way.

Thanks to all the collaborators that contributed to this project, especially Prof. Anja Schneider and the teams at the Klinik für Neurodegenerative Erkrankungen und Gerontopsychiatrie and DZNE Biorepository. Also, thanks to all the patients, without whom this work wouldn’t have been possible.

I would like to express my gratitude to my family and friends. A special mention goes to Dr. Iraad Bronner and Dr. Stephan Lorenz, whose belief in me helped start this journey. Finally, my incredible partner Bryony whose understanding and encouragement over the past few years have been indispensable.

9. References

Aibar, S., González-Blas, C. B., Moerman, T., Huynh-Thu, V. A., Imrichova, H., Hulselmans, G., Rambow, F., Marine, J. C., Geurts, P., Aerts, J., Van Den Oord, J., Atak, Z. K., Wouters, J., & Aerts, S. (2017). SCENIC: Single-cell regulatory network inference and clustering. *Nature Methods*, *14*(11), 1083–1086. https://doi.org/10.1038/nmeth.4463

Akıncıoğlu, H., & Gülçin, İ. (2020). Potent Acetylcholinesterase Inhibitors: Potential Drugs for Alzheimer's Disease. *Mini-Reviews in Medicinal Chemistry*, *20*(8), 703–715. https://doi.org/10.2174/1389557520666200103100521

Alberro, A., Iribarren-Lopez, A., Sáenz-Cuesta, M., Matheu, A., Vergara, I., & Otaegui, D. (2021). Inflammaging markers characteristic of advanced age show similar levels with frailty and dependency. *Scientific Reports*, *11*(1), 4358. https://doi.org/10.1038/S41598-021-83991-7

Alonso, A. D. C., Zaidi, T., Novak, M., Grundke-Iqbal, I., & Iqbal, K. (2001). Hyperphosphorylation induces self-assembly of tau into tangles of paired helical filaments/straight filaments. *Proceedings of the National Academy of Sciences of the United States of America*, *98*(12), 6923–6928. https://doi.org/10.1073/PNAS.121119298

Andreadis, A. (2006). Misregulation of tau alternative splicing in neurodegeneration and dementia. *Progress in Molecular and Subcellular Biology*, *44*, 89–107. https://doi.org/10.1007/978-3-540-34449-0_5

Aran, D., Looney, A. P., Liu, L., Wu, E., Fong, V., Hsu, A., Chak, S., Naikawadi, R. P., Wolters, P. J., Abate, A. R., Butte, A. J., & Bhattacharya, M. (2019). *Reference-based analysis of lung single-cell sequencing reveals a transitional profibrotic macrophage*. *20*(2), 163–172. https://doi.org/10.1038/s41590-018-0276-y

Ardura-Fabregat, A., Boddeke, E. W. G. M., Boza-Serrano, A., Brioschi, S., Castro-Gomez, S., Ceyzériat, K., Dansokho, C., Dierkes, T., Gelders, G., Heneka, M. T., Hoeijmakers, L., Hoffmann, A., Iaccarino, L., Jahnert, S., Kuhbandner, K., Landreth, G., Lonnemann, N., Löschmann, P. A., McManus, R. M., … Yang, Y. (2017). Targeting Neuroinflammation to Treat Alzheimer's Disease. *CNS Drugs*, *31*(12), 1057–1082. https://doi.org/10.1007/s40263-017-0483-3

Bachiller, S., Jiménez-Ferrer, I., Paulus, A., Yang, Y., Swanberg, M., Deierborg, T., & Boza-Serrano, A. (2018). Microglia in neurological diseases: A road map to brain-disease dependent-inflammatory response. *Frontiers in Cellular Neuroscience*, *12*, 488. https://doi.org/10.3389/FNCEL.2018.00488/BIBTEX

Ballard, C., Creese, B., Corbett, A., & Aarsland, D. (2011). Atypical antipsychotics for the treatment of behavioral and psychological symptoms in dementia, with a particular focus on longer term outcomes and mortality. *Expert Opinion on Drug Safety*, *10*(1), 35–43. https://doi.org/10.1517/14740338.2010.506711

Barbé-Tuana, F., Funchal, G., Schmitz, C. R. R., Maurmann, R. M., & Bauer, M. E. (2020). The interplay between immunosenescence and age-related diseases. In *Seminars in Immunopathology* (pp. 1–13). Springer. https://doi.org/10.1007/s00281-020-00806-z

Baßler, K., Fujii, W., Kapellos, T. S., Horne, A., Reiz, B., Dudkin, E., Lücken, M., Reusch, N., Osei-Sarpong, C., Warnat-Herresthal, S., Wagner, A., Bonaguro, L., Günther, P., Pizarro, C., Schreiber, T., Becker, M., Händler, K., Wohnhaas, C. T., Baumgartner, F., … Schultze, J. L. (2020). Alterations of multiple alveolar macrophage states in chronic obstructive pulmonary disease. *BioRxiv*, 1–82.

Bassler, K., Schulte-Schrepping, J., Warnat-Herresthal, S., Aschenbrenner, A. C., & Schultze, J. L. (2019). The Myeloid Cell Compartment-Cell by Cell. *Annu Rev Immunol*, *37*, 269–293. https://doi.org/10.1146/annurev-immunol-042718-041728

Bellenguez, C., Küçükali, F., Jansen, I. E., Kleineidam, L., Moreno-Grau, S., Amin, N., Naj, A. C., Campos-Martin, R., Grenier-Boley, B., Andrade, V., Holmans, P. A., Boland, A., Damotte, V., Lee, S. J., Costa, M. R., Kuulasmaa, T., Yang, Q., Rojas, I., Bis, J. C., … Lambert, J.-C. (2022). New insights into the genetic etiology of Alzheimer's disease and related dementias. *Nature Genetics 2022 54:4*, *54*(4), 412–436. https://doi.org/10.1038/s41588-022-01024-z

Bellettato, C. M., & Scarpa, M. (2018). Possible strategies to cross the blood-brain barrier 11 Medical and Health Sciences 1109 Neurosciences. *Italian Journal of Pediatrics*, *44*(2), 1DUNNY. https://doi.org/10.1186/S13052-018-0563-0/FIGURES/1

Bloom, G. S. (2014). Amyloid-β and Tau. *JAMA Neurology*, *71*(4), 505. https://doi.org/10.1001/jamaneurol.2013.5847

Boyko, A. A., Troyanova, N. I., Kovalenko, E. I., Sapozhnikov, A. M., Boyko, A. A., Troyanova, N. I., Kovalenko, E. I., & Sapozhnikov, A. M. (2017). Similarity and Differences in Inflammation-Related Characteristics of the Peripheral Immune System of Patients with Parkinson's and Alzheimer's Diseases. *International Journal of Molecular Sciences*, *18*(12), 2633. https://doi.org/10.3390/ijms18122633

Braak, H., & Braak, E. (1991). Acta H ' pathologica Neuropathological stageing of Alzheimer-related changes. In *Acta Neuropathol* (Vol. 82). https://link.springer.com/content/pdf/10.1007%2FBF00308809.pdf

Brioschi, S., Zhou, Y., & Colonna, M. (2020). Brain Parenchymal and Extraparenchymal Macrophages in Development, Homeostasis, and Disease. *Journal of Immunology (Baltimore, Md. : 1950)*, *204*(2), 294–305. https://doi.org/10.4049/JIMMUNOL.1900821

Brosseron, F., Maass, A., Kleineidam, L., Ravichandran, K. A., González, P. G., McManus, R. M., Ising, C., Santarelli, F., Kolbe, C. C., Häsler, L. M., Wolfsgruber, S., Marquié, M., Boada, M., Orellana, A., de Rojas, I., Röske, S., Peters, O., Cosma, N. C., Cetindag, A., … Heneka, M. T. (2022). Soluble TAM receptors sAXL and sTyro3 predict structural and functional protection in Alzheimer's disease. *Neuron*, *110*(6), 1009-1022.e4. https://doi.org/10.1016/j.neuron.2021.12.016

Brown, P. D., Davies, S. L., Speake, T., & Millar, I. D. (2004). Molecular Mechanisms of Cerebrospinal Fluid Production. *Neurosciencescience*, *129*(4), 957–970.

Buchhave, P., Minthon, L., Zetterberg, H., Wallin, Å. K., Blennow, K., & Hansson, O. (2012). Cerebrospinal Fluid Levels ofβ-Amyloid 1-42, but Not of Tau, Are Fully Changed Already 5 to 10 Years Before the Onset of Alzheimer Dementia. *Archives of General Psychiatry*, *69*(1), 98–106. https://doi.org/10.1001/ARCHGENPSYCHIATRY.2011.155

Bulk, M., Abdelmoula, W. M., Nabuurs, R. J. A., van der Graaf, L. M., Mulders, C. W. H., Mulder, A. A., Jost, C. R., Koster, A. J., van Buchem, M. A., Natté, R., Dijkstra, J., & van der Weerd, L. (2018). Postmortem MRI and histology demonstrate differential iron accumulation and cortical myelin organization in early- and late-onset Alzheimer's disease. *Neurobiology of Aging*, *62*, 231–242. https://doi.org/10.1016/J.NEUROBIOLAGING.2017.10.017

Burns, A., Byrne, E. J., & Maurer, K. (2002). Alzheimer's disease. *The Lancet*, *360*(9327), 163–165. https://doi.org/10.1016/S0140-6736(02)09420-5

Busse, S., Hoffmann, J., Michler, E., Hartig, R., Frodl, T., & Busse, M. (2021). Dementia-associated changes of immune cell composition within the cerebrospinal fluid. *Brain, Behavior, & Immunity - Health*, *14*, 100218. https://doi.org/10.1016/J.BBIH.2021.100218

Butler, A., Hoffman, P., Smibert, P., Papalexi, E., & Satija, R. (2018). Integrating single-cell transcriptomic data across different conditions, technologies, and species. *Nature Biotechnology*, *36*(5), 411–420. https://doi.org/10.1038/nbt.4096

Büttner, M., Ostner, J., Müller, C. L., Theis, F. J., & Schubert, B. (2021). scCODA is a Bayesian model for compositional single-cell data analysis. *Nature Communications 2021 12:1*, *12*(1), 1–10. https://doi.org/10.1038/s41467-021-27150-6

Calsolaro, V., Antognoli, R., Okoye, C., & Monzani, F. (2019). The use of antipsychotic drugs for treating behavioral symptoms in Alzheimer's disease. *Frontiers in Pharmacology*, *10*, 1465. https://doi.org/10.3389/FPHAR.2019.01465/BIBTEX

Cao, J., O'Day, D. R., Pliner, H. A., Kingsley, P. D., Deng, M., Daza, R. M., Zager, M. A., Aldinger, K. A., Blecher-Gonen, R., Zhang, F., Spielmann, M., Palis, J., Doherty, D., Steemers, F. J., Glass, I. A., Trapnell, C., & Shendure, J. (2020). A human cell atlas of fetal gene expression. *Science*, *370*(6518). https://doi.org/10.1126/SCIENCE.ABA7721/SUPPL_FILE/ABA7721_TABLESS1-S16.XLSX

Cao, J., Packer, J. S., Ramani, V., Cusanovich, D. A., Huynh, C., Daza, R., Qiu, X., Lee, C., Furlan, S. N., Steemers, F. J., Adey, A., Waterston, R. H., Trapnell, C., & Shendure, J. (2017). Comprehensive single-cell transcriptional profiling of a multicellular organism. *Science*, *357*(6352), 661–667. https://doi.org/10.1126/science.aam8940

Carroll, M. C., & Isenman, D. E. (2012). Regulation of Humoral Immunity by Complement. *Immunity*, *37*(2), 199–207. https://doi.org/10.1016/J.IMMUNI.2012.08.002

Chang, C., Nakamoto, M., Lai, J., Siddique, I., & Mortimer, S. (2019). Simultaneous mRNA, protein, and immune-repertoire profiling of thousands of single cells. *The Journal of Immunology*, *202*(1 Supplement).

Chen, I. T., Dixit, A., Rhoads, D. D., & Roufa, D. J. (1986). Homologous ribosomal proteins in bacteria, yeast, and humans. *Proceedings of the National Academy of Sciences of the United States of America*, *83*(18), 6907–6911. https://doi.org/10.1073/PNAS.83.18.6907

Chen, R., Wu, X., Jiang, L., & Zhang, Y. (2017). Single-Cell RNA-Seq Reveals Hypothalamic Cell Diversity. *Cell Reports*, *18*(13), 3227–3241. https://doi.org/10.1016/J.CELREP.2017.03.004

Chien, D. T., Bahri, S., Szardenings, A. K., Walsh, J. C., Mu, F., Su, M. Y., Shankle, W. R., Elizarov, A., & Kolb, H. C. (2013). Early Clinical PET Imaging Results with the Novel PHF-Tau Radioligand [F-18]-T807. *Journal of Alzheimer's Disease*, *34*(2), 457–468. https://doi.org/10.3233/JAD-122059

Ciudad, S., Puig, E., Botzanowski, T., Meigooni, M., Arango, A. S., Do, J., Mayzel, M., Bayoumi, M., Chaignepain, S., Maglia, G., Cianferani, S., Orekhov, V., Tajkhorshid, E., Bardiaux, B., & Carulla, N. (2020). Aβ(1-42) tetramer and octamer structures reveal edge conductivity pores as a mechanism for membrane damage. *Nature Communications 2020 11:1*, *11*(1), 1–14. https://doi.org/10.1038/s41467-020-16566-1

Clark, S. J., Argelaguet, R., Kapourani, C. A., Stubbs, T. M., Lee, H. J., Alda-Catalinas, C., Krueger, F., Sanguinetti, G., Kelsey, G., Marioni, J. C., Stegle, O., & Reik, W. (2018). scNMT-seq enables joint profiling of chromatin accessibility DNA methylation and transcription in single cells. *Nature Communications 2018 9:1*, *9*(1), 1–9. https://doi.org/10.1038/s41467-018-03149-4

Codeluppi, S., Borm, L. E., Zeisel, A., La Manno, G., van Lunteren, J. A., Svensson, C. I., & Linnarsson, S. (2018). *Spatial organization of the somatosensory cortex revealed by cyclic smFISH*. https://doi.org/10.1101/276097

Crinier, A., Dumas, P. Y., Escalière, B., Piperoglou, C., Gil, L., Villacreces, A., Vély, F., Ivanovic, Z., Milpied, P., Narni-Mancinelli, É., & Vivier, É. (2020). Single-cell profiling reveals the trajectories of natural killer cell differentiation in bone marrow and a stress signature induced by acute myeloid leukemia. *Cellular & Molecular Immunology 2020 18:5*, *18*(5), 1290–1304. https://doi.org/10.1038/s41423-020-00574-8

Dai, L., & Shen, Y. (2021). Insights into T-cell dysfunction in Alzheimer's disease. *Aging Cell*, *20*(12). https://doi.org/10.1111/ACEL.13511

De Graaf, M. T., Sillevis Smitt, P. A. E., Luitwieler, R. L., Van Velzen, C., Van Den Broek, P. D. M., Kraan, J., & Gratama, J. W. (2011). Central memory CD4+ T cells dominate the normal cerebrospinal fluid. *Cytometry Part B - Clinical Cytometry*, *80 B*(1), 43–50. https://doi.org/10.1002/cyto.b.20542

DeLaughter, D. M. (2018). The Use of the Fluidigm C1 for RNA Expression Analyses of Single Cells. *Current Protocols in Molecular Biology*, *122*(1), e55. https://doi.org/10.1002/CPMB.55

Deture, M. A., & Dickson, D. W. (2019). The neuropathological diagnosis of Alzheimer's disease. *Molecular Neurodegeneration 2019 14:1*, *14*(1), 1–18. https://doi.org/10.1186/S13024-019-0333-5

DeVos, S. L., Miller, R. L., Schoch, K. M., Holmes, B. B., Kebodeaux, C. S., Wegener, A. J., Chen, G., Shen, T., Tran, H., Nichols, B., Zanardi, T. A., Kordasiewicz, H. B., Swayze, E. E., Bennett, C. F., Diamond, M. I., & Miller, T. M. (2017). Tau reduction prevents neuronal loss and reverses pathological tau deposition and seeding in mice with tauopathy. *Science Translational Medicine*, *9*(374). https://doi.org/10.1126/SCITRANSLMED.AAG0481

Dobin, A., Davis, C. A., Schlesinger, F., Drenkow, J., Zaleski, C., Jha, S., Batut, P., Chaisson, M., & Gingeras, T. R. (2013). STAR: Ultrafast universal RNA-seq aligner. *Bioinformatics*, *29*(1), 15–21. https://doi.org/10.1093/bioinformatics/bts635

Donovan, J., Dufner, M., & Korennykh, A. (2013). Structural basis for cytosolic double-stranded RNA surveillance by human oligoadenylate synthetase 1. *Proceedings of the National Academy of Sciences of*

the United States of America, *110*(5), 1652–1657. https://doi.org/10.1073/PNAS.1218528110/SUPPL_FILE/SD01.TXT

Dunne, M. R., Phelan, J. J., Michielsen, A. J., Maguire, A. A., Dunne, C., Martin, P., Noonan, S., Tosetto, M., Geraghty, R., Fennelly, D., Sheahan, K., Ryan, E. J., & O'Sullivan, J. (2020). Characterising the prognostic potential of HLA-DR during colorectal cancer development. *Cancer Immunology, Immunotherapy*, *69*(8), 1577–1588. https://doi.org/10.1007/s00262-020-02571-2

El Khoury, J. B., Moore, K. J., Means, T. K., Leung, J., Terada, K., Toft, M., Freeman, M. W., & Luster, A. D. (2003). CD36 Mediates the Innate Host Response to β-Amyloid. *Journal of Experimental Medicine*, *197*(12), 1657–1666. https://doi.org/10.1084/JEM.20021546

Esaulova, E., Cantoni, C., Shchukina, I., Zaitsev, K., Bucelli, R. C., Wu, G. F., Artyomov, M. N., Cross, A. H., & Edelson, B. T. (2020). Single-cell RNA-seq analysis of human CSF microglia and myeloid cells in neuroinflammation. *Neurology - Neuroimmunology Neuroinflammation*, *7*(4), 732. https://doi.org/10.1212/NXI.0000000000000732

Fandos, N., Pérez-Grijalba, V., Pesini, P., Olmos, S., Bossa, M., Villemagne, V. L., Doecke, J., Fowler, C., Masters, C. L., & Sarasa, M. (2017). Plasma amyloid β 42/40 ratios as biomarkers for amyloid β cerebral deposition in cognitively normal individuals. *Alzheimer's & Dementia (Amsterdam, Netherlands)*, *8*, 179–187. https://doi.org/10.1016/J.DADM.2017.07.004

Fändrich, M., Meinhardt, J., & Grigorieff, N. (2009). Structural polymorphism of Alzheimer Abeta and other amyloid fibrils. *Prion*, *3*(2), 89–93. https://doi.org/10.4161/PRI.3.2.8859

Farhadian, S. F., Mehta, S. S., Zografou, C., Robertson, K., Price, R. W., Pappalardo, J., Chiarella, J., Hafler, D. A., & Spudich, S. S. (2019). Single-cell RNA sequencing reveals microglia-like cells in cerebrospinal fluid during virologically suppressed HIV. *JCI Insight*, *3*(18). https://doi.org/10.1172/JCI.INSIGHT.121718

Flores-Cordero, J. A., Pérez-Pérez, A., Jiménez-Cortegana, C., Alba, G., Flores-Barragán, A., & Sánchez-Margalet, V. (2022). Obesity as a Risk Factor for Dementia and Alzheimer's Disease: The Role of Leptin. *International Journal of Molecular Sciences*, *23*(9). https://doi.org/10.3390/IJMS23095202

Folstein, M. F., Folstein, S. E., & Mchugh, P. R. (1975). Mini-mental state" A practical method for grading the cognitive state of patients for the clinician Related papers 'MINI-MENTAL STATE' A PRACTICAL METHOD FOR GRADING THE COGNITIVE STATE OF PATIENTS FOR THE CLINICIAN*. *J. Gsychiaf. Res*, *12*, 189–198.

Fonseca, M. I., Zhou, J., Botto, M., & Tenner, A. J. (2004). Absence of C1q leads to less neuropathology in transgenic mouse models of Alzheimer's disease. *The Journal of Neuroscience : The Official Journal of the Society for Neuroscience*, *24*(29), 6457–6465. https://doi.org/10.1523/JNEUROSCI.0901-04.2004

Forabosco, P., Ramasamy, A., Trabzuni, D., Walker, R., Smith, C., Bras, J., Levine, A. P., Hardy, J., Pocock, J. M., Guerreiro, R., Weale, M. E., & Ryten, M. (2013). Insights into TREM2 biology by network analysis of human brain gene expression data. *Neurobiology of Aging*, *34*(12), 2699–2714. https://doi.org/10.1016/J.NEUROBIOLAGING.2013.05.001

Furman, D., Campisi, J., Verdin, E., Carrera-Bastos, P., Targ, S., Franceschi, C., Ferrucci, L., Gilroy, D. W., Fasano, A., Miller, G. W., Miller, A. H., Mantovani, A., Weyand, C. M., Barzilai, N., Goronzy, J. J., Rando, T. A., Effros, R. B., Lucia, A., Kleinstreuer, N., & Slavich, G. M. (2019). Chronic inflammation in the

etiology of disease across the life span. *Nature Medicine*, *25*(12), 1822–1832. https://doi.org/10.1038/s41591-019-0675-0

Gani, Z. (2021). *Complement System | British Society for Immunology*. British Society for Immunology. https://www.immunology.org/public-information/bitesized-immunology/systems-and-processes/complement-system

Gate, D., Saligrama, N., Leventhal, O., Yang, A. C., Unger, M. S., Middeldorp, J., Chen, K., Lehallier, B., Channappa, D., De Los Santos, M. B., McBride, A., Pluvinage, J., Elahi, F., Tam, G. K.-Y. Y., Kim, Y., Greicius, M., Wagner, A. D., Aigner, L., Galasko, D. R., … Wyss-Coray, T. (2020). Clonally expanded CD8 T cells patrol the cerebrospinal fluid in Alzheimer's disease. *Nature*, *577*(7790), 399–404. https://doi.org/10.1038/s41586-019-1895-7

Gierahn, T. M., Wadsworth, M. H., Hughes, T. K., Bryson, B. D., Butler, A., Satija, R., Fortune, S., Love, J. C., & Shalek, A. K. (2017). Seq-Well: portable, low-cost RNA sequencing of single cells at high throughput. *Nature Methods*, *14*(4), 395–398. https://doi.org/10.1038/nmeth.4179

Ginhoux, F., Greter, M., Leboeuf, M., Nandi, S., See, P., Gokhan, S., Mehler, M. F., Conway, S. J., Ng, L. G., Stanley, E. R., Samokhvalov, I. M., & Merad, M. (2010). Fate mapping analysis reveals that adult microglia derive from primitive macrophages. *Science*, *330*(6005), 841–845. https://doi.org/10.1126/SCIENCE.1194637/SUPPL_FILE/GINHOUX.SOM.PDF

Goedert, M. (2009). Oskar Fischer and the study of dementia. *Brain : A Journal of Neurology*, *132*(Pt 4), 1102–1111. https://doi.org/10.1093/BRAIN/AWN256

Golde, T. E. (2022). Alzheimer's disease – the journey of a healthy brain into organ failure. *Molecular Neurodegeneration 2022 17:1*, *17*(1), 1–19. https://doi.org/10.1186/S13024-022-00523-1

Goldmann, T., Jordão, M. J. C., Wieghofer, P., Prutek, F., Hagemeyer, N., Frenzel, K., Staszewski, O., Kierdorf, K., Amann, L., Krueger, M., Locatelli, G., Hochgarner, H., Zeiser, R., Epelman, S., Geissmann, F., Priller, J., Rossi, F., Bechmann, I., Kerschensteiner, M., … Prinz, M. (2016). Origin, fate and dynamics of macrophages at CNS interfaces HHS Public Access. *Nat Immunol*, *17*(7), 797–805. https://doi.org/10.1038/ni.3423

Gu, Z., Eils, R., & Schlesner, M. (2016). Complex heatmaps reveal patterns and correlations in multidimensional genomic data. *Bioinformatics*, *32*(18), 2847–2849. https://doi.org/10.1093/bioinformatics/btw313

Guan, E., Wang, J., & Norcross, M. A. (2001). Identification of Human Macrophage Inflammatory Proteins 1α and 1β as a Native Secreted Heterodimer. *Journal of Biological Chemistry*, *276*(15), 12404–12409. https://doi.org/10.1074/JBC.M006327200

Guedes, J. R., Lao, T., Cardoso, A. L., & El Khoury, J. (2018). Roles of microglial and monocyte chemokines and their receptors in regulating Alzheimer's disease-associated amyloid-β and tau pathologies. *Frontiers in Neurology*, *9*(AUG), 549. https://doi.org/10.3389/FNEUR.2018.00549/BIBTEX

Hafemeister, C., & Satija, R. (2019). Normalization and variance stabilization of single-cell RNA-seq data using regularized negative binomial regression. *Genome Biology*, *20*(1), 1–15. https://doi.org/10.1186/S13059-019-1874-1/FIGURES/6

Hamed, A. A., Kunz, D. J., El-Hamamy, I., Trinh, Q. M., Subedar, O. D., Richards, L. M., Foltz, W., Bullivant, G., Ware, M., Vladoiu, M. C., Zhang, J., Raj, A. M., Pugh, T. J., Taylor, M. D., Teichmann, S. A., Stein, L. D., Simons, B. D., & Dirks, P. B. (2022). A brain precursor atlas reveals the acquisition of developmental-like states in adult cerebral tumours. *Nature Communications*, *13*(1). https://doi.org/10.1038/S41467-022-31408-Y

Hampel, H., Cummings, J., Blennow, K., Gao, P., Jack, C. R., & Vergallo, A. (2021). Developing the ATX(N) classification for use across the Alzheimer disease continuum. *Nature Reviews Neurology 2021 17:9*, *17*(9), 580–589. https://doi.org/10.1038/s41582-021-00520-w

Hanisch, U. K., & Kettenmann, H. (2007). Microglia: active sensor and versatile effector cells in the normal and pathologic brain. *Nature Neuroscience 2007 10:11*, *10*(11), 1387–1394. https://doi.org/10.1038/nn1997

Hao, Y., Hao, S., Andersen-Nissen, E., Mauck, W. M., Zheng, S., Butler, A., Lee, M. J., Wilk, A. J., Darby, C., Zager, M., Hoffman, P., Stoeckius, M., Papalexi, E., Mimitou, E. P., Jain, J., Srivastava, A., Stuart, T., Fleming, L. M., Yeung, B., … Satija, R. (2021). Integrated analysis of multimodal single-cell data. *Cell*, *184*(13), 3573-3587.e29. https://doi.org/10.1016/J.CELL.2021.04.048

Haque, R. U., & Levey, A. I. (2019). Alzheimer's disease: A clinical perspective and future nonhuman primate research opportunities. *Proceedings of the National Academy of Sciences of the United States of America*, *116*(52), 26224–26229. https://doi.org/10.1073/PNAS.1912954116/ASSET/C0CAB292-2B2C-4EE3-81F8-C0FE20633BA6/ASSETS/GRAPHIC/PNAS.1912954116FIG01.JPEG

Harrow, J., Frankish, A., Gonzalez, J. M., Tapanari, E., Diekhans, M., Kokocinski, F., Aken, B. L., Barrell, D., Zadissa, A., Searle, S., Barnes, I., Bignell, A., Boychenko, V., Hunt, T., Kay, M., Mukherjee, G., Rajan, J., Despacio-Reyes, G., Saunders, G., … Hubbard, T. J. (2012). GENCODE: The reference human genome annotation for the ENCODE project. *Genome Research*, *22*(9), 1760–1774. https://doi.org/10.1101/gr.135350.111

Hashimshony, T., Wagner, F., Sher, N., & Yanai, I. (2012). CEL-Seq: Single-Cell RNA-Seq by Multiplexed Linear Amplification. *Cell Reports*, *2*(3), 666–673. https://doi.org/10.1016/J.CELREP.2012.08.003

Heneka, M. T., Carson, M. J., Khoury, J. El, Landreth, G. E., Brosseron, F., Feinstein, D. L., Jacobs, A. H., Wyss-Coray, T., Vitorica, J., Ransohoff, R. M., Herrup, K., Frautschy, S. A., Finsen, B., Brown, G. C., Verkhratsky, A., Yamanaka, K., Koistinaho, J., Latz, E., Halle, A., … Kummer, M. P. (2015). Neuroinflammation in Alzheimer's disease. *The Lancet Neurology*, *14*(4), 388–405. https://doi.org/10.1016/S1474-4422(15)70016-5

Herber, D. L., Cao, W., Nefedova, Y., Novitskiy, S. V., Nagaraj, S., Tyurin, V. A., Corzo, A., Cho, H. I., Celis, E., Lennox, B., Knight, S. C., Padhya, T., McCaffrey, T. V., McCaffrey, J. C., Antonia, S., Fishman, M., Ferris, R. L., Kagan, V. E., & Gabrilovich, D. I. (2010). Lipid accumulation and dendritic cell dysfunction in cancer. *Nature Medicine*, *16*(8), 880. https://doi.org/10.1038/NM.2172

Herman, J. S., Sagar, & Grün, D. (2018). FateID infers cell fate bias in multipotent progenitors from single-cell RNA-seq data. *Nature Methods*, *15*(5), 379–386. https://doi.org/10.1038/NMETH.4662

Holtzman, D. M., Morris, J. C., & Goate, A. M. (2011). Alzheimer's disease: the challenge of the second century. *Science Translational Medicine*, *3*(77). https://doi.org/10.1126/SCITRANSLMED.3002369

Hong, S., Dissing-Olesen, L., & Stevens, B. (2016). New insights on the role of microglia in synaptic pruning in health and disease. *Current Opinion in Neurobiology*, *36*, 128–134. https://doi.org/10.1016/J.CONB.2015.12.004

Hook, V., Yoon, M., Mosier, C., Ito, G., Podvin, S., Head, B. P., Rissman, R., O'Donoghue, A. J., & Hook, G. (2020). Cathepsin B in Neurodegeneration of Alzheimer's Disease, Traumatic Brain Injury, and Related Brain Disorders. *Biochimica et Biophysica Acta. Proteins and Proteomics*, *1868*(8), 140428. https://doi.org/10.1016/J.BBAPAP.2020.140428

Hu, M. yan, Lin, Y. yao, Zhang, B. jun, Lu, D. li, Lu, Z. qi, & Cai, W. (2019). Update of inflammasome activation in microglia/macrophage in aging and aging-related disease. *CNS Neuroscience and Therapeutics*, *25*(12), 1299–1307. https://doi.org/10.1111/CNS.13262

Ilicic, T., Kim, J. K., Kolodziejczyk, A. A., Bagger, F. O., McCarthy, D. J., Marioni, J. C., & Teichmann, S. A. (2016). Classification of low quality cells from single-cell RNA-seq data. *Genome Biology*, *17*(1), 1–15. https://doi.org/10.1186/S13059-016-0888-1/FIGURES/5

Islam, S., Kjällquist, U., Moliner, A., Zajac, P., Fan, J. B., Lönnerberg, P., & Linnarsson, S. (2011). Characterization of the single-cell transcriptional landscape by highly multiplex RNA-seq. *Genome Research*, *21*(7), 1160–1167. https://doi.org/10.1101/GR.110882.110

Jack, C. R., Bennett, D. A., Blennow, K., Carrillo, M. C., Feldman, H. H., Frisoni, G. B., Hampel, H., Jagust, W. J., Johnson, K. A., Knopman, D. S., Petersen, R. C., Scheltens, P., Sperling, R. A., & Dubois, B. (2016). A/T/N: An unbiased descriptive classification scheme for Alzheimer disease biomarkers. *Neurology*, *87*(5), 539–547. https://doi.org/10.1212/WNL.0000000000002923

Jack, C. R., Knopman, D. S., Jagust, W. J., Petersen, R. C., Weiner, M. W., Aisen, P. S., Shaw, L. M., Vemuri, P., Wiste, H. J., Weigand, S. D., Lesnick, T. G., Pankratz, V. S., Donohue, M. C., & Trojanowski, J. Q. (2013). Tracking pathophysiological processes in Alzheimer's disease: an updated hypothetical model of dynamic biomarkers. *The Lancet. Neurology*, *12*(2), 207–216. https://doi.org/10.1016/S1474-4422(12)70291-0

Jack Jr, C. R., Bennett, D. A., Blennow, K., Carrillo, M. C., Dunn, B., Budd Haeberlein, S., Holtzman, D. M., Jagust, W., Jessen, F., Karlawish, J., Liu, E., Luis Molinuevo, J., Montine, T., Phelps, C., Rankin, K. P., Rowe, C. C., Scheltens, P., Siemers, E., Snyder, H. M., … Dement Author manuscript, A. (2018). NIA-AA Research Framework: Toward a biological definition of Alzheimer's disease HHS Public Access Author manuscript. *Alzheimers Dement*, *14*(4), 535–562. https://doi.org/10.1016/j.jalz.2018.02.018

Jaitin, D. A., Kenigsberg, E., Keren-Shaul, H., Elefant, N., Paul, F., Zaretsky, I., Mildner, A., Cohen, N., Jung, S., Tanay, A., & Amit, I. (2014). Massively parallel single-cell RNA-seq for marker-free decomposition of tissues into cell types. *Science*, *343*(6172), 776–779. https://doi.org/10.1126/SCIENCE.1247651/SUPPL_FILE/TABLE_S6.XLS

Janelidze, S., Berron, D., Smith, R., Strandberg, O., Proctor, N. K., Dage, J. L., Stomrud, E., Palmqvist, S., Mattsson-Carlgren, N., & Hansson, O. (2021). Associations of Plasma Phospho-Tau217 Levels With Tau Positron Emission Tomography in Early Alzheimer Disease. *JAMA Neurology*, *78*(2), 149–156. https://doi.org/10.1001/JAMANEUROL.2020.4201

Jiang-Shieh, Y. F., Wu, C. H., Chang, M. L., Shieh, J. Y., & Wen, C. Y. (2003). Regional heterogeneity in immunoreactive macrophages/microglia in the rat pineal gland. *Journal of Pineal Research*, *35*(1), 45–53. https://doi.org/10.1034/J.1600-079X.2003.00054.X

Jordão, M. J. C., Sankowski, R., Brendecke, S. M., Sagar, Locatelli, G., Tai, Y. H., Tay, T. L., Schramm, E., Armbruster, S., Hagemeyer, N., Groß, O., Mai, D., Çiçek, Ö., Falk, T., Kerschensteiner, M., Grün, D., & Prinz, M. (2019). Neuroimmunology: Single-cell profiling identifies myeloid cell subsets with distinct fates during neuroinflammation. *Science*, *363*(6425). https://doi.org/10.1126/SCIENCE.AAT7554/SUPPL_FILE/AAT7554-JORDAO-SM.PDF

Kapellos, T. S., Bonaguro, L., Gemünd, I., Reusch, N., Saglam, A., Hinkley, E. R., & Schultze, J. L. (2019). Human monocyte subsets and phenotypes in major chronic inflammatory diseases. *Frontiers in Immunology*, *10*(AUG). https://doi.org/10.3389/fimmu.2019.02035

Kenkhuis, B., Somarakis, A., de Haan, L., Dzyubachyk, O., IJsselsteijn, M. E., de Miranda, N. F. C. C., Lelieveldt, B. P. F., Dijkstra, J., van Roon-Mom, W. M. C., Höllt, T., & van der Weerd, L. (2021). Iron loading is a prominent feature of activated microglia in Alzheimer's disease patients. *Acta Neuropathologica Communications*, *9*(1), 1–15. https://doi.org/10.1186/S40478-021-01126-5/FIGURES/6

Keren-Shaul, H., Spinrad, A., Weiner, A., Matcovitch-Natan, O., Dvir-Szternfeld, R., Ulland, T. K., David, E., Baruch, K., Lara-Astaiso, D., Toth, B., Itzkovitz, S., Colonna, M., Schwartz, M., & Amit, I. (2017). A Unique Microglia Type Associated with Restricting Development of Alzheimer's Disease. *Cell*, *169*(7), 1276-1290.e17. https://doi.org/10.1016/J.CELL.2017.05.018

Klein, A. M., Mazutis, L., Akartuna, I., Tallapragada, N., Veres, A., Li, V., Peshkin, L., Weitz, D. A., & Kirschner, M. W. (2015). Droplet Barcoding for Single-Cell Transcriptomics Applied to Embryonic Stem Cells. *Cell*, *161*(5), 1187–1201. https://doi.org/10.1016/J.CELL.2015.04.044

Koh, S. H., Kwon, H. S., Choi, S. H., Jeong, J. H., Na, H. R., Lee, C. N., Yang, Y. S., Lee, A. Y., Lee, J. H., Park, K. W., Han, H. J., Kim, B. C., Park, J. S., Lee, J. Y., Kim, S., & Lee, K. Y. (2021). Efficacy and safety of GV1001 in patients with moderate-to-severe Alzheimer's disease already receiving donepezil: a phase 2 randomized, double-blind, placebo-controlled, multicenter clinical trial. *Alzheimer's Research and Therapy*, *13*(1), 1–11. https://doi.org/10.1186/S13195-021-00803-W/TABLES/3

Korabecny, J., Spilovska, K., Mezeiova, E., Benek, O., Juza, R., Kaping, D., & Soukup, O. (2019). A Systematic Review on Donepezil-based Derivatives as Potential Cholinesterase Inhibitors for Alzheimer's Disease. *Current Medicinal Chemistry*, *26*(30), 5625–5648. https://doi.org/10.2174/0929867325666180517094023

Korsunsky, I., Millard, N., Fan, J., Slowikowski, K., Zhang, F., Wei, K., Baglaenko, Y., Brenner, M., Loh, P. ru, & Raychaudhuri, S. (2019). Fast, sensitive and accurate integration of single-cell data with Harmony. *Nature Methods*, *16*(12), 1289–1296. https://doi.org/10.1038/S41592-019-0619-0

Kunis, G., Baruch, K., Rosenzweig, N., Kertser, A., Miller, O., Berkutzki, T., & Schwartz, M. (2013). IFN-γ-dependent activation of the brain's choroid plexus for CNS immune surveillance and repair. *Brain*, *136*(11), 3427–3440. https://doi.org/10.1093/brain/awt259

Kurimoto, K., Yabuta, Y., Ohinata, Y., Ono, Y., Uno, K. D., Yamada, R. G., Ueda, H. R., & Saitou, M. (2006). An improved single-cell cDNA amplification method for efficient high-density oligonucleotide microarray analysis. *Nucleic Acids Research*, *34*(5), e42–e42. https://doi.org/10.1093/NAR/GKL050

Lai, K. S. P., Liu, C. S., Rau, A., Lanctôt, K. L., Köhler, C. A., Pakosh, M., Carvalho, A. F., & Herrmann, N. (2017). Peripheral inflammatory markers in Alzheimer's disease: a systematic review and meta-analysis of 175 studies. *Journal of Neurology, Neurosurgery, and Psychiatry*, *88*(10), 876–882. https://doi.org/10.1136/jnnp-2017-316201

Laman, J. D., & Weller, R. O. (2013). Drainage of Cells and Soluble Antigen from the CNS to Regional Lymph Nodes. *Journal of Neuroimmune Pharmacology*, *8*(4), 840. https://doi.org/10.1007/S11481-013-9470-8

Lane, R. M., Holly Kordasiewicz, B., Smith, A. E., Mignon, L., Miller, T., Narayanan, P., Swayze, E. E., Norris, D. A., Fitzsimmons, B., & Frank Bennett, C. (2017). *Rationale for and development of Ionis-MAPTRx, the first tau-lowering antisense oligonucleotide, in patients with mild AD*. www.ionispharma.com

Lee, W. Bin, Choi, W. Y., Lee, D. H., Shim, H., Kim-Ha, J., & Kim, Y. J. (2019). OAS1 and OAS3 negatively regulate the expression of chemokines and interferon-responsive genes in human macrophages. *BMB Reports*, *52*(2), 133–138. https://doi.org/10.5483/BMBREP.2019.52.2.129

Li, Q., Brown, J. B., Huang, H., & Bickel, P. J. (2011). Measuring reproducibility of high-throughput experiments. *Annals of Applied Statistics*, *5*(3), 1752–1779. https://doi.org/10.1214/11-AOAS466

Lim, K. R. Q., Maruyama, R., & Yokota, T. (2017). Eteplirsen in the treatment of Duchenne muscular dystrophy. *Drug Design, Development and Therapy*, *11*, 533–545. https://doi.org/10.2147/DDDT.S97635

Liu, J., Chang, L., Song, Y., Li, H., & Wu, Y. (2019). The role of NMDA receptors in Alzheimer's disease. *Frontiers in Neuroscience*, *13*(FEB), 43. https://doi.org/10.3389/FNINS.2019.00043/BIBTEX

Liu, J. L., Fan, Y. G., Yang, Z. S., Wang, Z. Y., & Guo, C. (2018). Iron and Alzheimer's disease: From pathogenesis to therapeutic implications. In *Frontiers in Neuroscience* (Vol. 12, Issue SEP, p. 632). Frontiers Media S.A. https://doi.org/10.3389/fnins.2018.00632

Liu, Q., Liu, X., Zhao, D., Ruan, X., Su, R., Shang, X., Wang, D., Yang, C., & Xue, Y. (2021). Pseudogene ACTBP2 increases blood-brain barrier permeability by promoting KHDRBS2 transcription through recruitment of KMT2D/WDR5 in Aβ 1-42 microenvironment. *Cell Death Discovery Press*, *7*(142). https://doi.org/10.1038/s41420-021-00531-y

Lumsden, A. L., Rogers, J. T., Majd, S., Newman, M., Sutherland, G. T., Verdile, G., & Lardelli, M. (2018). Dysregulation of neuronal iron homeostasis as an alternative unifying effect of mutations causing familial alzheimer's disease. *Frontiers in Neuroscience*, *12*(AUG), 533. https://doi.org/10.3389/FNINS.2018.00533/BIBTEX

Lun, M. P., Monuki, E. S., & Lehtinen, M. K. (2015). Development and functions of the choroid plexus–cerebrospinal fluid system. *Nature Reviews Neuroscience 2015 16:8*, *16*(8), 445–457. https://doi.org/10.1038/nrn3921

Ma, P., Li, Y., Zhang, W., Fang, F., Sun, J., Liu, M., Li, K., & Dong, L. (2019). Long Non-coding RNA MALAT1 Inhibits Neuron Apoptosis and Neuroinflammation While Stimulates Neurite Outgrowth and Its

Correlation With MiR-125b Mediates PTGS2, CDK5 and FOXQ1 in Alzheimer's Disease. *Current Alzheimer Research*, *16*(7), 596–612. https://doi.org/10.2174/1567205016666190725130134

Mabbott, N. A., Baillie, J. K., Brown, H., Freeman, T. C., & Hume, D. A. (2013). An expression atlas of human primary cells: Inference of gene function from coexpression networks. *BMC Genomics*, *14*(1), 1–13. https://doi.org/10.1186/1471-2164-14-632/FIGURES/4

Macaulay, I. C., Haerty, W., Kumar, P., Li, Y. I., Hu, T. X., Teng, M. J., Goolam, M., Saurat, N., Coupland, P., Shirley, L. M., Smith, M., Van Der Aa, N., Banerjee, R., Ellis, P. D., Quail, M. A., Swerdlow, H. P., Zernicka-Goetz, M., Livesey, F. J., Ponting, C. P., & Voet, T. (2015). G&T-seq: parallel sequencing of single-cell genomes and transcriptomes. *Nature Methods 2015 12:6*, *12*(6), 519–522. https://doi.org/10.1038/nmeth.3370

Macosko, E. Z., Basu, A., Satija, R., Nemesh, J., Shekhar, K., Goldman, M., Tirosh, I., Bialas, A. R., Kamitaki, N., Martersteck, E. M., Trombetta, J. J., Weitz, D. A., Sanes, J. R., Shalek, A. K., Regev, A., & McCarroll, S. A. (2015). Highly Parallel Genome-wide Expression Profiling of Individual Cells Using Nanoliter Droplets. *Cell*, *161*(5), 1202–1214. https://doi.org/10.1016/J.CELL.2015.05.002

Mansouri, L., Messalmani, M., Klai, S., Bedoui, I., Derbali, H., Gritli, N., Mrissa, R., & Fekih-Mrissa, N. (2015). Association of HLA-DR/DQ polymorphism with alzheimer's disease. *American Journal of the Medical Sciences*, *349*(4), 334–337. https://doi.org/10.1097/MAJ.0000000000000416

Marbac, M., Biernacki, C., & Vandewalle, V. (2017). Model-based clustering of Gaussian copulas for mixed data. *Communications in Statistics - Theory and Methods*, *46*(23), 11635–11656. https://doi.org/10.1080/03610926.2016.1277753

Masuda, takahiro, Sankowski, roman, Staszewski, O., Böttcher, C., Amann, L., Scheiwe, C., Nessler, S., Kunz, P., van Loo, G., Arnd Coenen, V., Christoph reinacher, P., Michel, A., Sure, U., Gold, ralf, Grün, D., Priller, J., Stadelmann, C., Prinz, M., Masuda, T., & Sankowski, R. (n.d.). Spatial and temporal heterogeneity of mouse and human microglia at single-cell resolution. *Nature*. https://doi.org/10.1038/s41586-019-0924-x

Mathys, H., Davila-Velderrain, J., Peng, Z., Gao, F., Mohammadi, S., Young, J. Z., Menon, M., He, L., Abdurrob, F., Jiang, X., Martorell, A. J., Ransohoff, R. M., Hafler, B. P., Bennett, D. A., Kellis, M., & Tsai, L.-H. (2019). Single-cell transcriptomic analysis of Alzheimer's disease. *Nature*, 1. https://doi.org/10.1038/s41586-019-1195-2

Mattsson, N., & Hansson, O. (2019). Primary fatty amides are potential plasma biomarkers for AD. *Nature Reviews Neurology*, *15*(9), 498–499. https://doi.org/10.1038/s41582-019-0229-6

McGinnis, C. S., Murrow, L. M., & Gartner, Z. J. (2019). DoubletFinder: Doublet Detection in Single-Cell RNA Sequencing Data Using Artificial Nearest Neighbors. *Cell Systems*, *8*(4), 329-337.e4. http://www.cell.com/article/S2405471219300730/fulltext

McInnes, L., Healy, J., & Melville, J. (2018). *UMAP: Uniform Manifold Approximation and Projection for Dimension Reduction*.

McInnes, L., Healy, J., Saul, N., & Großberger, L. (2018). UMAP: Uniform Manifold Approximation and Projection. *Journal of Open Source Software*, *3*(29), 861. https://doi.org/10.21105/joss.00861

McKhann, G., Drachman, D., Folstein, M., Katzman, R., Price, D., & Stadlan, E. M. (1984). Clinical diagnosis of Alzheimer's disease. *Neurology*, *34*(7), 939–939. https://doi.org/10.1212/WNL.34.7.939

Medeiros, R., Baglietto-Vargas, D., & Laferla, F. M. (2011). The Role of Tau in Alzheimer's Disease and Related Disorders. *CNS Neuroscience & Therapeutics*, *17*(5), 514. https://doi.org/10.1111/J.1755-5949.2010.00177.X

Meng, J. X., Zhang, Y., Saman, D., Haider, A. M., De, S., Sang, J. C., Brown, K., Jiang, K., Humphrey, J., Julian, L., Hidari, E., Lee, S. F., Balmus, G., Floto, R. A., Bryant, C. E., Benesch, J. L. P., Ye, Y., Klenerman, D., & Zhang, Y. . (2022). Hyperphosphorylated tau self-assembles into amorphous aggregates eliciting TLR4-dependent responses. *Nature Communications 2022 13:1*, *13*(1), 1–16. https://doi.org/10.1038/s41467-022-30461-x

Menten, P., Wuyts, A., & Van Damme, J. (2002). Macrophage inflammatory protein-1. *Cytokine & Growth Factor Reviews*, *13*(6), 455–481. https://doi.org/10.1016/S1359-6101(02)00045-X

Mezeiova, E., Chalupova, K., Nepovimova, E., Gorecki, L., Prchal, L., Malinak, D., Kuca, K., Soukup, O., & Korabecny, J. (2019). Donepezil Derivatives Targeting Amyloid-β Cascade in Alzheimer's Disease. *Current Alzheimer Research*, *16*(9), 772–800. https://doi.org/10.2174/1567205016666190228122956

Mielke, M. M., Hagen, C. E., Xu, J., Chai, X., Vemuri, P., Lowe, V. J., Airey, D. C., Knopman, D. S., Roberts, R. O., Machulda, M. M., Jack, C. R., Petersen, R. C., & Dage, J. L. (2018). Plasma phospho-tau181 increases with Alzheimer's disease clinical severity and is associated with tau- and amyloid-positron emission tomography. *Alzheimer's & Dementia : The Journal of the Alzheimer's Association*, *14*(8), 989–997. https://doi.org/10.1016/J.JALZ.2018.02.013

MOE. (2017). Global action plan on the public health response to dementia 2017 - 2025. *Geneva: World Health Organization*, 27. http://apps.who.int/bookorders.

Monaco, G., Lee, B., Xu, W., Mustafah, S., Hwang, Y. Y., Carré, C., Burdin, N., Visan, L., Ceccarelli, M., Poidinger, M., Zippelius, A., Pedro de Magalhães, J., & Larbi, A. (2019). RNA-Seq Signatures Normalized by mRNA Abundance Allow Absolute Deconvolution of Human Immune Cell Types. *Cell Reports*, *26*(6), 1627-1640.e7. https://doi.org/10.1016/J.CELREP.2019.01.041

Morena, F., Argentati, C., Trotta, R., Crispoltoni, L., Stabile, A., Pistilli, A., di Baldassarre, A., Calafiore, R., Montanucci, P., Basta, G., Pedrinolla, A., Smania, N., Venturelli, M., Schena, F., Naro, F., Emiliani, C., Rende, M., & Martino, S. (2017). A Comparison of Lysosomal Enzymes Expression Levels in Peripheral Blood of Mild- and Severe-Alzheimer's Disease and MCI Patients: Implications for Regenerative Medicine Approaches. *International Journal of Molecular Sciences 2017, Vol. 18, Page 1806*, *18*(8), 1806. https://doi.org/10.3390/IJMS18081806

Mori, H., Takio, K., Ogawara, M., & Selkoe, D. J. (1992). Mass spectrometry of purified amyloid beta protein in Alzheimer's disease. *Journal of Biological Chemistry*, *267*(24), 17082–17086. https://doi.org/10.1016/S0021-9258(18)41896-0

Mullard, A. (2021). Landmark Alzheimer's drug approval confounds research community. *Nature*, *594*(7863), 309–310. https://doi.org/10.1038/D41586-021-01546-2

Näslund, J., Schierhorn, A., Hellman, U., Lannfelt, L., Roses, A. D., Tjernberg, L. O., Silberring, J., Gandy, S. E., Winblad, B., Greengard, P., Nordstedt, C., & Terenius, L. (1994). Relative abundance of Alzheimer Aβ amyloid peptide variants in Alzheimer disease and normal aging. *Proceedings of the National Academy of Sciences of the United States of America*, *91*(18), 8378–8382. https://doi.org/10.1073/PNAS.91.18.8378

Nathan, C. (2002). Points of control in inflammation. *Nature 2002 420:6917*, *420*(6917), 846–852. https://doi.org/10.1038/nature01320

Neil, E. E., & Bisaccia, E. K. (2019). Nusinersen: A Novel Antisense Oligonucleotide for the Treatment of Spinal Muscular Atrophy. *The Journal of Pediatric Pharmacology and Therapeutics : JPPT : The Official Journal of PPAG*, *24*(3), 194–203. https://doi.org/10.5863/1551-6776-24.3.194

Noble, W., Hanger, D. P., Miller, C. C. J., & Lovestone, S. (2013). The Importance of Tau Phosphorylation for Neurodegenerative Diseases. *Frontiers in Neurology*, *4*. https://doi.org/10.3389/FNEUR.2013.00083

Ochocka, N., Segit, P., Walentynowicz, K. A., Wojnicki, K., Cyranowski, S., Swatler, J., Mieczkowski, J., & Kaminska, B. (2021). Single-cell RNA sequencing reveals functional heterogeneity of glioma-associated brain macrophages. *Nature Communications 2021 12:1*, *12*(1), 1–14. https://doi.org/10.1038/s41467-021-21407-w

Olah, M., Menon, V., Habib, N., Taga, M. F., Ma, Y., Yung, C. J., Cimpean, M., Khairallah, A., Coronas-Samano, G., Sankowski, R., Grün, D., Kroshilina, A. A., Dionne, D., Sarkis, R. A., Cosgrove, G. R., Helgager, J., Golden, J. A., Pennell, P. B., Prinz, M., … De Jager, P. L. (2020). Single cell RNA sequencing of human microglia uncovers a subset associated with Alzheimer's disease. *Nature Communications 2020 11:1*, *11*(1), 1–18. https://doi.org/10.1038/s41467-020-19737-2

Pang, B., Wang, Q., Ning, S., Wu, J., Zhang, X., Chen, Y., & Xu, S. (2019). Landscape of tumor suppressor long noncoding RNAs in breast cancer. *Journal of Experimental and Clinical Cancer Research*, *38*(1), 1–18. https://doi.org/10.1186/S13046-019-1096-0/FIGURES/10

Paouri, E., & Georgopoulos, S. (2019). Systemic and CNS inflammation crosstalk: implications for Alzheimer's Disease. *Current Alzheimer Research*, *16*. https://doi.org/10.2174/1567205016666190321154618

Petersen, R. C., Caracciolo, B., Brayne, C., Gauthier, S., Jelic, V., & Fratiglioni, L. (2014). Mild cognitive impairment: a concept in evolution. *Journal of Internal Medicine*, *275*(3), 214–228. https://doi.org/10.1111/JOIM.12190

Picelli, S., Björklund, Å. K., Faridani, O. R., Sagasser, S., Winberg, G., & Sandberg, R. (2013). Smart-seq2 for sensitive full-length transcriptome profiling in single cells. *Nature Methods*, *10*(11), 1096–1098. https://doi.org/10.1038/nmeth.2639

Piehl, N., van Olst, L., Ramakrishnan, A., Teregulova, V., Simonton, B., Zhang, Z., Tapp, E., Channappa, D., Oh, H., Losada, P. M., Rutledge, J., Trelle, A. N., Mormino, E. C., Elahi, F., Galasko, D. R., Henderson, V. W., Wagner, A. D., Wyss-Coray, T., & Gate, D. (2022). Cerebrospinal fluid immune dysregulation during healthy brain aging and cognitive impairment. *Cell*, *185*(26), 5028-5039.e13. https://doi.org/10.1016/J.CELL.2022.11.019

Pietronigro, E., Zenaro, E., & Constantin, G. (2016). Imaging of Leukocyte Trafficking in Alzheimer's Disease. *Frontiers in Immunology*, *7*(FEB), 1. https://doi.org/10.3389/FIMMU.2016.00033

Pillai, J. A., Maxwell, S., Bena, J., Bekris, L. M., Rao, S. M., Chance, M., Lamb, B. T., & Leverenz, J. B. (2019). Key inflammatory pathway activations in the MCI stage of Alzheimer's disease. *Annals of Clinical and Translational Neurology*, *6*(7), 1248–1262. https://doi.org/10.1002/ACN3.50827

Pospich, S., & Raunser, S. (2017). The molecular basis of Alzheimer's plaques. *Science*, *358*(6359), 45–46. https://doi.org/10.1126/SCIENCE.AAP8002/ASSET/0827D90B-FB2D-45FC-AFF4-49334A9E6193/ASSETS/GRAPHIC/358_45_F1.JPEG

Proulx, S. T. (2021). Cerebrospinal fluid outflow: a review of the historical and contemporary evidence for arachnoid villi, perineural routes, and dural lymphatics. *Cellular and Molecular Life Sciences 2021 78:6*, *78*(6), 2429–2457. https://doi.org/10.1007/S00018-020-03706-5

Raivo Kolde. (2019). *Package 'pheatmap'*.

Ransohoff, R. M., & Engelhardt, B. (2012). The anatomical and cellular basis of immune surveillance in the central nervous system. *Nature Reviews Immunology 2012 12:9*, *12*(9), 623–635. https://doi.org/10.1038/nri3265

Reitz, C., Rogaeva, E., & Beecham, G. W. (2020). Late-onset vs nonmendelian early-onset Alzheimer disease: A distinction without a difference? *Neurology: Genetics*, *6*(5). https://doi.org/10.1212/NXG.0000000000000512

Revi, M. (2020). Alzheimer's Disease Therapeutic Approaches. *Advances in Experimental Medicine and Biology*, *1195*, 105–116. https://doi.org/10.1007/978-3-030-32633-3_15

Rinaldi, C., & Wood, M. J. A. (2018). Antisense oligonucleotides: the next frontier for treatment of neurological disorders. *Nature Reviews Neurology*, *14*(1), 9–21. https://doi.org/10.1038/nrneurol.2017.148

Roostaei, T., Diaconu, C., Touil, H., Harbison, C., Zhang, Y., Epstein, S., Tuddenham, J., Thakur, K., Bryois, J., Wiendl, H., Meyer, G., Hörste, Z., Malhotra, D., Riley, C., Menon, V., & De Jager, P. L. (2021). Defining the architecture of cerebrospinal fluid cellular communities in neuroinflammatory diseases. *BioRxiv*, 2021.11.01.466797. https://doi.org/10.1101/2021.11.01.466797

Rozenblatt-Rosen, O., Stubbington, M. J. T., Regev, A., & Teichmann, S. A. (2017). The Human Cell Atlas: From vision to reality. In *Nature* (Vol. 550, Issue 7677, pp. 451–453). Nature Publishing Group. https://doi.org/10.1038/550451a

Rucker, P., Torti, F. M., & Torti, S. V. (1996). Role of H and L subunits in mouse ferritin. *The Journal of Biological Chemistry*, *271*(52), 33352–33357. https://doi.org/10.1074/JBC.271.52.33352

Rui, W., Xiao, H., Fan, Y., Ma, Z., Xiao, M., Li, S., & Shi, J. (2021). Systemic inflammasome activation and pyroptosis associate with the progression of amnestic mild cognitive impairment and Alzheimer's disease. *Journal of Neuroinflammation*, *18*(1), 1–14. https://doi.org/10.1186/S12974-021-02329-2/FIGURES/7

Sakka, L., Coll, G., & Chazal, J. (2011). Anatomy and physiology of cerebrospinal fluid. In *European Annals of Otorhinolaryngology, Head and Neck Diseases* (Vol. 128, Issue 6, pp. 309–316). Elsevier Masson SAS. https://doi.org/10.1016/j.anorl.2011.03.002

Sala Frigerio, C., Wolfs, L., Fattorelli, N., Thrupp, N., Voytyuk, I., Schmidt, I., Mancuso, R., Chen, W. T., Woodbury, M. E., Srivastava, G., Möller, T., Hudry, E., Das, S., Saido, T., Karran, E., Hyman, B., Perry, V. H., Fiers, M., & De Strooper, B. (2019). The Major Risk Factors for Alzheimer's Disease: Age, Sex, and Genes Modulate the Microglia Response to Aβ Plaques. *Cell Reports*, *27*(4), 1293-1306.e6. https://doi.org/10.1016/J.CELREP.2019.03.099

Salih, D. A., Bayram, S., Guelfi, S., Reynolds, R. H., Shoai, M., Ryten, M., Brenton, J. W., Zhang, D., Matarin, M., Botia, J. A., Shah, R., Brookes, K. J., Guetta-Baranes, T., Morgan, K., Bellou, E., Cummings, D. M., Escott-Price, V., & Hardy, J. (2019). Genetic variability in response to amyloid beta deposition influences Alzheimer's disease risk. *Brain Communications*, *1*(1). https://doi.org/10.1093/BRAINCOMMS/FCZ022

Sandin, L., Bergkvist, L., Nath, S., Kielkopf, C., Janefjord, C., Helmfors, L., Zetterberg, H., Blennow, K., Li, H., Nilsberth, C., Garner, B., Brorsson, A., & Kågedal, K. (2016). Beneficial effects of increased lysozyme levels in Alzheimer's disease modelled in *Drosophila melanogaster*. *The FEBS Journal*, *283*(19), 3508–3522. https://doi.org/10.1111/febs.13830

Sankowski, R., Böttcher, C., Masuda, T., Geirsdottir, L., Sagar, Sindram, E., Seredenina, T., Muhs, A., Scheiwe, C., Shah, M. J., Heiland, D. H., Schnell, O., Grün, D., Priller, J., & Prinz, M. (2019). Mapping microglia states in the human brain through the integration of high-dimensional techniques. *Nature Neuroscience 2019 22:12*, *22*(12), 2098–2110. https://doi.org/10.1038/s41593-019-0532-y

Schäfer, M. K.-H., Schwaeble, W. J., Post, C., Salvati, P., Calabresi, M., Sim, R. B., Petry, F., Loos, M., & Weihe, E. (2000). Complement C1q Is Dramatically Up-Regulated in Brain Microglia in Response to Transient Global Cerebral Ischemia. *The Journal of Immunology*, *164*(10), 5446–5452. https://doi.org/10.4049/JIMMUNOL.164.10.5446

Schafflick, D., Xu, C. A., Hartlehnert, M., Cole, M., Schulte-Mecklenbeck, A., Lautwein, T., Wolbert, J., Heming, M., Meuth, S. G., Kuhlmann, T., Gross, C. C., Wiendl, H., Yosef, N., & Meyer zu Horste, G. (2020). Integrated single cell analysis of blood and cerebrospinal fluid leukocytes in multiple sclerosis. *Nature Communications*, *11*(1), 1–14. https://doi.org/10.1038/s41467-019-14118-w

Schmidt, M., Sachse, C., Richter, W., Xu, C., Fändrich, M., & Grigorieff, N. (2009). Comparison of Alzheimer Aβ(1-40) and Aβ(1-42) amyloid fibrils reveals similar protofilament structures. *Proceedings of the National Academy of Sciences of the United States of America*, *106*(47), 19813–19818. https://doi.org/10.1073/PNAS.0905007106/SUPPL_FILE/0905007106SI.PDF

Schulte-Schrepping, J., Reusch, N., Paclik, D., Baßler, K., Schlickeiser, S., Zhang, B., Krämer, B., Krammer, T., Brumhard, S., Bonaguro, L., De Domenico, E., Wendisch, D., Grasshoff, M., Kapellos, T. S., Beckstette, M., Pecht, T., Saglam, A., Dietrich, O., Mei, H. E., … Ziebuhr, J. (2020). Severe COVID-19 Is Marked by a Dysregulated Myeloid Cell Compartment. *Cell*, *182*(6), 1419-1440.e23. https://doi.org/10.1016/j.cell.2020.08.001

Schwartz, M., & Baruch, K. (2014). The resolution of neuroinflammation in neurodegeneration: leukocyte recruitment via the choroid plexus. *The EMBO Journal*, *33*(1), 7–22. https://doi.org/10.1002/EMBJ.201386609

Selkoe, D. J., & Hardy, J. (2016). The amyloid hypothesis of Alzheimer's disease at 25 years. *EMBO Molecular Medicine*, *8*(6), 595–608. https://doi.org/10.15252/emmm.201606210

Serrano-Pozo, A., Frosch, M. P., Masliah, E., & Hyman, B. T. (2011). Neuropathological alterations in Alzheimer disease. *Cold Spring Harbor Perspectives in Medicine*, *1*(1). https://doi.org/10.1101/CSHPERSPECT.A006189

Sevigny, J., Chiao, P., Bussière, T., Weinreb, P. H., Williams, L., Maier, M., Dunstan, R., Salloway, S., Chen, T., Ling, Y., O'Gorman, J., Qian, F., Arastu, M., Li, M., Chollate, S., Brennan, M. S., Quintero-Monzon, O., Scannevin, R. H., Arnold, H. M., … Sandrock, A. (2016). The antibody aducanumab reduces Aβ plaques in Alzheimer's disease. *Nature 2016 537:7618*, *537*(7618), 50–56. https://doi.org/10.1038/nature19323

Shahan, R. (2019). The future is now: Gene expression dynamics at single cell resolution. *Plant Cell*, *31*(5), 933–934. https://doi.org/10.1105/tpc.19.00247

Shechter, R., Miller, O., Yovel, G., Rosenzweig, N., London, A., Ruckh, J., Kim, K. W., Klein, E., Kalchenko, V., Bendel, P., Lira, S. A., Jung, S., & Schwartz, M. (2013). Recruitment of Beneficial M2 Macrophages to Injured Spinal Cord Is Orchestrated by Remote Brain Choroid Plexus. *Immunity*, *38*(3), 555–569. https://doi.org/10.1016/J.IMMUNI.2013.02.012

Shechter, R., & Schwartz, M. (2013). Harnessing monocyte-derived macrophages to control central nervous system pathologies: no longer 'if' but 'how'. *The Journal of Pathology*, *229*(2), 332–346. https://doi.org/10.1002/PATH.4106

Shemer, A., Grozovski, J., Tay, T. L., Tao, J., Volaski, A., Süß, P., Ardura-Fabregat, A., Gross-Vered, M., Kim, J. S., David, E., Chappell-Maor, L., Thielecke, L., Glass, C. K., Cornils, K., Prinz, M., & Jung, S. (2018). Engrafted parenchymal brain macrophages differ from microglia in transcriptome, chromatin landscape and response to challenge. *Nature Communications 2018 9:1*, *9*(1), 1–16. https://doi.org/10.1038/s41467-018-07548-5

Shen, Q., Zheng, J., Wang, X., Hu, W., Jiang, Y., & Jiang, Y. (2020). LncRNA SNHG5 regulates cell apoptosis and inflammation by miR-132/PTEN axis in COPD. *Biomedicine & Pharmacotherapy = Biomedecine & Pharmacotherapie*, *126*, 110016–110016. https://doi.org/10.1016/J.BIOPHA.2020.110016

Ståhl, P. L., Salmén, F., Vickovic, S., Lundmark, A., Navarro, J. F., Magnusson, J., Giacomello, S., Asp, M., Westholm, J. O., Huss, M., Mollbrink, A., Linnarsson, S., Codeluppi, S., Borg, Å., Pontén, F., Costea, P. I., Sahlén, P., Mulder, J., Bergmann, O., … Frisén, J. (2016). Visualization and analysis of gene expression in tissue sections by spatial transcriptomics. *Science*, *353*(6294), 78–82. https://doi.org/10.1126/SCIENCE.AAF2403/SUPPL_FILE/AAF2403_STAHL_SM.PDF

Steele, N. Z. R., Carr, J. S., Bonham, L. W., Geier, E. G., Damotte, V., Miller, Z. A., Desikan, R. S., Boehme, K. L., Mukherjee, S., Crane, P. K., Kauwe, J. S. K., Kramer, J. H., Miller, B. L., Coppola, G., Hollenbach, J. A., Huang, Y., & Yokoyama, J. S. (2017). Fine-mapping of the human leukocyte antigen locus as a risk factor for Alzheimer disease: A case–control study. *PLoS Medicine*, *14*(3), e1002272. https://doi.org/10.1371/journal.pmed.1002272

Steinbusch, M. M. F., Fang, Y., Milner, P. I., Clegg, P. D., Young, D. A., Welting, T. J. M., & Peffers, M. J. (2017). Serum snoRNAs as biomarkers for joint ageing and post traumatic osteoarthritis. *Scientific Reports*, *7*(1), 1–11. https://doi.org/10.1038/srep43558

Stelzmann, R. A., Norman Schnitzlein, H., & Reed Murtagh, F. (1995). An English translation of Alzheimer's 1907 paper, 'Uber eine eigenartige Erkankung der Hirnrinde'. *Clinical Anatomy (New York, N.Y.)*, *8*(6), 429–431. https://doi.org/10.1002/CA.980080612

Stepanov, G. A., Filippova, J. A., Komissarov, A. B., Kuligina, E. V., Richter, V. A., Semenov, D. V., & Tang, T. H. (2015). Regulatory role of Small nucleolar RNAs in human diseases. In *BioMed Research International* (Vol. 2015, pp. 206849–206849). Hindawi Publishing Corporation. https://doi.org/10.1155/2015/206849

Stoeckius, M., Hafemeister, C., Stephenson, W., Houck-Loomis, B., Chattopadhyay, P. K., Swerdlow, H., Satija, R., & Smibert, P. (2017). Simultaneous epitope and transcriptome measurement in single cells. *Nature Methods 2017 14:9*, *14*(9), 865–868. https://doi.org/10.1038/nmeth.4380

Stoeckius, M., Zheng, S., Houck-Loomis, B., Hao, S., Yeung, B. Z., Mauck 3rd, W. M., Smibert, P., & Satija, R. (2018). Cell Hashing with barcoded antibodies enables multiplexing and doublet detection for single cell genomics. *Genome Biol*, *19*(1), 224. https://doi.org/10.1186/s13059-018-1603-1

Streit, W. J., Braak, H., Del Tredici, K., Leyh, J., Lier, J., Khoshbouei, H., Eisenlöffel, C., Müller, W., & Bechmann, I. (2018). Microglial activation occurs late during preclinical Alzheimer's disease. *Glia*, *66*(12), 2550–2562. https://doi.org/10.1002/GLIA.23510

Stuart, T., Butler, A., Hoffman, P., Hafemeister, C., Papalexi, E., Mauck, W. M., Hao, Y., Stoeckius, M., Smibert, P., & Satija, R. (2019). Comprehensive Integration of Single-Cell Data. *Cell*, *177*(7), 1888-1902.e21.

Sud, R., Geller, E. T., & Schellenberg, G. D. (2014). Antisense-mediated Exon Skipping Decreases Tau Protein Expression: A Potential Therapy For Tauopathies. *Molecular Therapy - Nucleic Acids*, *3*, e180. https://doi.org/10.1038/mtna.2014.30

Sundelöf, J., Sundström, J., Hansson, O., Eriksdotter-Jönhagen, M., Giedraitis, V., Larsson, A., Degerman-Gunnarsson, M., Ingelsson, M., Minthon, L., Blennow, K., Kilander, L., Basun, H., & Lannfelt, L. (2010). Higher Cathepsin B Levels in Plasma in Alzheimer's Disease Compared to Healthy Controls. *Journal of Alzheimer's Disease*, *22*(4), 1223–1230. https://doi.org/10.3233/JAD-2010-101023

Svensson, V., Vento-Tormo, R., & Teichmann, S. A. (2018). Exponential scaling of single-cell RNA-seq in the past decade. *Nature Protocols 2018 13:4*, *13*(4), 599–604. https://doi.org/10.1038/nprot.2017.149

Sweeney, M. D., Sagare, A. P., & Zlokovic, B. V. (2018). Blood–brain barrier breakdown in Alzheimer disease and other neurodegenerative disorders. *Nature Reviews Neurology 2018 14:3*, *14*(3), 133–150. https://doi.org/10.1038/nrneurol.2017.188

Tabet, N. (2006). Acetylcholinesterase inhibitors for Alzheimer's disease: anti-inflammatories in acetylcholine clothing! *Age and Ageing*, *35*(4), 336–338. https://doi.org/10.1093/AGEING/AFL027

Tang, F., Barbacioru, C., Wang, Y., Nordman, E., Lee, C., Xu, N., Wang, X., Bodeau, J., Tuch, B. B., Siddiqui, A., Lao, K., & Surani, M. A. (2009). mRNA-Seq whole-transcriptome analysis of a single cell. *Nature Methods 2009 6:5*, *6*(5), 377–382. https://doi.org/10.1038/nmeth.1315

Tang, W., Shen, Z., Guo, J., & Sun, S. (2016). Screening of long non-coding RNA and TUG1 inhibits proliferation with TGF-β induction in patients with COPD. *International Journal of Chronic Obstructive Pulmonary Disease*, *11*(1), 2951–2964. https://doi.org/10.2147/COPD.S109570

Taura, M., Frank, J. A., Takahashi, T., Kong, Y., Kudo, E., Song, E., Tokuyama, M., & Iwasaki, A. (2022). APOBEC3A regulates transcription from interferon-stimulated response elements. *Proceedings of the National Academy of Sciences of the United States of America*, *119*(20). https://doi.org/10.1073/PNAS.2011665119/-/DCSUPPLEMENTAL

Terai, K., Walker, D. G., McGeer, E. G., & McGeer, P. L. (1997). Neurons express proteins of the classical complement pathway in Alzheimer disease. *Brain Research*, *769*(2), 385–390. https://doi.org/10.1016/S0006-8993(97)00849-4

Thomson, A. M., Cahill, C. M., Cho, H. H., Kassachau, K. D., Epis, M. R., Bridges, K. R., Leedman, P. J., & Rogers, J. T. (2005). The Acute Box cis-Element in Human Heavy Ferritin mRNA 5′-Untranslated Region Is a Unique Translation Enhancer That Binds Poly(C)-binding Proteins. *Journal of Biological Chemistry*, *280*(34), 30032–30045. https://doi.org/10.1074/JBC.M502951200

Tracey, K. J. (2002). The inflammatory reflex. *Nature 2002 420:6917*, *420*(6917), 853–859. https://doi.org/10.1038/nature01321

van Dyck CH, Swanson CJ, Aisen P, Bateman RJ, Chen C, Gee M, Kanekiyo M, Li D, Reyderman L, Cohen S, Froelich L, Katayama S, Sabbagh M, Vellas B, Watson D, Dhadda S, Irizarry M, Kramer LD, & Iwatsubo T. (2023). Lecanemab in Early Alzheimer's Disease. *New England Journal of Medicine*, *388*(17), 1630–1632. https://doi.org/10.1056/NEJMC2301380

Van Hove, H., Martens, L., Scheyltjens, I., De Vlaminck, K., Pombo Antunes, A. R., De Prijck, S., Vandamme, N., De Schepper, S., Van Isterdael, G., Scott, C. L., Aerts, J., Berx, G., Boeckxstaens, G. E., Vandenbroucke, R. E., Vereecke, L., Moechars, D., Guilliams, M., Van Ginderachter, J. A., Saeys, Y., & Movahedi, K. (2019). A single-cell atlas of mouse brain macrophages reveals unique transcriptional identities shaped by ontogeny and tissue environment. *Nature Neuroscience 2019 22:6*, *22*(6), 1021–1035. https://doi.org/10.1038/s41593-019-0393-4

Vandooren, J., & Itoh, Y. (2021). Alpha-2-Macroglobulin in Inflammation, Immunity and Infections. *Frontiers in Immunology*, *12*, 5411. https://doi.org/10.3389/FIMMU.2021.803244/BIBTEX

Veglia, F., Perego, M., & Gabrilovich, D. (2018). Myeloid-derived suppressor cells coming of age. *Nature Immunology 2018 19:2*, *19*(2), 108–119. https://doi.org/10.1038/s41590-017-0022-x

Venet, F., Demaret, J., Gossez, M., & Monneret, G. (2021). Myeloid cells in sepsis-acquired immunodeficiency. *Annals of the New York Academy of Sciences*, *1499*(1), 3–17. https://doi.org/10.1111/NYAS.14333

Villemagne, V. L., Fodero-Tavoletti, M. T., Masters, C. L., & Rowe, C. C. (2015). Tau imaging: early progress and future directions. *The Lancet Neurology*, *14*(1), 114–124. https://doi.org/10.1016/S1474-4422(14)70252-2

Villemagne, V. L., Furumoto, S., Fodero-Tavoletti, M. T., Mulligan, R. S., Hodges, J., Harada, R., Yates, P., Piguet, O., Pejoska, S., Doré, V., Yanai, K., Masters, C. L., Kudo, Y., Rowe, C. C., & Okamura, N. (2014). In vivo evaluation of a novel tau imaging tracer for Alzheimer's disease. *European Journal of Nuclear*

Medicine and Molecular Imaging, *41*(5), 816–826. https://doi.org/10.1007/S00259-013-2681-7/FIGURES/3

Wang, P., & Wang, Z. Y. (2017). Metal ions influx is a double edged sword for the pathogenesis of Alzheimer's disease. In *Ageing Research Reviews* (Vol. 35, pp. 265–290). Elsevier Ireland Ltd. https://doi.org/10.1016/j.arr.2016.10.003

Wang, X., Allen, W. E., Wright, M. A., Sylwestrak, E. L., Samusik, N., Vesuna, S., Evans, K., Liu, C., Ramakrishnan, C., Liu, J., Nolan, G. P., Bava, F. A., & Deisseroth, K. (2018). Three-dimensional intact-tissue sequencing of single-cell transcriptional states. *Science*, *361*(6400). https://doi.org/10.1126/SCIENCE.AAT5691/SUPPL_FILE/AAT5691_WANG_SM_TABLE-S2.XLSX

Ward, R. J., Zucca, F. A., Duyn, J. H., Crichton, R. R., & Zecca, L. (2014). The role of iron in brain ageing and neurodegenerative disorders. *The Lancet Neurology*, *13*(10), 1045–1060. https://doi.org/10.1016/S1474-4422(14)70117-6

Weiner, H. L., & Selkoe, D. J. (2002). Inflammation and therapeutic vaccination in CNS diseases. *Nature 2002 420:6917*, *420*(6917), 879–884. https://doi.org/10.1038/nature01325

Weingarten, M. D., Lockwood, A. H., Hwo, S. Y., & Kirschner, M. W. (1975). A protein factor essential for microtubule assembly. *Proceedings of the National Academy of Sciences of the United States of America*, *72*(5), 1858–1862. https://doi.org/10.1073/PNAS.72.5.1858

Wendeln, A. C., Degenhardt, K., Kaurani, L., Gertig, M., Ulas, T., Jain, G., Wagner, J., Hasler, L. M., Wild, K., Skodras, A., Blank, T., Staszewski, O., Datta, M., Centeno, T. P., Capece, V., Islam, M. R., Kerimoglu, C., Staufenbiel, M., Schultze, J. L., … Neher, J. J. (2018). Innate immune memory in the brain shapes neurological disease hallmarks. *Nature*, *556*(7701), 332–338. https://doi.org/10.1038/s41586-018-0023-4

Wendisch, D., Dietrich, O., Mari, T., von Stillfried, S., Ibarra, I. L., Mittermaier, M., Mache, C., Chua, R. L., Knoll, R., Timm, S., Brumhard, S., Krammer, T., Zauber, H., Hiller, A. L., Pascual-Reguant, A., Mothes, R., Bülow, R. D., Schulze, J., Leipold, A. M., … Sander, L. E. (2021). SARS-CoV-2 infection triggers profibrotic macrophage responses and lung fibrosis. *Cell*, *184*(26), 6243. https://doi.org/10.1016/J.CELL.2021.11.033

Wickham, H. (2016). ggplot2 Elegant Graphics for Data Analysis. In *Journal of the Royal Statistical Society: Series A (Statistics in Society)* (Vol. 174, Issue 1). Springer International Publishing. https://doi.org/10.1007/978-3-319-24277-4

Wirth, M., Madison, C. M., Rabinovici, G. D., Oh, H., Landau, S. M., & Jagust, W. J. (2013). Alzheimer's disease neurodegenerative biomarkers are associated with decreased cognitive function but not-amyloid in cognitively normal older individuals. *Journal of Neuroscience*, *33*(13), 5553–5563. https://doi.org/10.1523/JNEUROSCI.4409-12.2013

Wolock, S. L., Lopez, R., & Klein, A. M. (2019). Scrublet: Computational Identification of Cell Doublets in Single-Cell Transcriptomic Data. *Cell Systems*, *8*(4), 281-291.e9. https://doi.org/10.1016/J.CELS.2018.11.005

World Health Organization. (2017). Global action plan on the public health response to dementia. *Global Action Plan on the Public Health Response to Dementia 2017 - 2025. Geneva World Heal. Organ.*, *27*. http://apps.who.int/bookorders.

Wyss-Coray, T., & Rogers, J. (2012). Inflammation in Alzheimer Disease—A Brief Review of the Basic Science and Clinical Literature. *Cold Spring Harbor Perspectives in Medicine*, *2*(1). https://doi.org/10.1101/CSHPERSPECT.A006346

Xi, N. M., & Li, J. J. (2021). Benchmarking Computational Doublet-Detection Methods for Single-Cell RNA Sequencing Data. *Cell Systems*, *12*(2), 176-194.e6. https://doi.org/10.1016/J.CELS.2020.11.008

Xu, H., & Jia, J. (2021). Single-Cell RNA Sequencing of Peripheral Blood Reveals Immune Cell Signatures in Alzheimer's Disease. *Frontiers in Immunology*, *12*, 2727. https://doi.org/10.3389/FIMMU.2021.645666/BIBTEX

Xu, J., Li, J., Xiao, K., Zou, S., Yan, P., Xie, X., & Xie, L. (2020). Dynamic changes in human HLA-DRA gene expression and Th cell subsets in sepsis: Indications of immunosuppression and associated outcomes. *Scandinavian Journal of Immunology*, *91*(1). https://doi.org/10.1111/sji.12813

Young, M. D., & Behjati, S. (2020). SoupX removes ambient RNA contamination from droplet-based single-cell RNA sequencing data. *GigaScience*, *9*(12), 1–10. https://doi.org/10.1093/GIGASCIENCE/GIAA151

Yu, G., Wang, L. G., Han, Y., & He, Q. Y. (2012). clusterProfiler: an R Package for Comparing Biological Themes Among Gene Clusters. *OMICS : A Journal of Integrative Biology*, *16*(5), 284. https://doi.org/10.1089/OMI.2011.0118

Zakeri, N., Hall, A., Swadling, L., Pallett, L. J., Schmidt, N. M., Diniz, M. O., Kucykowicz, S., Amin, O. E., Gander, A., Pinzani, M., Davidson, B. R., Quaglia, A., & Maini, M. K. (2022). Characterisation and induction of tissue-resident gamma delta T-cells to target hepatocellular carcinoma. *Nature Communications 2022 13:1*, *13*(1), 1–16. https://doi.org/10.1038/s41467-022-29012-1

Zeisel, A., M͡oz-Manchado, A. B., Codeluppi, S., Lönnerberg, P., Manno, G. La, Juréus, A., Marques, S., Munguba, H., He, L., Betsholtz, C., Rolny, C., Castelo-Branco, G., Hjerling-Leffler, J., & Linnarsson, S. (2015). Brain structure. Cell types in the mouse cortex and hippocampus revealed by single-cell RNA-seq. *Science (New York, N.Y.)*, *347*(6226), 1138–1142. https://doi.org/10.1126/SCIENCE.AAA1934

Zhang, Y., Li, P., Feng, J., & Wu, M. (2016). Dysfunction of NMDA receptors in Alzheimer's disease. *Neurological Sciences*, *37*(7), 1039–1047. https://doi.org/10.1007/S10072-016-2546-5/FIGURES/2

Zhao, Q., Wang, J., Levichkin, I. V., Stasinopoulos, S., Ryan, M. T., & Hoogenraad, N. J. (2002). A mitochondrial specific stress response in mammalian cells. *The EMBO Journal*, *21*(17), 4411–4419. https://doi.org/10.1093/EMBOJ/CDF445

Zheng, G. X. Y., Terry, J. M., Belgrader, P., Ryvkin, P., Bent, Z. W., Wilson, R., Ziraldo, S. B., Wheeler, T. D., McDermott, G. P., Zhu, J., Gregory, M. T., Shuga, J., Montesclaros, L., Underwood, J. G., Masquelier, D. A., Nishimura, S. Y., Schnall-Levin, M., Wyatt, P. W., Hindson, C. M., … Bielas, J. H. (2017). Massively parallel digital transcriptional profiling of single cells. *Nature Communications 2017 8:1*, *8*(1), 1–12. https://doi.org/10.1038/ncomms14049